USGS
science for a changing world

Studies by the U.S. Geological Survey in Alaska, 2008–2009

Depositional Setting and Geochemistry of Phosphorites and Metalliferous Black Shales in the Carboniferous-Permian Lisburne Group, Northern Alaska

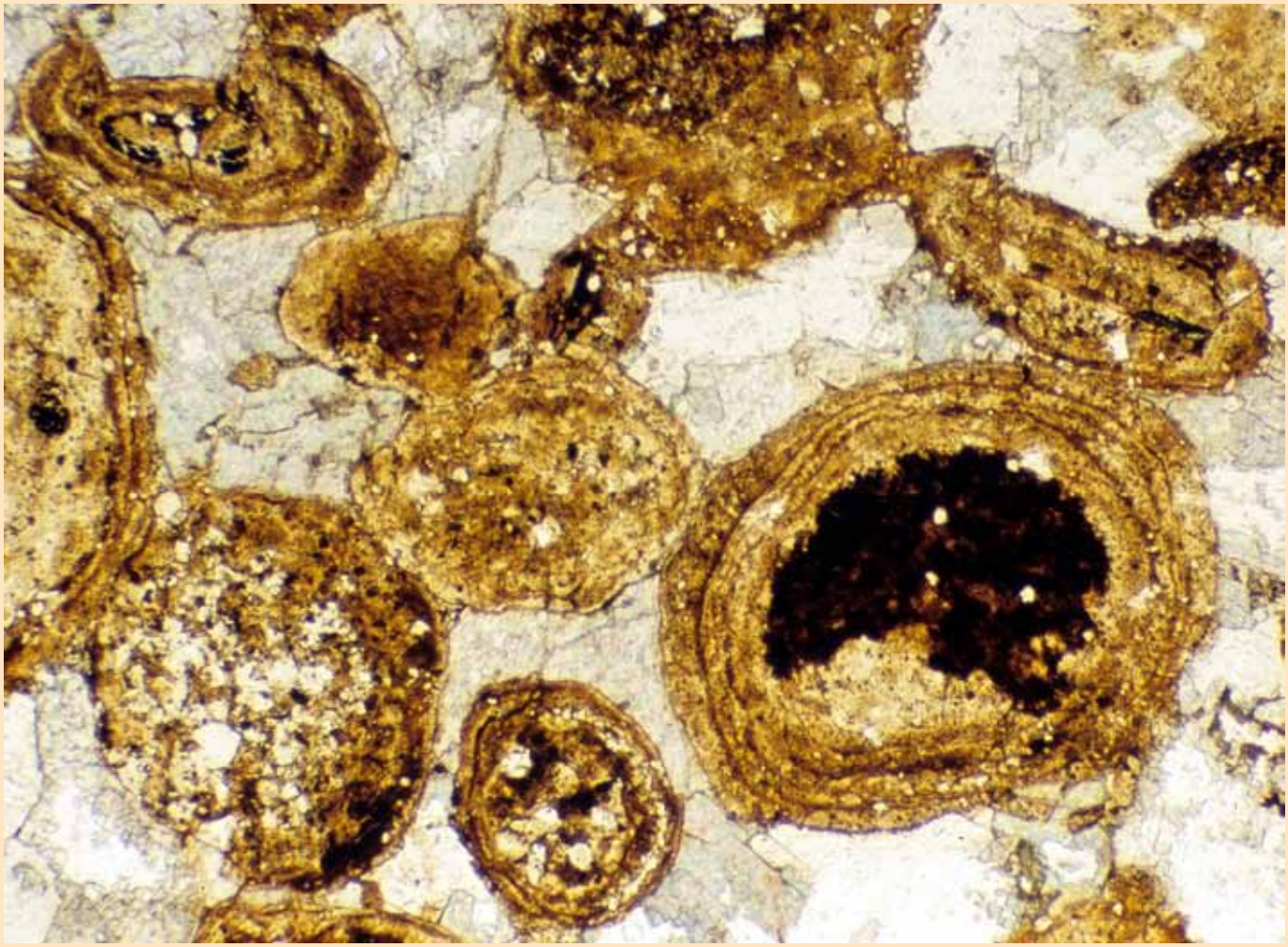

Professional Paper 1776-C

U.S. Department of the Interior
U.S. Geological Survey

Cover photograph: Photomicrograph of phosphatic ooids and peloids in carbonate cement.

Studies by the U.S. Geological Survey in Alaska, 2008–2009

Depositional Setting and Geochemistry of Phosphorites and Metalliferous Black Shales in the Carboniferous-Permian Lisburne Group, Northern Alaska

By Julie A. Dumoulin, John F. Slack, Michael T. Whalen, and Anita G. Harris

Professional Paper 1776-C

U.S. Department of the Interior
U.S. Geological Survey

U.S. Department of the Interior
KEN SALAZAR, Secretary

U.S. Geological Survey
Marcia K. McNutt, Director

U.S. Geological Survey, Reston, Virginia: 2011

This report and any updates to it are available online at:
http://pubs.usgs.gov/pp/1776/c/

For additional information write to:
U.S. Geological Survey
Box 25046, Mail Stop 421, Denver Federal Center
Denver, CO 80225-0046

Additional USGS publications can be found at:
http://geology.usgs.gov/index.htm

For more information about the USGS and its products:
Telephone: 1–888–ASK–USGS (1-888-275-8747)
World Wide Web: http://www.usgs.gov/

Suggested Citation
Dumoulin, J.A., Slack, J.F., Whalen, M.T., and Harris, A.G., 2011, Depositional setting and geochemistry of phosphorites and metalliferous black shales in the Carboniferous-Permian Lisburne Group, northern Alaska, Dumoulin, J.A., and Galloway, J.P., eds., Studies by the U.S. Geological Survey in Alaska, 2008–2009: U.S. Geological Survey Professional Paper 1776–C, 64 p.

Contents

Figures

Tables

Studies by the U.S. Geological Survey in Alaska, 2008–2009
Edited by Julie A. Dumoulin and John P. Galloway
U.S. Geological Survey Professional Paper 1776–C

Depositional Setting and Geochemistry of Phosphorites and Metalliferous Black Shales in the Carboniferous-Permian Lisburne Group, Northern Alaska

By Julie A. Dumoulin[1], John F. Slack[2], Michael T. Whalen[3], and Anita G. Harris[4]

Abstract

Phosphatic rocks are distributed widely in the Lisburne Group, a mainly Carboniferous carbonate succession that occurs throughout northern Alaska. New sedimentologic, paleontologic, and geochemical data presented here constrain the geographic and stratigraphic extent of these strata and their depositional and paleogeographic settings. Our findings support models that propose very high oxygen contents of the Permo-Carboniferous atmosphere and oceans, and those that suggest enhanced phosphogenesis in iron-limited sediments; our data also have implications for Carboniferous paleogeography of the Arctic.

Lisburne Group phosphorites range from granular to nodular, are interbedded with black shale and lime mudstone rich in radiolarians and sponge spicules, and accumulated primarily in suboxic outer- to middle-ramp environments. Age constraints from conodonts, foraminifers, and goniatite cephalopods indicate that most are middle Late Mississippian (early Chesterian; early late Visean). Phosphorites form 2- to 40-cm-thick beds of sand- to pebble-sized phosphatic peloids, coated grains, and (or) bioclasts cemented by carbonate, silica, or phosphate that occur through an interval ≤12 m thick. High gamma-ray response through this interval suggests strongly condensed facies related to sediment starvation and development of phosphatic hardgrounds. Phosphorite textures, such as unconformity-bounded coated grains, record multiple episodes of phosphogenesis and sedimentary reworking. Sharp bed bases and local grading indicate considerable redeposition of phosphatic material into deeper water by storms and (or) gravity flows.

Lisburne Group phosphorites contain up to 37 weight percent P_2O_5, 7.6 weight percent F, 1,030 ppm Y, 517 ppm La, and 166 ppm U. Shale-normalized rare earth element (REE) plots show uniformly large negative Ce anomalies (avg. Ce/Ce*=0.11±0.03) that are interpreted to reflect phosphate deposition in seawater that was greatly depleted in Ce due to increased oxygenation of the atmosphere and oceans during the Carboniferous evolution of large vascular land plants.

Black shales within the phosphorite sections have up to 20.2 weight percent C_{org} and are potential petroleum source rocks. Locally, these strata also are metalliferous, with up to 1,690 ppm Cr, 2,831 ppm V, 551 ppm Ni, 4,670 ppm Zn, 312 ppm Cu, 43.5 ppm Ag, and 12.3 ppm Tl; concentrations of these metals covary broadly with C_{org}, suggesting coupled redox variations. Calculated marine fractions (MF) of Cr, V, and Mo, used to evaluate the paleoredox state of the bottom waters, show generally high Cr_{MF}/Mo_{MF} and V_{MF}/Mo_{MF} ratios that indicate deposition of the black shales under suboxic denitrifying conditions; Re/Mo ratios also plot mainly within the suboxic field and support this interpretation. Predominantly seawater and biogenic sources are indicated for Cr, V, Mo, Zn, Cd, Ni, and Cu in the black shales, with an additional hydrothermal contribution inferred for Zn, Cd, Ag, and Tl in some samples.

Lisburne Group phosphorites formed in the Ikpikpuk Basin and along both sides of the mud- and chert-rich Kuna Basin, which hosts giant massive sulfide and barite deposits of the Red Dog district. Lisburne Group phosphatic strata are coeval with these deposits and formed in response to a nutrient-rich upwelling regime. Phosphate deposition occurred mainly in suboxic bottom waters based on data for paleoredox proxies (Cr, V, Mo, Re) within contemporaneous black shales. Recent global reconstructions are consistent with Carboniferous upwelling in northern Alaska, but differ in the type of upwelling expected (zonal versus meridional). Paleoenvironmental data suggest that meridional upwelling may better explain phosphorite deposition in the Lisburne Group.

Introduction

Phosphatic rocks form a small but conspicuous and widespread part of the Lisburne Group, a chiefly Carboniferous carbonate-platform succession found throughout northern Alaska (fig. 1; Armstrong and Mamet, 1977, 1978; Dumoulin

[1]U.S. Geological Survey, Anchorage, Alaska.

[2]U.S. Geological Survey, Reston, Virginia.

[3]University of Alaska, Fairbanks.

[4]U.S. Geological Survey, Reston, Virginia (retired).

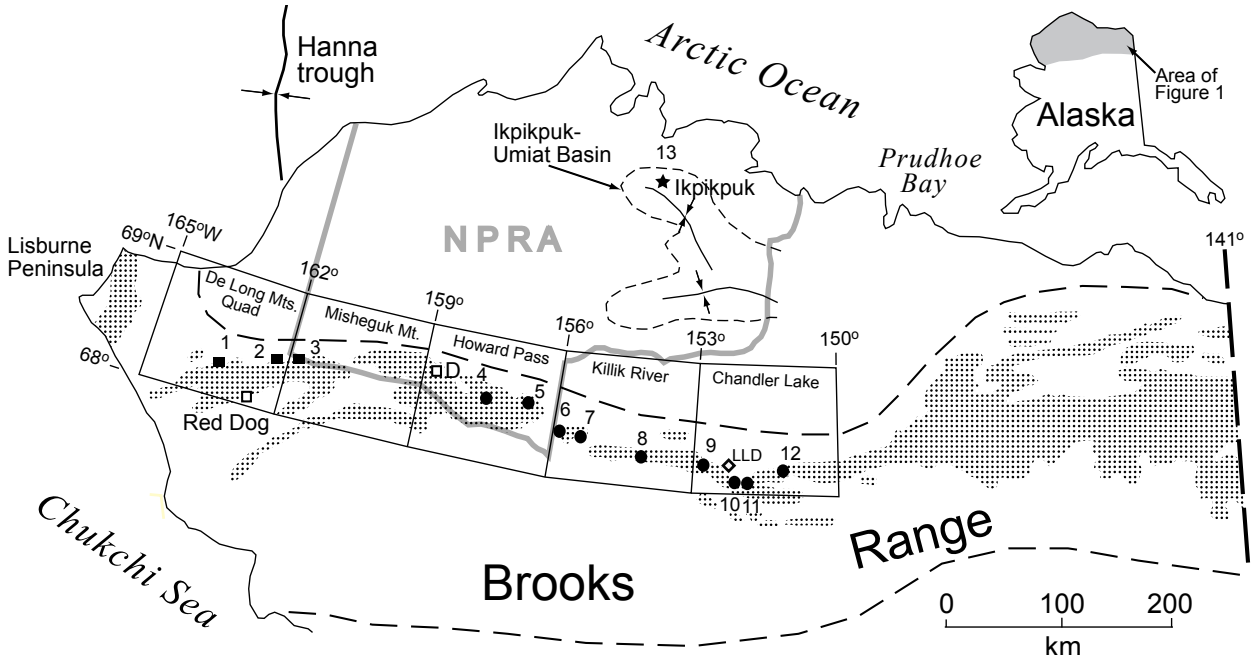

Figure 1. Outcrop belt of the Lisburne Group (shaded) in northern Alaska (modified from Armstrong and Mamet, 1978) and location of major phosphorite occurrences, quadrangles, and localities mentioned in the text (see table 1 for additional data). D, Drenchwater deposit; LLD, Lawrence Livermore Laboratory drill holes; gray line, boundary of NPRA (National Petroleum Reserve–Alaska). See Mayfield and others (1988), Young (2004), and references therein for details of allochthon distribution; individual allochthons are imbricated internally and made up of plates and thrust sheets, some of which are named. Endicott Mountains Allochthon (EMA) occurs throughout the western and central Brooks Range; Kelly River Allochthon (KRA) is found chiefly west of 159°; Picnic Creek Allochthon (PCA) chiefly west of 155°; localities 1–3 are in KRA, localities 4–12 occur in EMA, and locality 13 is in parautochthonous subsurface strata. Skimo and Tiglukpuk thrust sheets (Dumoulin and others, 2008) occur in the Chandler Lake quadrangle and are two of numerous imbricated thrust sheets that make up the EMA.

and Bird, 2001; Dumoulin and others, 2004). Lisburne Group phosphorites are of middle Late Mississippian (mainly early Chesterian) age and are interbedded with organic-rich black shale and lime mudstone; radiolarians and sponge spicules are common components of all three lithologies. The black shales are potential petroleum source rocks (Dumoulin and others, 2008) and locally are metalliferous, with high concentrations of Cr, V, Ni, Zn, Cu, Ag, Se, and Tl (Dumoulin and others, 2006b, 2006c). Phosphorites in the Lisburne Group formed at a time of great geologic activity in northern Alaska. They are coeval with the formation of world-class deposits of zinc and barite in the Red Dog district (Kelley and Jennings, 2004; fig. 1) and with the drowning of carbonate platforms across much of north-western and north-central Alaska (Dumoulin and others, 2004, 2008; Whalen and others, 2006).

Carboniferous phosphorites are uncommon worldwide (for example, Shields and others, 2000), and granular phosphorites that correlate precisely with those of the Lisburne Group have not been reported elsewhere. The purpose of this paper is to present new sedimentological, paleontological, and geochemical data that allow us to define the geographic and stratigraphic extent and depositional setting of these temporally unusual phosphorites. Our findings have implications for oxygen levels of the Permo-Carboniferous atmosphere and oceans, support recent models of phosphogenesis in suboxic iron-limited sediments, and constrain paleogeographic reconstructions of the Arctic.

Geologic Framework

The mainly Carboniferous Lisburne Group crops out throughout the Brooks Range (fig. 1) and is found in the subsurface beneath much of northern Alaska and adjacent offshore areas, where locally it is as young as Permian. The Lisburne Group consists chiefly of carbonate rocks that were deposited in a range of shallow- and deep-water settings. Shallow water, as used here, implies peritidal to subtidal photic-zone settings; deep water refers to outer-ramp to basin environments (for example, Burchette and Wright, 1992; Wright and Burchette, 1998). Facies patterns of the Lisburne Group reflect a complex late Paleozoic paleogeography that was rearranged by later tectonism. The unit was deposited on an uneven topography shaped by extensional and transpressional deformation that began in the Devonian and persisted into the Permian (Dumoulin and Bird, 2001; Dumoulin and others, 2004). Structural features that were active during Carboniferous time include the Ikpikpuk-Umiat Basin beneath the west-central North Slope

and the Kuna Basin in the western Brooks Range (Bird, 2001; Young, 2004) as well as a number of other basins and intervening highs (see fig. 8 by Hubbard and others, 1987). Thrust and extensional faulting during the Mesozoic and Tertiary Brooks Range orogeny further complicated facies distribution of the Lisburne Group; we use the nomenclature of Young (2004) and Dumoulin and others (2008) for structural features such as allochthons that formed in this orogeny.

The diverse facies of the Lisburne Group are part of a single, structurally dismembered depositional system (fig. 2). Deep-water facies of the Lisburne Group predominate in parts of the Endicott Mountains Allochthon (EMA) in the western Brooks Range and throughout the structurally higher Picnic Creek and Ipnavik River allochthons; shallow-water strata prevail elsewhere in the EMA and throughout most of the Kelly River Allochthon (KRA; Dumoulin and others, 2004). The Lisburne Group in the subsurface formed mainly in shallow water, but includes some deeper-water rocks (Dumoulin and Bird, 2001). Palinspastic models of Mayfield and others (1988) and Young (2004) imply that deep-water strata of the Lisburne Group accumulated in a sediment-starved, extensional basin about 200 km wide by 600 km long (Kuna Basin), which was bounded on the north and southwest (present-day coordinates) by extensive carbonate platforms. The platforms consist largely of shallow-water carbonate rocks, but include local tongues of deeper-water strata (Dumoulin and others, 2004; Whalen and

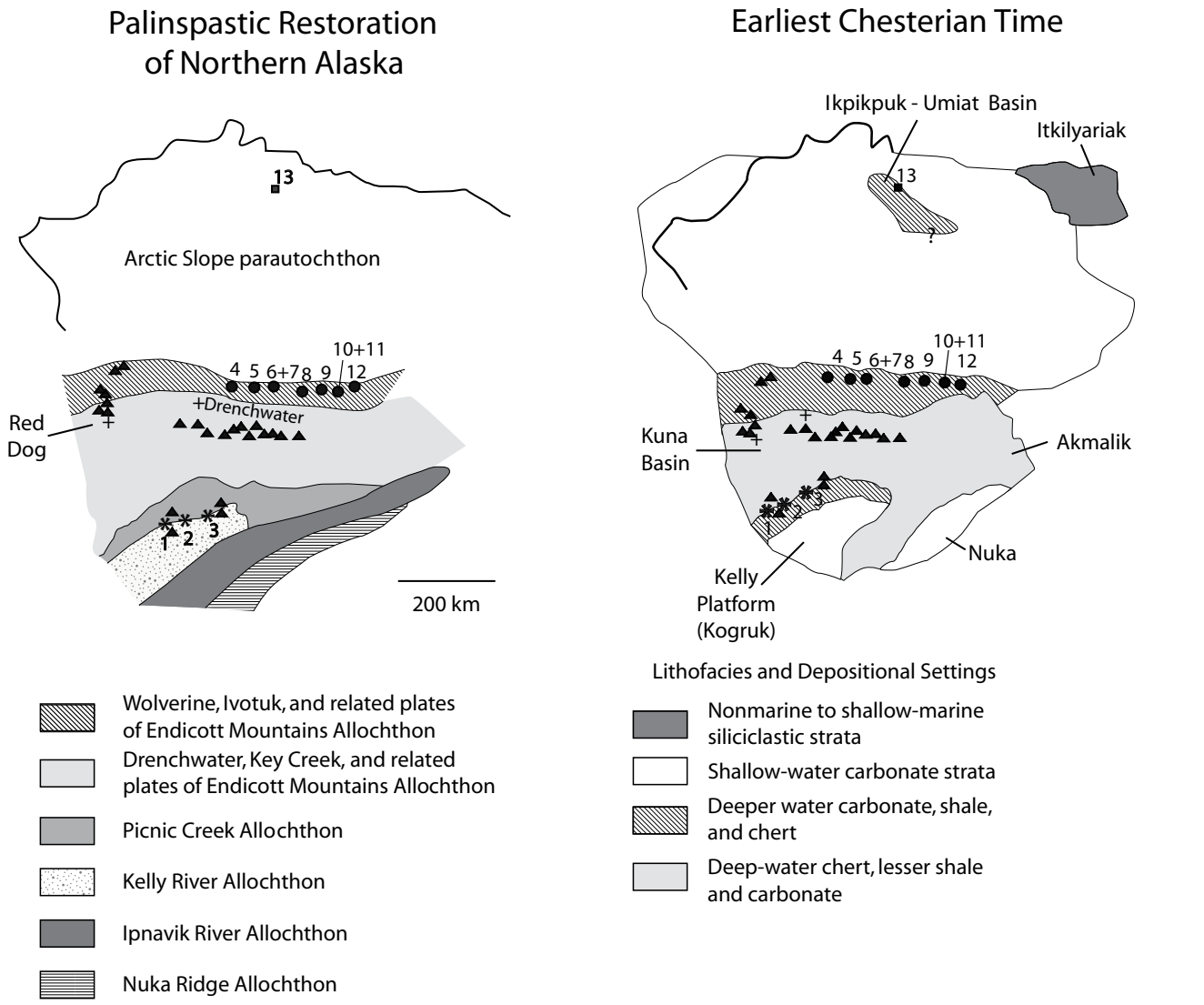

Figure 2. Palinspastic restoration of northern Alaska, adapted from Young (2004); subsurface data from Dumoulin and Bird (2001). Lisburne Group phosphorites formed during late Meramecian-early Chesterian time along the margin of the Ikpikpuk-Umiat Basin and on both sides of the Kuna Basin, which encompasses all deeper water and deep-water facies shown in southern part of reconstruction; triangles indicate approximately coeval occurrences of less-phosphatic strata (1-6 weight percent P_2O_5) in the Lisburne. Other occurrences of less-phosphatic rocks in the Lisburne Group that likely are older (Osagean) or younger (Morrowan or younger) are not shown here but are listed in table 2 and are found, respectively, west of and mainly east of locality 8.

others, 2006). Facies patterns indicate that the southern margin of the main (northern) platform was not uniform, but changed from a gently sloping homoclinal ramp in the east to a distally-steepened margin along which locally abundant carbonate turbidites accumulated in the west (Dumoulin and others, 2004). Basins farther north in the subsurface beneath the Arctic coastal plain, such as the ~200 by 150 km Ikpikpuk-Umiat Basin (figs. 1, 2), were filled with thick, rapidly deposited, chiefly shallow-water strata that include some deeper-water intervals (Dumoulin and Bird, 2001).

Strata deposited in the Kuna Basin (fig. 2) mainly are organic-rich, biosiliceous black shale and mudstone and lesser calcareous radiolarite and carbonate turbidites of the Kuna Formation and related units (Dumoulin and others, 2004). Geochemical, petrographic, and sedimentologic data indicate that black shales of the Kuna Formation accumulated under chiefly suboxic, denitrifying depositional conditions (Dumoulin and others, 2004; Slack and others, 2004a; this paper).

Following Patton and Matzko (1959), Trappe (1998), and Cook and Shergold (2005), we define phosphorites as rocks that contain ≥18 weight percent P_2O_5, and we use the term phosphate rock to refer to samples having 13–17 weight percent P_2O_5. Phosphorites in the Lisburne Group contain 18–37 weight percent P_2O_5. They are most abundant in, and were first described from, the EMA (figs. 1, 2; Patton and Matzko, 1959; Kelley and Mull, 1995; Kurtak and others, 1995; Whalen and others, 2006; Dumoulin and others, 2008). Similar phosphorites were recognized more recently in the KRA in the western Brooks Range and in the parautochthonous subsurface succession in the Ikpikpuk well (Dumoulin and Bird, 2001; Dumoulin and others, 2004, 2006b, 2006c) and also may occur in parautochthonous strata of the Lisburne Peninsula (Armstrong and Mamet, 1977). All of these phosphorites are of late Meramecian-early Chesterian age (fig. 3) and occur within a distinctive subunit of the Lisburne Group, typically ~3–35 m thick, which also contains black shale, characteristic carbonate lithologies (described below), and local chert (fig. 4).

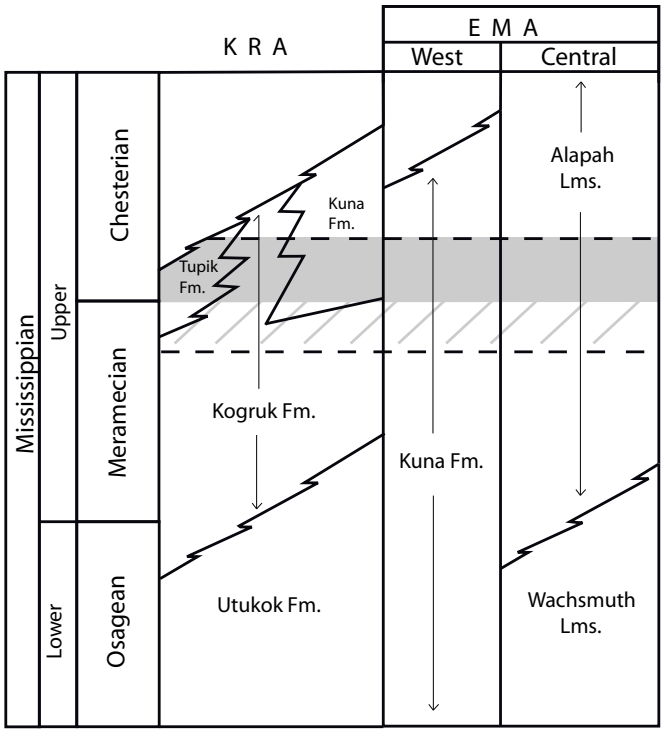

Figure 3. Stratigraphic nomenclature of the Mississippian part of the Lisburne Group in the Kelly River Allochthon (KRA) and Endicott Mountains Allochthon (EMA). Dashed lines indicate approximate age range (late Meramecian-early Chesterian) of phosphorite interval, based on conodonts, foraminifers, and goniatite cephalopods; where most tightly dated, phosphorites are early Chesterian (shaded interval).

Various formal and informal stratigraphic names have been applied to the phosphorite-bearing interval of the Lisburne Group in the western and central Brooks Range (fig. 3). Workers in the central Brooks Range have called these strata the lower Kiruktagiak member (Brosgé and Reiser, 1951), the black chert and shale member (Bowsher and Dutro, 1957; Patton and Matzko, 1959), the shale and phosphorite unit (in the Skimo thrust sheet of the EMA; Dumoulin and others, 2008), and the chert and phosphorite unit (in the Tiglukpuk thrust sheet of the EMA; Dumoulin and others, 2008); all of these are considered subunits of the Alapah Limestone. In the western Brooks Range, equivalent rocks have been referred to as the Tupik and Kuna Formations (Curtis and others, 1984, 1990), or are included in the Kogruk Formation (Dumoulin and others, 2004).

Less-phosphatic rocks (1–6 weight percent P_2O_5) occur more widely throughout the Lisburne Group. Some are coeval with the major episode of Lisburne phosphorite formation, but others are older (late Early Mississippian; Osagean) or younger (latest Mississippian-Middle Pennsylvanian; late early Chesterian-Morrowan). These less-phosphatic strata occur in the western and central Brooks Range in the EMA and KRA, and in the Picnic Creek Allochthon (PCA), and include phosphatic black shale in the Kuna Formation and phosphatic limestone in various units of the Lisburne Group (Slack and others, 2004a, 2004c, 2004d; Dumoulin and others, 2006c).

Methods and Terminology

We studied phosphatic rocks of the Lisburne Group as part of regional mineral and energy resource assessments by the U.S. Geological Survey (USGS) that were focused on the western Brooks Range (Red Dog area) and Chandler Lake quadrangle (fig. 1). Phosphatic strata in the Lisburne Group were investigated and sampled at 54 outcrop localities in the west, west-central, and central Brooks Range, and also were examined in cuttings from the Lisburne and Ikpikpuk wells and in drill cores from the Red Dog district (figs. 1, 2; tables 1, 2; note that tables 1–3 are found at the back of this report). We visited and sampled most Lisburne Group phosphorites reported in the literature and discovered several new occurrences during the course of our studies. Sections were measured through the phosphorite-bearing interval of the

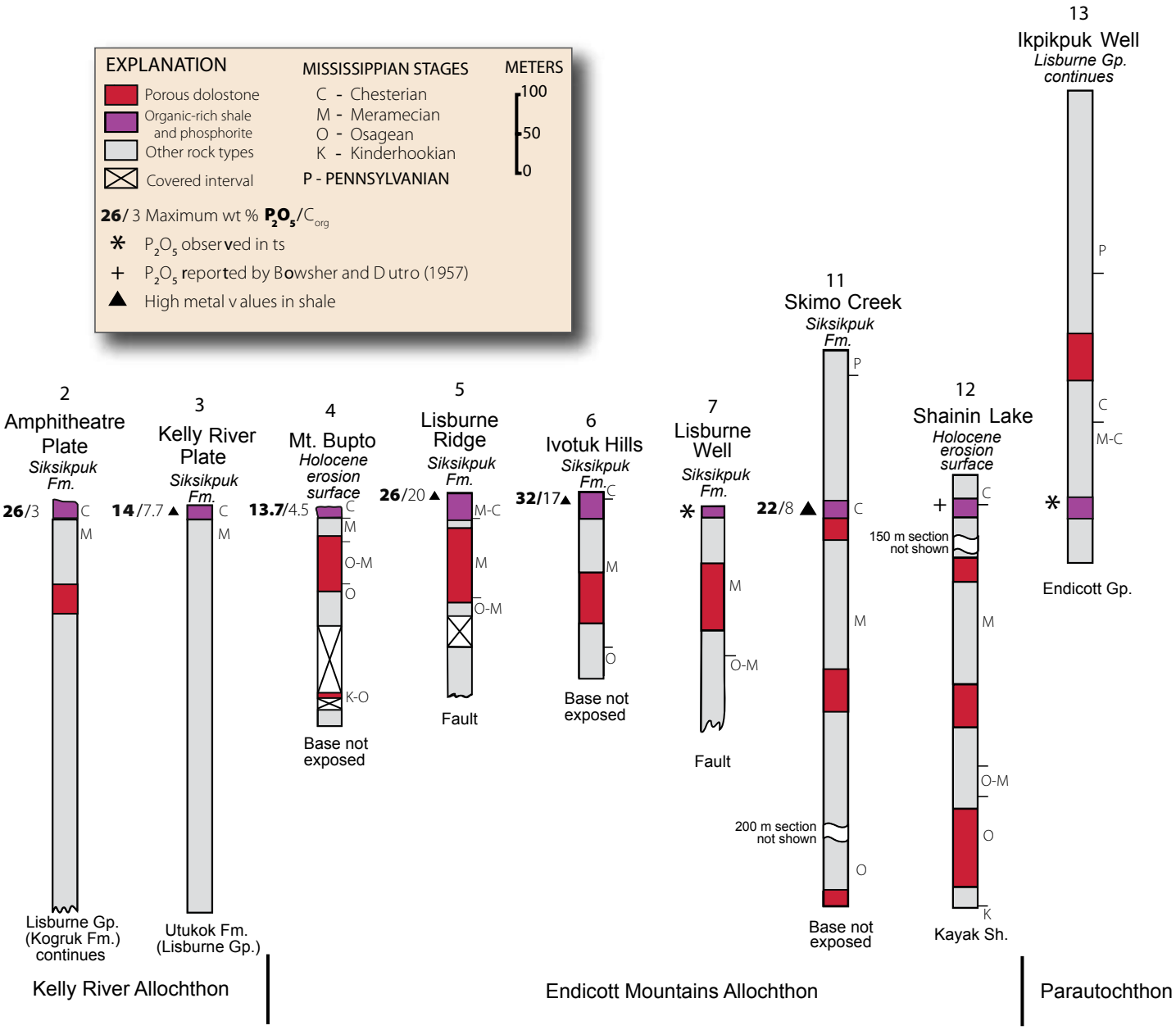

Figure 4. Stratigraphic position of phosphorites in the Lisburne Group; section locations shown in figure 1. Lower part of sections 2 and 3 are modified from Armstrong (1970).

Lisburne Group at all localities where strata were sufficiently well exposed (see table 1 for details). Age control for the sections comes mainly from conodonts, augmented by data from foraminifers and goniatite cephalopods (Dumoulin and Bird, 2001; Dover and others, 2004; Dumoulin and others, 2006a, 2008 and references therein). Petrographic interpretations are based on examination of 389 thin sections (tables 1, 2). Carbonate rocks are classified according to the scheme of Dunham (1962), as modified by Embry and Klovan (1972). We use the term "supportstone" to encompass packstone and grainstone.

Phosphorites in the Lisburne Group have two main forms: (1) Granular phosphorites are grain-supported lenses or beds made up of >90 volume percent phosphatic grains, which are mostly sand-sized and vary in type and texture (fig. 5*A*,*B*). (2) Phosphorite nodules are round to ovoid and range from a few millimeters to more than 15 cm long; most are made up of sand-sized phosphatic grains in a matrix of carbonate or silica cement, but some nodules consist mainly of fine-grained phosphate and lesser carbonate and (or) siliceous material (fig. 5*C*). Phosphate rocks are similar to granular phosphorites in outcrop and thin section texture, but contain more nonphosphatic material—mainly carbonate

cement, lime mud matrix, and calcareous and (or) silicified bioclasts (fig. 5*D*).

We obtained a spectral gamma-ray profile from the upper part of the Lisburne Group at Skimo Creek (loc. 11, fig. 1) using a Scintrex model 512 gamma-ray spectrometer that measures naturally occurring gamma-ray emissions (Dumoulin and others, 2008). This section was selected for profiling because it contains one of the thickest and most complete exposures of the phosphorite-bearing interval observed in this study, and because contacts with overlying and underlying subunits are well exposed. Measurements were taken every 0.5 m within the shale and phosphorite unit. The instrument provides total gamma-ray counts, as well as quantitative K (percent), U (ppm), and Th (ppm) concentrations.

Geochemical samples were selected to maximize geographic and lithologic coverage (fig. 1, table 1); we attempted to sample only fresh, unweathered rock but all samples analyzed for this study are from outcrop. At some localities with a range of phosphorite lithologies, several samples were taken to represent this range. Samples used for geochemical analysis were trimmed of weathered surfaces and veins and then pulverized in an alumina-ceramic mortar. All analyses were done at Activation Laboratories in Ancaster, Ontario. Major, selected trace, and rare earth elements (REE) were determined by inductively coupled plasma-mass spectrometry (ICP-MS) on rock powders fused with lithium metaborate/tetraborate in order to insure complete acid dissolution of minerals such as zircon, monazite, xenotime, and barite prior to analysis. Instrumental neutron activation analysis (INAA) was used for As, Sb, Sc, and Cr. Concentrations of Li, B, Ga, Co, Cd, Au, Pb, Mo, Re, Te, and Se were acquired by high-precision ICP-MS following a multi-acid digestion of powders. Analyses were made on duplicate samples

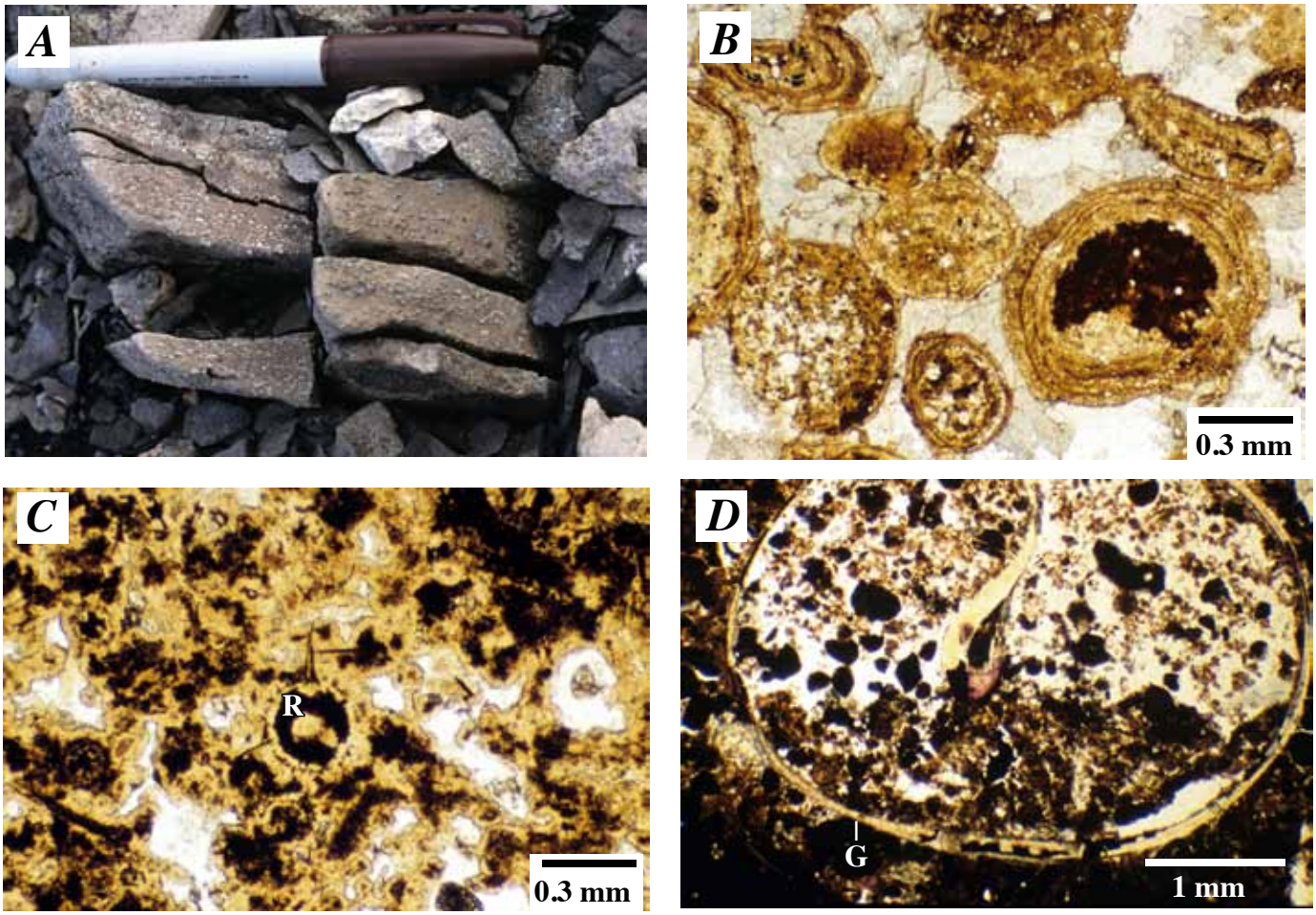

Figure 5. Phosphorite and phosphate rock in the Lisburne Group. *A*, Granular phosphorite (21–26 weight percent P_2O_5) in EMA at Lisburne Ridge (loc. 5, fig. 1). *B*, Photomicrograph of bed shown in *A* contains phosphatic ooids and peloids in carbonate cement; phosphatic grain in lower left includes abundant white quartz silt. *C*, Photomicrograph of phosphorite nodule (4 cm maximum diameter; 31 weight percent P_2O_5) in KRA (loc. 1, fig. 1); it consists of finely intergrown phosphatic and lesser chalcedonic cement with abundant partly pyritized radiolarians (R) and sponge spicules. *D*, Photomicrograph of phosphate rock (14 weight percent P_2O_5) in KRA (loc. 3, fig. 1); it consists of phosphatic peloids and partly silicified calcareous bioclasts in a matrix of mud and carbonate cement; large shell (G) is a gastropod.

and on 8–12 standards. Precision and accuracy for concentrations ≥100 times the minimum detection limit (MDL) generally were better than ±5-percent relative, and in many cases, such as for major elements, were better than ±1-percent relative. For concentrations approximately 10 times the MDL, precision and accuracy were about ±10–20-percent relative depending on the method used. Details of the various analytical methods are available online at www.actlabs.com.

Geographic and Stratigraphic Variation of Phosphorites

Phosphatic rocks in the Lisburne Group occur in a number of structural and geographic settings (tables 1, 2). The palinspastic models of Young (2004) and subsurface data of Dumoulin and Bird (2001) provide a basis for a reconstruction of North Alaskan paleogeography during Late Mississippian time (fig. 2). Lisburne Group phosphorites (P_2O_5 ≥18 weight percent) and phosphate rock (P_2O_5 13–17 weight percent)—the focus of this paper—formed at least locally along the margin of the Ikpikpuk-Umiat Basin and along both sides of the mud-rich Kuna Basin. Roughly coeval occurrences of less-phosphatic rocks (P_2O_5 1–6 weight percent) occur in the Wolverine and Key Creek plates of the EMA, the PCA, and the KRA; these strata accumulated adjacent to the major phosphorites along both margins of the Kuna Basin and within the basin (fig. 2). Less-phosphatic rocks also are found in the slope and basin succession of the Kuna Formation of the Lisburne Group and in platformal successions that commonly contain glauconite. In contrast, glauconite is absent from virtually all intervals of phosphorite and phosphate rocks we studied in the Lisburne Group.

EMA—Central and West-Central Brooks Range

Lisburne Group phosphorites in the EMA occur in a discontinuous belt that extends through the Chandler Lake, Killik River, and Howard Pass quadrangles for >250 km (figs. 1, 2, locs. 4–12; table 1). Phosphatic strata in this belt have many similarities, but differ from east to west in cumulative thickness and relative stratigraphic position (fig. 4). We examined phosphorites from 14 surface localities throughout this belt (table 1) and from drill cores of the Lisburne 1 well (loc. 7, fig. 1). Phosphorites also occur in cuttings from two boreholes drilled by Lawrence Livermore Laboratory (fig. 1; table 1; Brosgé and Armstrong, 1977). Occurrences of conodonts, foraminifers, and goniatite cephalopods indicate that all phosphorite strata in this belt are late Meramecian-early Chesterian, and where most tightly dated are early Chesterian (table 1; Dumoulin and others, 2006a, 2006c, 2008).

In the eastern part of the EMA phosphorite belt (from the central Killik River quadrangle eastward; locs. 8–12, figs. 1, 2; table 1), the phosphatic interval occurs in the upper (but not uppermost) part of the Lisburne Group (fig. 4). The thickness of Lisburne strata overlying the phosphate zone increases to the east, from 18 m in the central Killik River quadrangle (loc. 8, fig. 1; C.G. Mull, written commun., 2005) to 60 m near Monotis Creek (loc. 9, fig. 1; Patton and Matzko, 1959) to 170 m at Skimo Creek (loc. 11, fig. 1; Dumoulin and others, 2008).

Granular phosphorites in the Lisburne Group are most abundant in the western half of the Chandler Lake quadrangle (locs. 9–11, fig. 1), where they occur chiefly in the Skimo and Tiglukpuk thrust sheets of Dumoulin and others (2008) and consist of 2- to 40-cm-thick beds of sand- to pebble-sized phosphatic peloids, coated grains, and (or) bioclasts in a matrix of calcite, silica, or phosphate ± fluorite cement and (or) lime or phosphatic mud. Phosphorite nodules, typically a few millimeters to 2 cm in diameter, also occur at most localities. As many as 10 discrete granular phosphorite beds have been found in some outcrops; most have a lens-like form and cannot be traced laterally for more than a few hundred meters. Phosphorites are interbedded with organic-rich black shale and lime mudstone (Dumoulin and others, 2008), contain 18–37 weight percent P_2O_5, and occur through an interval ≤12 m thick. Shale and limestone interbeds in this interval have as much as 10 weight percent P_2O_5 (Patton and Matzko, 1959). Sections as much as 6 m thick averaging 19–26 weight percent P_2O_5 have been documented at several localities (Patton and Matzko, 1959; Kurtak and others, 1995).

Where detailed studies have been made in the central Chandler Lake quadrangle, Lisburne phosphorites were found in several distinct thrust sheets in the EMA (Dumoulin and others, 2008). They occur at the same stratigraphic level in all sheets, based on fossil age control and sequence stratigraphic analysis, but differ in thickness and associated lithofacies. Phosphorite layers are thicker, more numerous, and associated with greater amounts of black shale in the Skimo thrust sheet than in the Tiglukpuk thrust sheet to the north. Coeval phosphorites also were reported from thrust sheets south of the Skimo sheet (Porter, 1966; Armstrong and Mamet, 1978) but little lithologic detail is available for these strata. Paleogeographic reconstructions and structural studies indicate that Lisburne strata in the Skimo thrust sheet accumulated in a more distal setting, ~12–17 km seaward of coeval strata in the Tiglukpuk sheet (Dumoulin and others, 2008); equivalent rocks in thrust sheets south of the Skimo sheet were deposited still further offshore, but precise lateral displacements for these thrust sheets have not yet been determined.

The western part of the EMA phosphorite belt is in rocks of the Ivotuk plate (Young, 2004) and includes occurrences at Mount Bupto and Lisburne Ridge (fig. 5*A*,*B*) in the Howard Pass quadrangle, and in the Ivotuk Hills and Lisburne 1 well in the western Killik River quadrangle (locs. 4–7, figs. 1, 2, 4; table 1). The phosphorite interval here has similar lithofacies, P_2O_5 content, and associated rock types, but is thinner (generally ≤1–3 m thick) and occurs at or just below the top of the Lisburne Group. Granular phosphorites like those that crop out in the Ivotuk Hills (Kelley and Mull, 1995) also occur in the subsurface just to the east in the Lisburne 1 well (Dumoulin and Bird, 2002), which penetrated five imbricated thrust sheets

made up mostly of the Lisburne Group (Cole and others, 1997). We observed granular phosphorites in cuttings ~7–20 m below the top of the Lisburne in four of the five thrust sheets (sheets 1, 2, 4, and 5).

KRA—Western Brooks Range

Lisburne Group phosphorites in the KRA are found mainly in the eastern De Long Mountains and western Misheguk Mountain quadrangles (locs. 1–3, figs. 1, 2; table 1), where they crop out at scattered localities in the Wulik Peaks, Amphitheatre, and Kelly thrust plates (Dumoulin and others, 2004). Phosphatic rocks within this allochthon occur in a zone of organic-rich black shale ≤15 m thick at the top of the Lisburne Group (fig. 4) and consist of layers of ovoid phosphorite nodules as much as 15 cm long (26–31 weight percent P_2O_5; fig. 5*C*) and lenses, typically 10–30 cm thick, of phosphatic limestone grading to granular phosphate rock (2–14 weight percent P_2O_5; fig. 5*D*). Black shale at these localities has as much as 10 weight percent P_2O_5, chiefly as disseminated phosphatic peloids and small nodules. Nodules contain abundant and locally very well-preserved radiolarians (fig. 5*C*), as well as lesser sponge spicules and rare nautiloid(?) fragments. Chemical analyses and thin-section examinations (tables 1, A1) indicate that granular phosphatic strata in the KRA have more nonphosphatic grains (mostly calcareous bioclasts) than equivalent strata in the EMA. Conodonts from phosphatic limestone at several KRA localities are early Chesterian (Dumoulin and others, 2004, 2006a).

Ikpikpuk Well—North Slope

The Ikpikpuk well (loc. 13, figs. 1, 2; table 1) was drilled on the northwestern flank of the Ikpikpuk-Umiat Basin, a large complex sag initiated in Early Mississippian or Devonian time (Dumoulin and Bird, 2001). More than 1,000 m of parautochthonous Lisburne Group strata, ranging in age from Late Mississippian through Permian, were penetrated in this well. Cuttings through a 12-m-thick zone ~990 m below the top of the Lisburne Group (fig. 4; 14,600–650 ft depths) contain grains of calcite-cemented granular phosphorite, texturally identical to those seen elsewhere in the Lisburne, associated with dark mudstone, spiculite, and muddy skeletal packstone. Foraminifers indicate an age of late Meramecian-early Chesterian for these rocks (Dumoulin and Bird, 2001).

Lithologic Features of Phosphorites and Associated Rocks

Phosphorites

Granular phosphorites in the Lisburne Group vary in composition and texture among localities and between (and within) individual beds at a single locality. Most are grainstones, packstones, or rudstones in which virtually all grains are phosphatic (fig. 6*A–F*). Rare beds contain <10 percent nonphosphatic grains, mainly calcareous lithic clasts or bioclasts. The phosphate grains typically are packed loosely and cemented by coarsely crystalline sparry calcite (less commonly, dolomite or silica), but some layers are packed tightly and contain little matrix or cement; these highly compacted samples generally are cemented by phosphate or fibrous chalcedony (fig. 6*A*,*B*,*D*). Lime or phosphatic mud forms the matrix in some samples, and patchy purple fluorite occurs locally. A few phosphorite layers are graded normally, whereas others show reverse grading, or coarse-tail grading (fig. 6*B*,*F*). Bed bases typically are sharp.

Phosphatic particles in the granular phosphorites mainly are peloids, coated grains, and bioclasts that range in size from very fine sand to pebbles (fig. 6*B*). Peloids (structureless phosphatic particles, see Föllmi, 1996) vary from round to elongate to irregular; most are internally featureless but some contain silt- to sand-sized fragments of quartz, carbonate, or organic material (fig. 5*B*). Many of the coated grains have rims made up of either one or a few different-colored phosphatic laminae, but some have thick rims with >10 laminae; color variation may reflect different amounts of organic material in the laminae (fig. 6*B*,*D*). Some coated grains contain internal discordances and appear to be unconformity-bounded coated grains as defined by Pufahl and Grimm (2003). Most coated-grain nuclei are phosphatic peloids, but quartz grains, possible lithic clasts, and bioclasts also were observed (fig. 6*E*). Phosphatic bioclasts chiefly are conodonts and ichthyoliths; phosphatized bioclasts are less common and include crinoid, bryozoan, and brachiopod fragments. Composite grains—aggregates of two or more peloids or coated grains—occur locally (fig. 6*B*,*C*).

Peloids are the dominant phosphatic particle in most Lisburne Group samples, but coated grains are unusually abundant (≥50 percent of all grains) at Lisburne Ridge (western EMA; loc. 5, fig. 1) and near the middle of the phosphatic section at Confusion Creek (eastern EMA; Skimo thrust sheet; loc. 10, fig. 1). Phosphatized bioclasts are a notable component at Tiglukpuk Creek (eastern EMA; Tiglukpuk thrust sheet; 7 km north of loc. 11, fig. 1). Composite grains are most common in the upper part of the phosphatic zone in the Confusion Creek and Skimo Creek sections (locs. 10 and 11, fig. 1).

Complex textural variations occur locally at a microscopic scale in the granular phosphorites. Thin sections indicate that some phosphorite intervals, 1–7 cm thick, which appear homogeneous in outcrop, contain ≥4 distinct layers, 3–10 mm thick (fig. 6*F*). These layers have erosional bases, different matrix compositions (including various proportions of lime and phosphatic mud and calcite, silica, phosphate, and fluorite cement), and different proportions of phosphatic particle types (some layers are dominated by coated grains, others by peloids). Layers also differ in average grain size and type of grading (normal, coarse-tail, or reverse). Boundaries between some layers appear to be truncation surfaces, are marked by burrows or borings and rare truncated grains, and may be

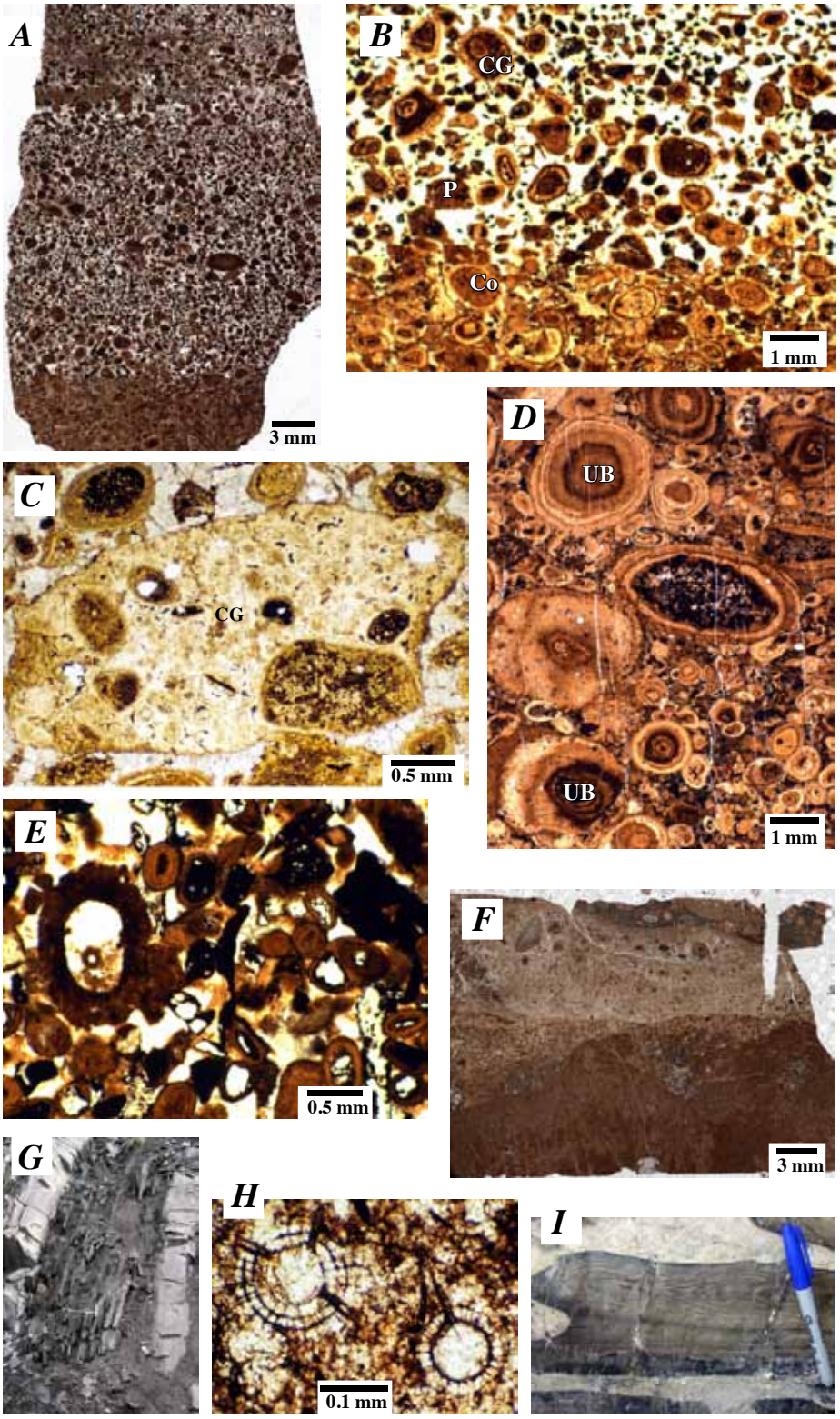

Figure 6. Lithologic features of phosphorites and related rocks in the Lisburne Group; all samples are from EMA. *A* and *F* are thin section scans; *B*-*E* and *H* are photomicrographs; *G* and *I* are outcrop views. *A* and *B*, Phosphorite (19 weight percent P_2O_5) from Monotis Creek (loc. 9, fig. 1), composed of a loosely packed layer with white silica cement above a tightly packed layer with phosphatic cement; *B* shows coarse-tail grading and variety of phosphatic peloids (P), coated grains (Co), and composite grains (CG). *C*, Large composite phosphatic grain (CG) made up of numerous smaller grains, Lisburne Ridge (loc. 5, fig. 1). *D*, Tightly packed phosphorite with phosphatic cement (37 weight percent P_2O_5), Killik River area (loc. 8, fig. 1); prominent grain left of center contains numerous radiolarians (dark spots) and several grains (UB) have internal discordances and appear to be unconformity bounded (Pufahl and Grimm, 2003). *E*, *F*, and *I*, Tiglukpuk Creek (7 km north of loc. 11, fig. 1); *E*, Phosphorite (21 weight percent P_2O_5) in which quartz grains and possible lithic clasts form nuclei for many phosphatic clasts. *F*, Complex phosphorite representing multiple episodes of reworking and redeposition; note the four distinct layers (that differ in composition, grain size, packing, and grading; the light layer near top is graded reversely) bounded by truncation surfaces that may be hardgrounds; phosphatic cement decreases upwards; the small zone of coarser-grained material in the center of the photo likely is a burrow or boring *I*, A chert nodule with laminated (wood-grained) texture. *G*, Black shale interbedded with light-gray-weathering lime mudstone, Skimo Creek (loc. 11, fig. 1). *H*, Carbonate concretion with well-preserved radiolarian tests (replaced by pyrite and calcite) in a matrix of fine-grained carbonate, Akmagolik Creek (10 km east of loc. 11, fig. 1).

hardgrounds (fig. 6*F*). Composite phosphorite intervals are especially abundant in the eastern EMA.

Phosphorite nodules occur in beds and lenses of granular phosphorite and are scattered within, or along, discrete horizons in black shale and lime mudstone. They are largest (3–>15 cm long) and most abundant at several localities in the KRA and also are notable at the tops of granular phosphorite beds at Skimo and Confusion Creeks. Some nodules have internal textures similar to those of granular phosphorites and consist of closely packed phosphatic peloids cemented by calcite or phosphate. Others are made mostly of massive phosphate, complexly intergrown with chalcedony or calcite, and may contain abundant bioclasts (chiefly radiolarians) and (or) minor siliciclastic or carbonate detritus (fig. 5*C*).

Radiolarians and lesser sponge spicules are important constituents of both granular and nodular phosphatic rocks in the Lisburne Group. Thin-section observations indicate that radiolarian tests, commonly coated with probable organic matter and (or) replaced by pyrite, occur in phosphatic nodules in the KRA (fig. 5*C*) and in phosphatic peloids and both rims and cores of coated grains (fig. 6*D*) at numerous localities in the EMA (table 1).

Black Shales

Fissile black shales (fig. 6*G*) are interbedded with phosphorites at virtually all known phosphorite localities in the EMA and KRA. Shales are mildly to moderately calcareous and organic-rich (1.34–20.2 weight percent C_{org}) and some are phosphatic (0.54–11.54 weight percent P_2O_5; 5 samples have >7 weight percent P_2O_5). Shale intervals are 0.1–5 m thick, laminated in thin section and outcrop, and generally lack evidence of bioturbation, although a few samples contain irregular concentrations of silt that could reflect some microbioturbation. Signs of floccule ripple bedding (Schieber and others, 2007) are absent. At Confusion Creek (loc. 10, fig. 1), shales contain 5–50 volume percent elongate (flattened?) clasts of carbonate and (or) phosphate; carbonate clasts (made mostly of micrite; 0.2–3 mm long) and disseminated micrite and calcite silt increase upward through the section. Carbonate clasts were not seen in shales at other localities, but scattered, fine-grained carbonate is common; dolomite euhedra are notable in shale samples from Mount Bupto and Lisburne Ridge (locs. 4, 5, fig. 1). Phosphatic peloids, ubiquitous in shale beds interbedded with phosphorites at all localities, are mostly ovoid to irregular and are 0.1–0.6 mm in diameter. They typically are disseminated, but locally are concentrated into layers and lenses a few millimeters thick, making up 1–30 volume percent of most shale samples. Rare bioclasts in shale beds include phosphatic skeletal fragments, calcareous and siliceous spicules, radiolarians, ostracodes, and possible calcispheres.

Carbonate Rocks and Chert

Lime mudstone is the main carbonate rock type interbedded with phosphorites in the eastern EMA (Chandler Lake quadrangle), whereas bioclastic supportstone predominates in the KRA. Carbonate rocks associated with phosphorite in the western EMA (Howard Pass and western Killik River quadrangles) are dolomitized extensively, but include protoliths ranging from bioclastic packstone to mudstone. Calcareous strata intercalated with phosphorite in the Ikpikpuk well also range from bioclastic (in part spiculitic) packstone to mudstone.

In the eastern EMA, lime mudstone to wackestone, intercalated with phosphorite, forms laterally continuous beds a few centimeters to >1.5 m thick (fig. 6*G*), as well as subordinate round to ellipsoidal concretions 0.1–1.3 m in maximum diameter (fig. 6*H*). Most beds are finely laminated, but a few appear partly bioturbated. Micritic clasts and phosphatic peloids, like those in the black-shale interbeds, occur locally, and many samples contain abundant radiolarians (fig. 6*H*) and (or) calcareous or siliceous sponge spicules. Goniatite cephalopods were found at several localities (Gordon, 1957; Dumoulin and others, 2008).

Carbonate associated with phosphorite in the KRA is mainly thin- to medium-bedded bioclastic supportstone and lesser wacke-packstone in intervals 0.3–>1.0 m thick. Some beds contain abundant phosphatic grains (typically 10–30 volume percent, locally as much as 80 volume percent), in places grading into granular phosphate rock. Bioclasts in these strata are brachiopod and pelmatozoan fragments with lesser ostracodes, gastropods, and coral debris (fig. 5*D*).

Bored bioclasts are a notable component of carbonate beds in the phosphorite zone of the KRA and western EMA and a less common constituent of equivalent strata in the eastern EMA. Borings occur chiefly in brachiopod shells in supportstone and phosphatic limestone, are 10–40 μm in diameter, as much as 0.4 mm long, and of unknown origin; most borings are filled with dark, noncarbonate mud, but some contain phosphatic material.

Biofacies of conodont faunas from lime mudstones intercalated with phosphorites in the EMA and from phosphatic limestones in the KRA indicate that most assemblages accumulated as distal winnows into deeper-water settings (Dumoulin and others, 2006a, 2008). A radiolarian-rich carbonate concretion in the eastern EMA (loc. 9, fig. 1) contains a conodont assemblage characteristic of a deep-water, poorly oxygenated setting (table 1; Dumoulin and others, 2008).

Black to dark gray chert forms local, decimeter-thick concretions and lenses in phosphorite-bearing sections throughout the EMA. Many samples contain abundant sponge spicules and (or) radiolarians. In some occurrences, chert is complexly intergrown with, or partly to completely replaces, calcite or dolomite. Chert lenses in the western EMA retain well-preserved textures of skeletal packstone; bioclasts include pelmatozoans, bryozoans, brachiopods (locally bored), and nautiloids, as well as spicules and radiolarians. Several cherty layers in the eastern EMA are laminated concentrically (fig. 6*I*); different proportions of chert, organic material, and fine-grained carbonate define the laminae.

Lithofacies Associations

Granular phosphorites in the eastern EMA are interbedded with black shale and lime mudstone to wackestone. Coarsening-upward sequences, 0.5–1.5 m thick, of shale grading up into lime wackestone and capped by granular phosphorite or phosphate rock, occur at Confusion and Skimo Creeks (fig. 7). Sections in the western EMA and KRA contain dolostone and bioclastic supportstone, respectively, in place of lime mudstone, but are otherwise similar to those in the eastern EMA. Exact compositions of beds in the Ikpikpuk well are less certain, but detailed study of cuttings composited over 10-ft intervals suggests similarities to lithofacies in the eastern EMA. Phosphorite nodules are most abundant near or at the tops of granular phosphorite layers; in the KRA, they also are notable in black shale layers.

Less-Phosphatic Strata

Intervals within the Lisburne Group, mostly ≤2 m thick, that contain minor to moderate amounts of phosphate, but no true phosphorites, have been found at 50 outcrop and subsurface localities in the western and central Brooks Range (fig. 2; table 2). These rocks typically contain ≤30 volume percent phosphatic grains visible in thin section, abundant phosphatic grains and (or) phosphatized bioclasts in conodont sample residues, and 1–6 weight percent P_2O_5 where chemical analyses are available. Most such strata appear to be coeval with the late Meramecian-early Chesterian Lisburne Group phosphorites, but others definitely are older or younger.

Less-phosphatic intervals that likely are coeval with the main episode of Lisburne Group phosphorite formation have been found in drowned platform facies near the top of the Lisburne in the western Brooks Range (Wolverine plate of EMA; KRA) and in slope and basinal facies of the Kuna Formation in the western and west-central Brooks Range (Red Dog and Key Creek plates of EMA; PCA). Intervals younger than the main Lisburne Group phosphorites occur mainly at the top of shallow-water sections of the Lisburne in the central Brooks Range (EMA); conodont data and regional correlations indicate that some of these are late early Chesterian-earliest Morrowan but others are early Morrowan (Early Pennsylvanian) or younger. Phosphatic intervals of Early Mississippian (Osagean) age are less common, but have been found in basinal strata in the western Brooks Range (PCA, EMA?) and in the lower part of the Lisburne Group in the Ivotuk Hills and the Lisburne well (locs. 6, 7, fig. 1; Dumoulin and Harris, 1993). Phosphatic grains in all of these sections mainly are sand-sized peloids and phosphatic and phosphatized bioclasts disseminated in skeletal supportstones (platform facies) or in shales and carbonate turbidites (basinal facies). Coated phosphatic grains and (or) millimeter-scale phosphatic nodules occur in some younger samples. Glauconite is a notable component of many of the younger phosphatic intervals and of Osagean phosphatic strata in the Ivotuk Hills area (Dumoulin and Bird, 2002); it occurs chiefly as scattered, sand-sized grains mixed with phosphate particles in skeletal supportstone and makes up as much as 30–40 volume percent of some samples.

Whole-Rock Geochemistry

Black Shales

We obtained whole-rock geochemical data (tables 3, A1) for 17 samples of Lisburne Group black shales interbedded with phosphorite including 13 samples from 7 locations in the EMA and 4 samples from 3 locations in the KRA; 6 of the EMA samples are from a single section through the phosphorite-bearing interval at Confusion Creek. Factor analysis of the whole-rock data (table A2) shows four main factors, which in decreasing order of abundance are marine, hydrothermal, detrital, and phosphate. Compared to contemporaneous black shales of the Kuna Formation (Slack and others, 2004a), the phosphorite-related black shales in our present sample set typically are less siliceous and more calcareous and phosphatic. Phosphorite-associated black shales also are characterized by higher C_{org} values, mostly in the range of 4–6 weight percent, and include three very C_{org}-rich (>15 weight percent) samples from the Ivotuk Hills and Lisburne Ridge. Rock-eval analysis of a black shale from Lisburne Ridge yields a C_{org} value of 20.2 weight percent. Molar C_{org}/molar P ratios vary widely, from 1.56 to 116, with a median of 25.3. For comparison, molar C_{org}/molar P ratios of 42 black shales of the Kuna Formation (Slack and others, 2004a) range from 1.37 to 396, with a similar median of 22.8. With few exceptions, manganese concentrations in the phosphorite-related black shales are very low (≤0.01 weight percent MnO) as are those in black shales of the Kuna Formation (Slack and others, 2004a). C_{org}-rich (>4 weight percent) Lisburne black shales are depleted in S compared to typical oxidized marine sediments (fig. 8); data for these low-S samples plot mainly within the field of sulfate- and iron-limited sediments. An important caveat here is that all of these samples come from surface outcrops or talus, not from drill cores as is preferred for such analyses of black shales.

Noteworthy in many of our samples are very high contents of Cr and V, ranging up to 1,690 ppm and 2,831 ppm, respectively. These maximum values are much higher than those in the Kuna Formation (Slack and others, 2004a); they are within the upper range of concentrations of Cr and V reported for black shales worldwide (for example, Desborough and Poole, 1983; Yudovich and Ketris, 1997; Coveney, 2003) and for modern organic-rich sediments (Brumsack, 2006). Data for both Cr and V covary broadly with C_{org} (fig. 9*A*,*B*), but no trends exist with respect to Al_2O_3 or K_2O. Molybdenum, which varies from 15.8 to 135 ppm in the black shales (table 3), shows broad correlations with both C_{org} and S (fig. 9*C*,*D*). Other metals that are concentrated locally in the phosphorite-related black shales include Zn (up to 4,670 ppm),

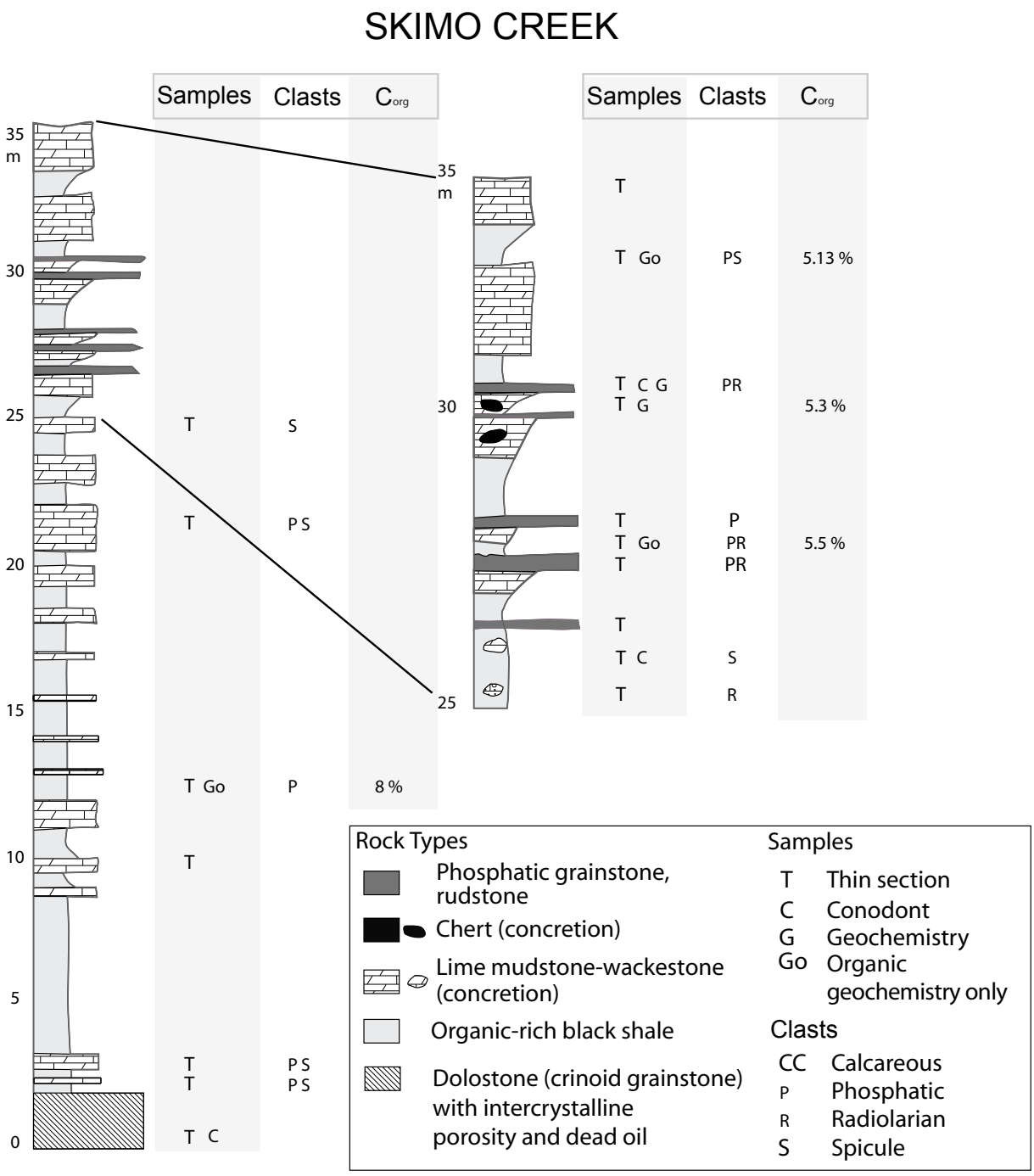

Figure 7. Detailed stratigraphy of the phosphorite-bearing interval at Confusion and Skimo Creeks (locs. 10, 11, figs. 1, 2). Phosphorite beds are interbedded with organic-rich black shale and fine-grained radiolarian and spiculitic limestone. C_{org} values are shown only for shale samples. See figure 14 for a spectral gamma-ray profile of the Skimo Creek section.

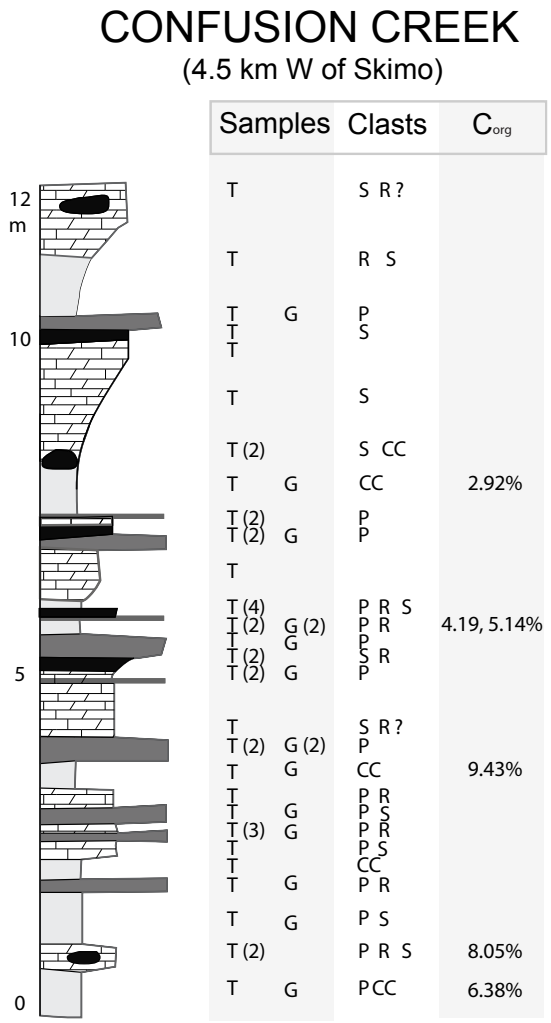

Figure 7. Detailed stratigraphy of the phosphorite-bearing interval at Confusion and Skimo Creeks (locs. 10, 11, figs. 1, 2). Phosphorite beds are interbedded with organic-rich black shale and fine-grained radiolarian and spiculitic limestone. C_{org} values are shown only for shale samples. See figure 14 for a spectral gamma-ray profile of the Skimo Creek section.—Continued.

Ni (up to 551 ppm), Cu (up to 312 ppm), U (up to 118 ppm), As (up to 78 ppm), Se (up to 111 ppm), Cd (up to 142 ppm), Ag (up to 43.5 ppm), and Tl (up to 12.3 ppm).

With few exceptions, data for the calculated marine fractions of Mo versus those of V and Cr for the black shales plot above the sulfate-reducing lines (fig. 10), consistent with deposition under suboxic conditions (see Perkins and others, 2008). These diagrams ignore possible contributions of the biogenic fraction, which for Mo, V, and Cr are negligible (Piper, 1994). Several samples, all from the KRA, plot on or close to these lines; these samples also have anomalously high contents of MnO (0.10–0.19 weight percent) relative to the other phosphorite-related black shales (<0.01 weight percent). A plot of the marine fraction of Mo versus Re (fig. 11) indicates that samples plot within the suboxic field, except for four black shales from the EMA. All of these data reflect paleoredox conditions in bottom waters, with limited influence from authigenic reactions involving pore fluids (Piper and Calvert, 2009, and references therein).

Data for REE in the phosphorite-related black shales are broadly similar with respect to overall patterns and magnitude of Ce anomalies (fig. 12*A*). For most samples, shale-normalized data show consistent trends with abundance levels (excluding Ce) of ~0.5 to ~5x Post Archean Average Shale (PAAS), and middle REE (MREE) < heavy REE (HREE). This range of REE abundance levels mainly reflects relative proportions of phosphate, terrigenous detrital material, and biogenic silica. Characteristic are large, negative Ce anomalies (calculated Ce/Ce*; table 3) of 0.16–0.34, and no Eu anomalies. Smaller negative Ce anomalies (Ce/Ce*=0.46–0.78) occur in three samples, all of which are from the KRA; data for two of these samples also fall off the expected inverse trend between P_2O_5 and Ce/Ce* (fig. 13*D*).

Phosphorites

Whole-rock analyses were obtained for 24 granular phosphorites from 13 locations in the EMA and 3 phosphorite nodules from 2 locations in the KRA; 9 samples are from a single section through the phosphorite interval at Confusion Creek. Major differences in bulk composition among the granular phosphorites (table 3) mainly reflect variations in the amount of silica cement and the amount and type of carbonate cement, including relative proportions of calcite and dolomite. Compared to the black shales, the phosphorites typically contain less C_{org}, although one

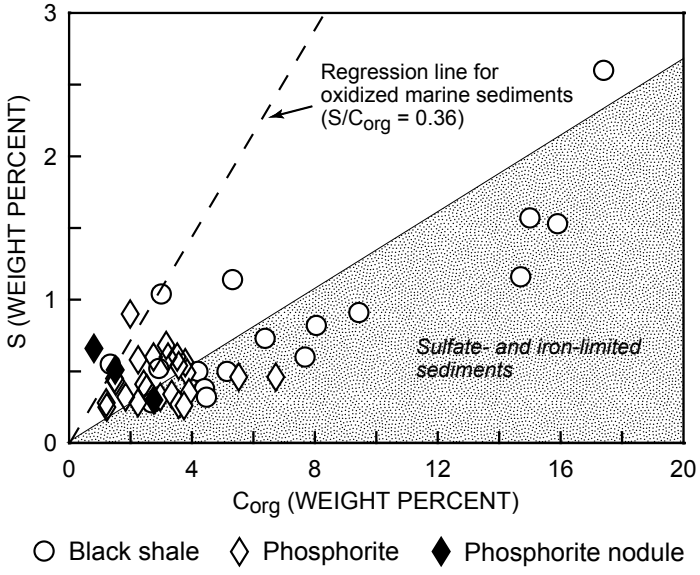

Figure 8. Total organic carbon (C_{org}) versus S plot, showing that most Lisburne Group phosphorite-related black shales have low S/C_{org} ratios, falling within the field of sulfate- and iron-limited sediments, similar to black shales of the Kuna Formation (Slack and others, 2004a).

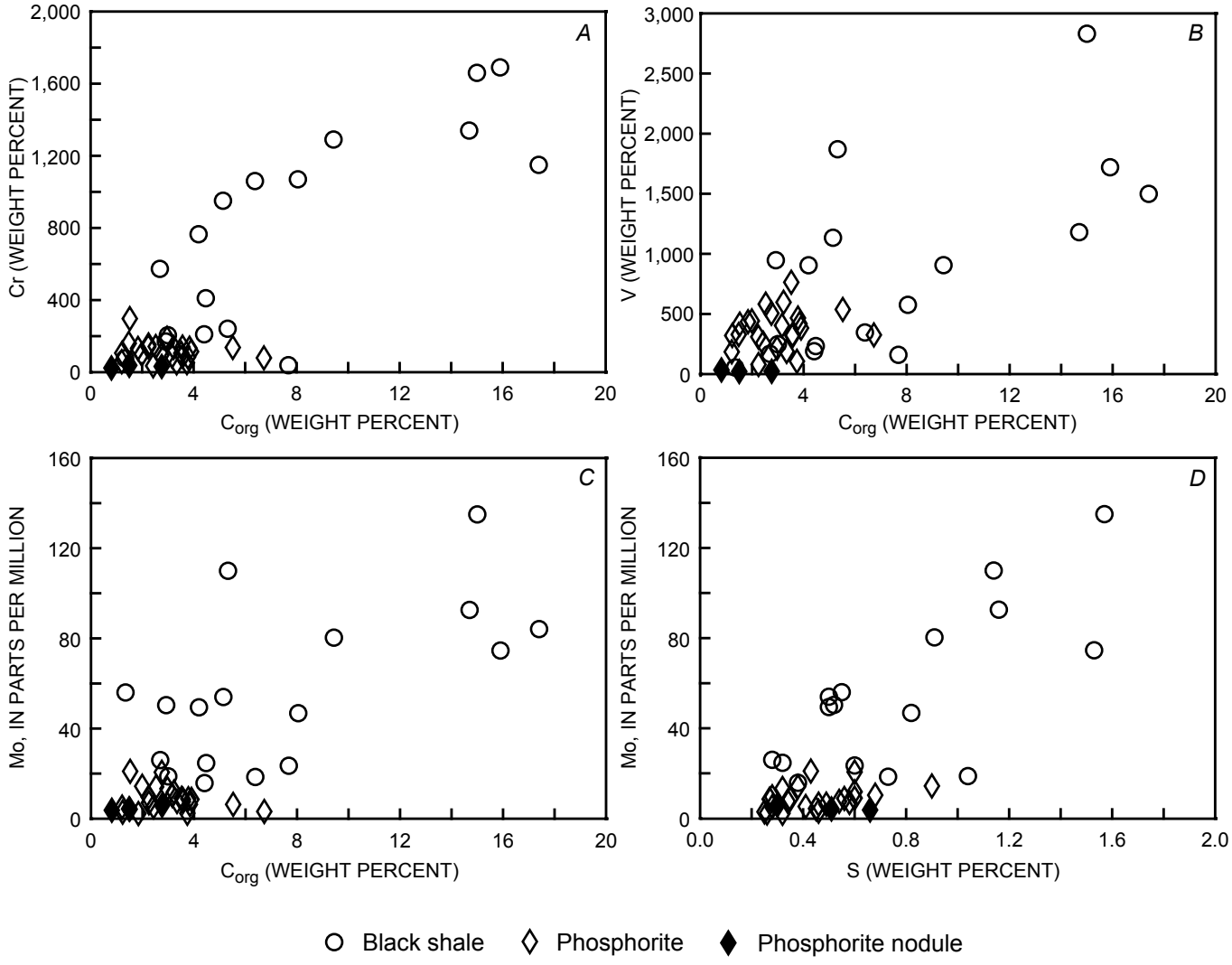

Figure 9. Binary trace-element plots. *A*, C_{org} versus Cr. *B*, C_{org} versus V. *C*, C_{org} versus Mo. *D*, S versus Mo. C_{org}, total organic carbon.

sample has 6.7 weight percent. As a result of these generally low C_{org} contents, metal concentrations that occur in the black shales mostly are absent from the phosphorites (fig. 9), except for locally elevated V (up to 763 ppm). Factor analysis of the whole-rock data (table A3) shows four main factors, which in decreasing order of loadings likely are phosphate, LREE+Y, detrital, and marine components.

Abundances of some trace elements covary with P_2O_5. Such trends are shown by F and Sr, and to a lesser extent by U (fig. 13*A*–*C*). The three phosphorite nodules are distinctive in having much higher Sr concentrations than do the granular phosphorites (fig. 13*B*). Shale-normalized REE data show overall abundances (excluding Ce) of ~0.4 to 15x PAAS, MREE < HREE, uniformly large, negative Ce anomalies (Ce/Ce*) of 0.08–0.19, and no Eu anomalies (fig. 12*B*). The three phosphorite nodules, in contrast, have much smaller negative Ce anomalies of 0.61–0.79 (figs. 12*C*, 13*D*).

Discussion

Depositional Setting

Lisburne Group phosphorites are intercalated with lithofacies, such as organic-rich black shale and radiolarian-bearing lime mudstone and chert, that contrast strongly with those of underlying (and in the eastern EMA and Ikpikpuk well, overlying) platformal-carbonate successions (fig. 4). This lithologic change marks an abrupt shift in the depositional regime of the Lisburne Group linked to widespread drowning of carbonate platforms (Dumoulin and others, 2004, 2008; Whalen and others, 2006), primarily those adjacent to the Kuna Basin (fig. 2).

We interpret granular phosphorites in the Lisburne Group as a hybrid of condensed and allochthonous phosphate (Föllmi, 1996). Complex textures of individual phosphatic

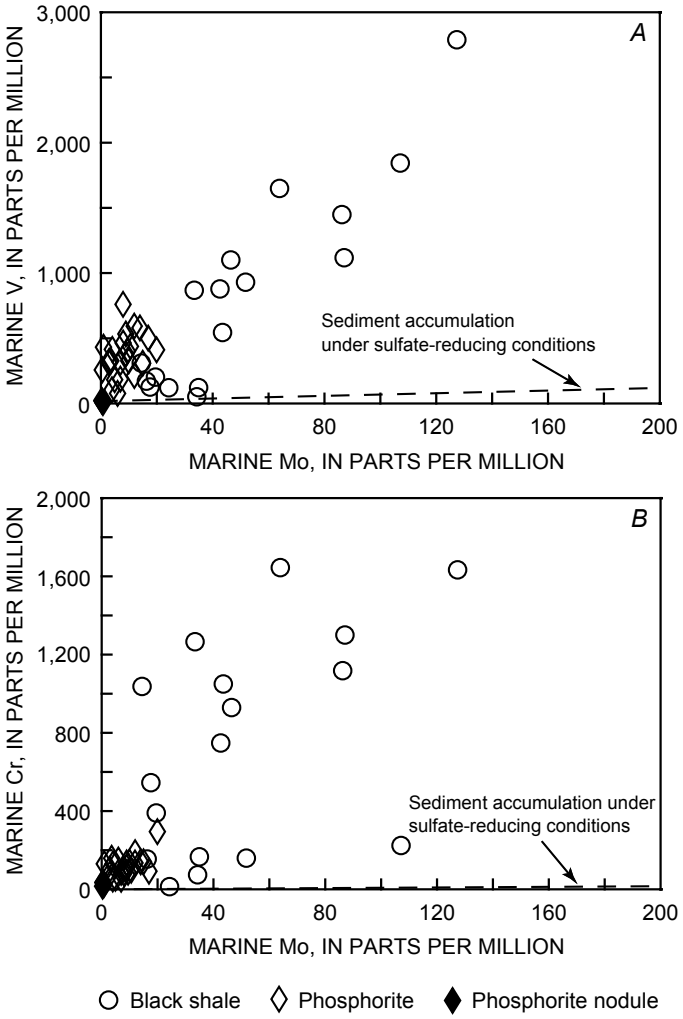

Figure 10. Binary plots discriminating suboxic denitrifying depositional conditions from sulfate-reducing conditions (dashed lines). *A*, marine Mo versus marine V. *B*, marine Mo versus marine Cr. Marine fractions of Mo, V, and Cr were determined by using the methods of Perkins and others (2008).

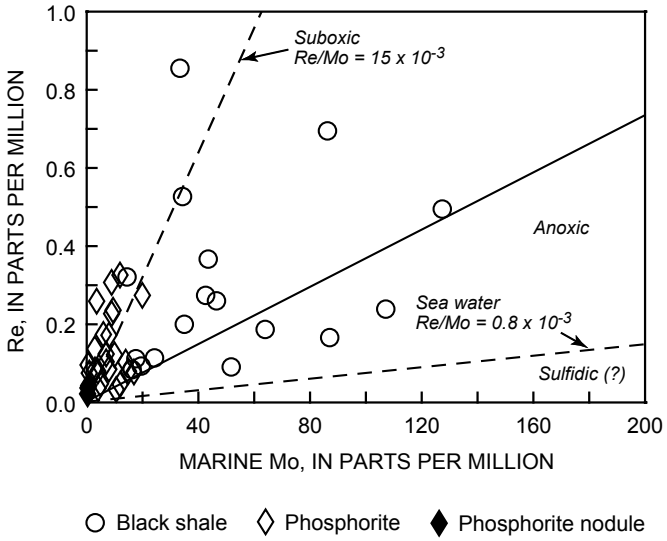

Figure 11. Binary marine Mo versus Re plot discriminating suboxic, anoxic, and euxinic depositional settings. Data for Re (total concentrations) are considered equivalent to the marine fraction (see text). Fields are from Ross and Bustin (2009).

grains, such as composite grains and unconformity-bounded coated grains (fig. 6*B*–*D*), as well as the co-occurrence of peloids and coated grains within individual phosphorite layers (figs. 5*B*, 6*B*), reflect multiple episodes of phosphogenesis and sedimentary reworking during times of stratigraphic condensation (for example, Pufahl and Grimm, 2003). Composite phosphorite intervals, internally bounded by truncation surfaces that may be hardgrounds (fig. 6*F*), further support this model. Sharp bed bottoms and local grading (fig. 6*B*,*F*), however, suggest redeposition of phosphatic particles into deeper water settings by storms or gravity flows; many Lisburne Group phosphorites and phosphatic limestones show some evidence of redeposition. Some composite phosphorites may be amalgamated allochthonous beds.

In the Skimo thrust sheet of the EMA (locs. 9-11, fig. 1; table 1), Lisburne Group phosphorites are interbedded with >30 m of black shale and fine-grained limestone (fig. 7) that accumulated as hemipelagic strata in an outer-ramp to basinal environment (Dumoulin and others, 2008). Conodont biofacies, a limited, largely pelagic fauna, and scarce evidence of bioturbation all suggest a deep-water, poorly oxygenated setting. Rare benthic faunal elements in these lithologies appear transported. Thin concentrations of calcareous clasts in shale and limestone are most likely distal-storm or gravity-flow deposits. Phosphatic rocks in this thrust sheet also are at least partly allochthonous, although local phosphate cement indicates some in-place phosphatization. The source of most phosphorites likely was no shallower than the middle ramp because radiolarians are abundant, both within and among phosphatic grains, and because definitively shallow-water bioclasts are absent.

A spectral gamma-ray profile (fig. 14) through the shale and phosphorite unit at Skimo Creek (loc. 11, fig. 1) provides additional support for condensed sedimentation. High gamma-ray response occurs throughout the unit and suggests that these facies underwent considerable condensation, probably due to sediment starvation and development of phosphatic hardgrounds (Loutit and others, 1988; Föllmi, 1996; Lanci and others, 2002). U dominates the gamma-ray response, with little of the signal originating from K or Th. Uranium enrichment of phosphorites and black shales is corroborated by our geochemical analyses (fig. 13*C*) and likely reflects the suboxic, reducing depositional setting interpreted for these strata. Although the identification of uranium-enriched intervals is not unequivocal evidence of condensation (Posamentier and Allen, 1999), condensed sections typically show high

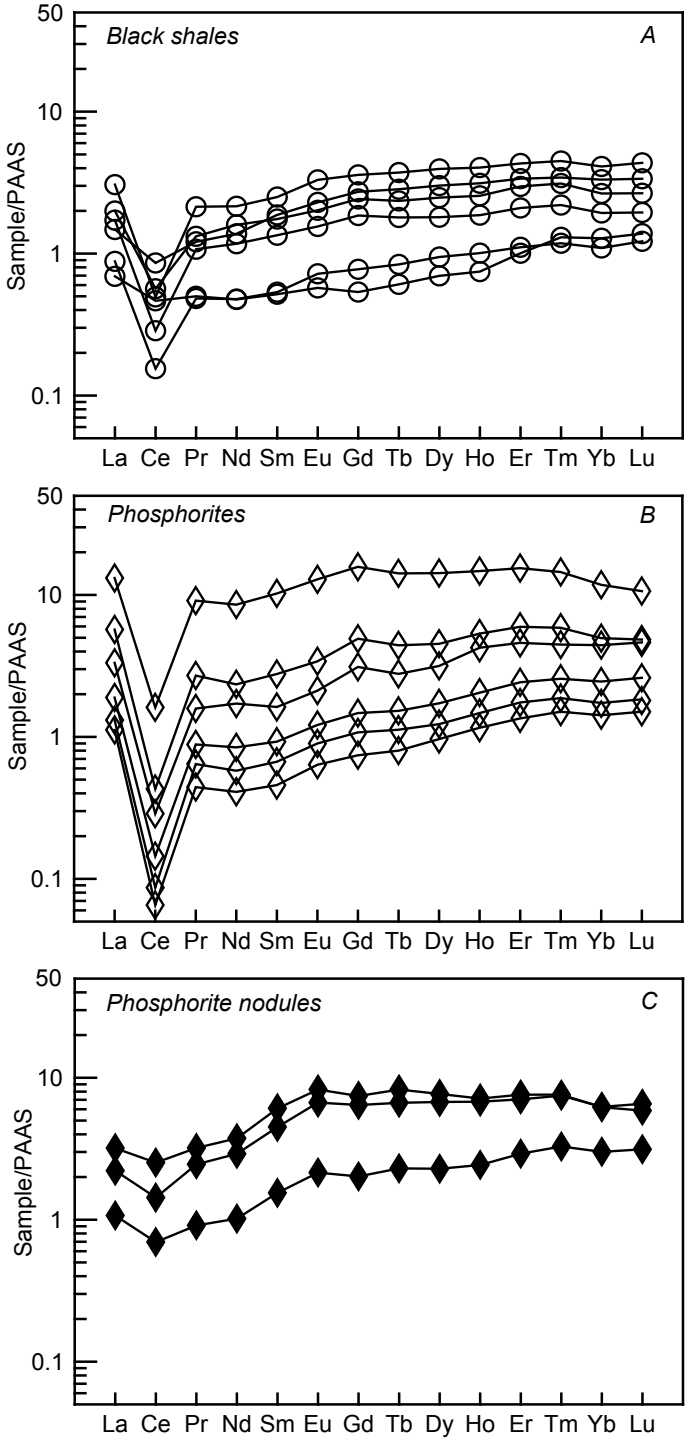

Figure 12. Shale-normalized REE plots showing representative data. *A*, Black shales; *B*, phosphorites; *C*, phosphorite nodules. Normalizing values from PAAS (Taylor and McLennan, 1985).

gamma-ray response (Creaney and Peasey, 1993; Lanci and others, 2002).

In the Tiglukpuk thrust sheet of the eastern EMA (table 1), western EMA, KRA, and Ikpikpuk well, phosphorites also formed through both condensation and redeposition and are associated with organic-rich shale and (or) radiolarian or spiculitic lime mudstone and chert. However, the interval containing these distinctive lithologies generally is thinner (3–20 m versus 30 m) and has more bioclastic supportstone and fewer discrete phosphorite beds. Radiolarians and sponge spicules are abundant in these phosphorites, but a more varied biota occurs in the carbonate supportstone interbeds. Rounded to angular quartz grains and quartzose lithic clasts form nuclei for many coated grains in the Tiglukpuk phosphorites (fig. 6*E*). These differences suggest somewhat shallower settings on the middle to outer ramp. Structural studies indicate that strata in the Tiglukpuk thrust sheet accumulated ~12–17 km landward of coeval strata in the Skimo thrust sheet (Dumoulin and others, 2008); if the slope of the Lisburne ramp was ~0.15–0.25° (Burchette and Wright, 1992), these distances imply a water-depth differential of 35–75 m between the two sections. It is likely that phosphorites in the western EMA, KRA, and Ikpikpuk well also were deposited closer to land (further upramp) than those in the Skimo thrust sheet.

In the KRA and western EMA, phosphorites occur at or very near the top of the Lisburne Group (fig. 4) and formed during final drowning of the Lisburne carbonate platform. Shallow-water carbonate deposition never resumed in these areas during Paleozoic time. Phosphorites in the eastern EMA and the Ikpikpuk well, however, are overlain by >100 m, and nearly 1,000 m, respectively, of latest Mississippian and younger Lisburne Group strata, indicating that platform drowning associated with phosphatization in these areas was temporary. Final drowning of the Lisburne carbonate platform occurred during the Early Pennsylvanian (Morrowan) in the central Brooks Range (Dumoulin and others, 2008), but did not take place until the Early Permian in the Ikpikpuk-Umiat Basin (Dumoulin and Bird, 2001).

Evidence for Upwelling

Paleontologic and sedimentologic data are consistent with the hypothesis that Lisburne Group phosphorites formed as part of a nutrient-rich, upwelling regime (Dumoulin and others, 2004, 2008). Abundant radiolarians within the phosphorites, as well as within associated limestone, shale, and chert, may be analogous to modern plankton accumulations in high-productivity upwelling zones. Faunal shifts in the Lisburne Group provide additional evidence for nutrient-rich conditions during phosphatization. In the Skimo Creek section, 200 m of middle- to inner-ramp carbonate strata that underlie the phosphorite and black shale interval show a clear faunal and lithologic progression indicative of increasing eutrophication (for example, Caplan and others, 1996): coralline biotas are succeeded by faunas that lack corals but contain algae and foraminifers, which are in turn overlain by pelmatozoan- and

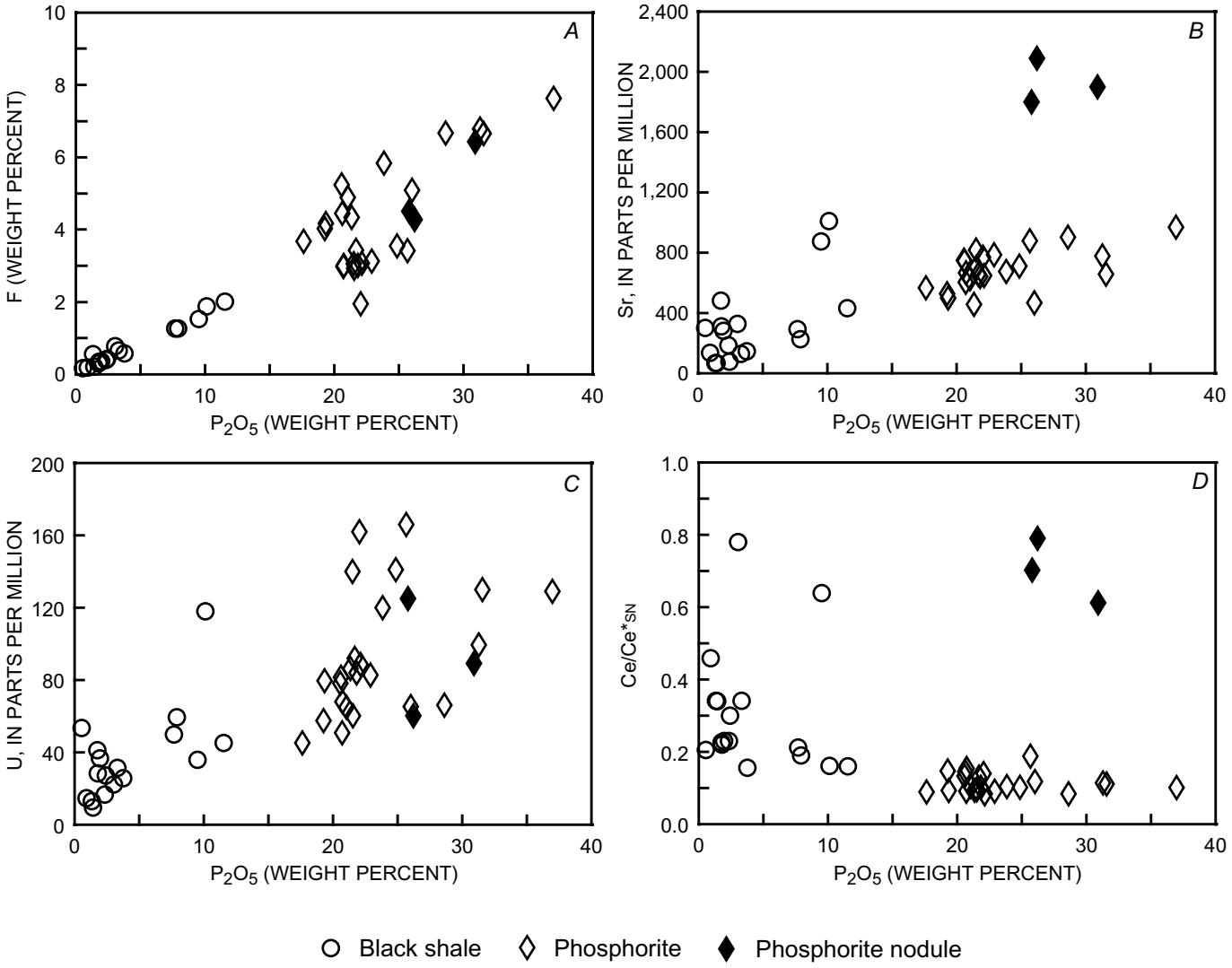

Figure 13. Binary P_2O_5 plots. *A*, P_2O_5 versus F; *B*, P_2O_5 versus Sr; *C*, P_2O_5 versus U; *D*, P_2O_5 versus Ce/Ce*. Ce/Ce* is the calculated Ce anomaly, relative to PAAS; see table 3 headnote for formula used.

bryozoan-rich assemblages. Calcareous peloids and micritized grains become less abundant upward and are absent from the pelmatozoan- and bryozoan-dominated rocks. A mirror image of this succession is seen in 100 m of ramp carbonate strata that overlie the phosphatic zone. Less detailed faunal studies suggest that similar patterns characterize other Lisburne Group sections that contain phosphorites.

Occurrences of organic-rich shale and multiple beds of granular phosphorite also suggest a setting with high productivity (for example, Parrish, 1982). Final drowning of the Lisburne carbonate platform in the western Brooks Range, and its penultimate drowning in the central Brooks Range (fig. 4), were synchronous with phosphatization associated with suboxic conditions near the upwelling-induced oxygen minimum zone; thus, the Lisburne platform drowning likely was due, at least partly, to nutrification produced by upwelling (Dumoulin and others, 2004, 2008; Whalen and others, 2006). High productivity also has been linked to metallogenesis in the Red Dog Zn-Pb-Ag district (fig. 1), which is approximately coeval with the major episode of phosphogenesis in the Lisburne Group. Abundant organic carbon in host black shales of the Kuna Formation there served as an important reductant during mineralization (Kelley and others, 2004b), and biosiliceous cap rocks may have focused mineralizing fluids in the shallow subsurface (Slack and others, 2004a).

Carbon-Sulfur Relationships

The low C_{org}/S ratios of the black shales (fig. 8) could reflect surficial weathering, nonmarine deposition, or an iron-poor provenance (Slack and others, 2004a, and references therein). Given the absence of extensive weathering

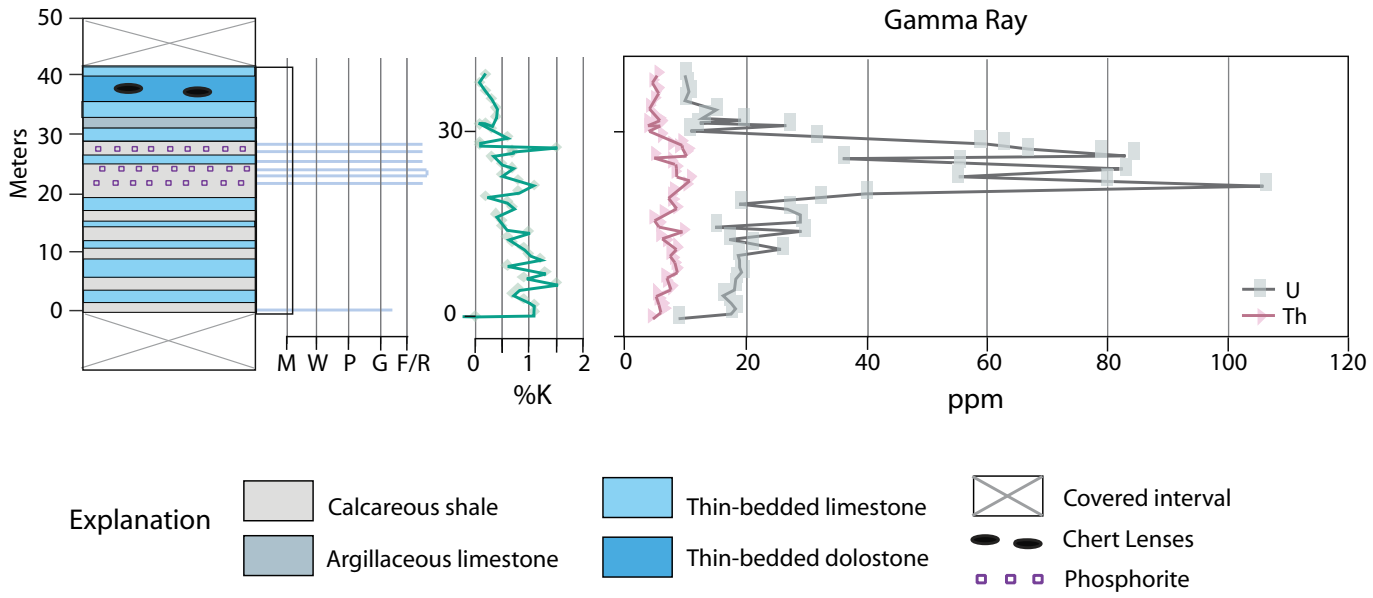

Figure 14. Lithofacies and spectral gamma-ray response of the shale and phosphorite unit (~30 m thick) at Skimo Creek (loc. 11, fig. 1). M, mudstone; W, wackestone; P, packstone: G, grainstone; F/R, floatstone/rudstone. To the right of the lithologic column are quantitative spectral gamma-ray data illustrating percent K and ppm U and Th. Shales in the lower 20 m of the unit have slightly elevated K contents, reflecting an abundance of clay minerals. Elevated U contents in the upper 10 m reside mainly in phosphorites (see fig. 13*C*).

of our samples, selective oxidation of iron sulfides is considered unlikely. Nonmarine deposition is precluded, based on widespread occurrence of marine fauna in the sampled sections (Dumoulin and Harris, 1993; Dumoulin and others, 2006a, 2008). As a result, we infer that an iron-poor sedimentary provenance is the most reasonable explanation for S-deficiency in the Lisburne Group black shales, as in the interpretation of Slack and others (2004a) for black shales of the correlative Kuna Formation (avg Fe/Ti=6.34; n=49). This model is supported by the low average Fe/Ti ratio of 5.12 for 17 black shales of the Lisburne Group, compared to the ratio of 10.5 for the North American Shale Composite (Gromet and others, 1984).

Element Trends and Mineralogical Residence

Trends between some elements in the black shales and phosphorites allow for interpretations of mineralogical residence of the elements. Broad covariance of both Cr and V with C_{org} (fig. 9*A*,*B*) suggests residence mainly in organic matter (for example, Algeo and Maynard, 2004), whereas the lack of trends with respect to Al_2O_3 or K_2O (not shown) argues against a clay-mineral host (cf. Peacor and others, 2000). Trends between Mo and C_{org} and S (fig. 9*C*,*D*) imply a dual residence of Mo in organic matter and pyrite (Ripley and others, 1990; Algeo and Lyons, 2006). Mineralogical hosts of Zn, Cu, Ag, As, Se, Cd, and Tl concentrations in the black shales are unknown, but likely are in both organic matter and sulfides (Slack and others, 2004a, 2004b, and references therein). High contents of Se and Cd that characterize these strata (tables 3, A1) may present environmental problems due to the toxicity of such elements, in elevated concentrations, to animals and people (for example, Piper and others, 2000).

Among the phosphorites, the covariance of P_2O_5 and F (fig. 13*A*) is consistent with fluorapatite and francolite (carbonate fluorapatite) being the dominant host minerals for both components. Data points that fall off this trend, and others involving Sr and U (fig. 13*B*,*C*), may reflect dilution by other phases, or in the case of anomalously high values, enrichment during diagenesis. The latter explanation is favored for a phosphorite sample that contains 1,030 ppm Y and 517 ppm La, which could record the presence of one or more discrete Y- and (or) REE-rich minerals, such as xenotime, monazite, and bastnaesite (Vallini and others, 2002; Baturin and Dubinchuk, 2005).

Redox Conditions during Sedimentation

Myriad studies have used whole-rock geochemistry to evaluate the redox state of bottom waters and pore waters during marine sedimentation. The focus of many such studies has been on black shales, utilizing data for a variety of components including Mn, C_{org}, S, and the redox-sensitive trace elements V, Cr, U, Ni, Mo, Re, and Ce (for example, Rimmer, 2004; Piper and others, 2007; Algeo and Maynard, 2008; Ross and Bustin, 2009). Paleoredox conditions of phosphorite deposition have been investigated chiefly through the use of

shale-normalized REE patterns, especially the nature and magnitude of Ce anomalies (for example, McArthur and Walsh, 1984; Piper and others, 1988; Watkins and others, 1995; Baturin, 2005; Daessle and Carriquiry, 2008). Early paleoredox studies of black shales typically produced conflicting or equivocal results, in many cases because the whole-rock analyses were not screened to use data selectively for the marine fraction and to exclude the terrigenous and biogenic fractions (Piper, 1994, 2001; Perkins and others, 2008). In the present study, we adopt this newer approach and use calculated marine fractions of selected elements in evaluating paleoredox conditions during black-shale and phosphorite deposition within the Lisburne Group. It is important to note here that the biogenic fractions for V, Cr, and Mo are quantitatively unimportant, constituting less than a few parts per million each based on analogy with compositions of modern marine plankton (Piper, 1994); thus, we have not applied correction factors to our data for any biogenic fraction that may be present. For Re, the total (uncorrected) concentration is used because the terrigenous fraction of this element is less than 0.5 ppb based on data for average continental crust, and the biogenic fraction likely is negligible given the very low Re/Mo ratios of about 10^{-2} to 10^{-4} that characterize black shales elsewhere (Crusius and others, 1996); hence, the marine fraction of Re in our samples is considered equivalent, within analytical uncertainty, to the total concentration. Significantly, the redox conditions inferred here, based on marine fractions of V, Cr, Mo, and Re, lack major influence from pore fluids during diagenesis because accumulation of high contents of these hydrogeneous elements (for example, V) requires renewal of bottom waters from overlying seawater (Piper and Calvert, 2009), a process that is not quantitatively important in subsurface pore fluids.

Geochemical analyses of the phosphorite-related black shales suggest deposition under suboxic, denitrifying conditions. Evidence for this redox setting is provided by high V/Mo and Cr/Mo ratios (all marine fractions) of most samples (fig. 10), based on the destabilization of aqueous V- and Cr-bearing species within denitrifying regions of modern oxygen-minimum zones (Piper, 2001; Sageman and others, 2003). Similarly, the generally high Re/Mo ratios (fig. 11) reflect preferential reduction of Re, relative to Mo, in suboxic bottom waters (Crusius and others, 1996). Also significant are the high Cr+V marine fractions (MF), showing a mean of 1,572 ppm, with most samples having 1,594–4,422 ppm $Cr_{MF}+V_{MF}$. Among all 17 samples, Cr_{MF}/V_{MF} ratios vary widely (0.12–4.33), suggesting different degrees of denitrification (Piper, 1994), the low and high ratios implying strongly and mildly denitrifying conditions, respectively. Most Cr_{MF}/V_{MF} ratios are 0.8 to 1.9, which indicate moderate to strong denitrification. In the Confusion Creek section, Cr_{MF}/V_{MF} ratios for five samples decrease systematically upsection, from 3.34 (0.4 m above base) to 0.17 (7.5 m above base); this pattern suggests increased denitrification with time, accompanying a shallowing-upward trend as defined by petrographic and biotic data. In a geochemical study of Devonian black shales of the Appalachian Basin, Sageman and others (2003) interpreted high contents of Cr+V as reflecting both redox oscillations in denitrifying bottom waters and the extent of sediment condensation. Gamma-ray profiles of the Skimo Creek section (fig. 14; Dumoulin and others, 2008) also suggest that this interval of black shale and phosphorite is highly condensed. We conclude, therefore, that phosphorite-related black shales of the Lisburne Group mainly formed by condensed sedimentation under suboxic denitrifying conditions. Exceptions occur for coeval black shales of the KRA, which have relatively high MnO contents (0.10–0.19 weight percent) and lower V_{MF}/Mo_{MF} and Cr_{MF}/Mo_{MF} ratios (fig. 10) compared to other phosphorite-related black shales of the Lisburne Group. These data suggest that the KRA black shales were deposited in more oxidizing bottom waters, although probably not fully oxic waters as exist typically in modern oceans. Their smaller negative Ce anomalies (fig. 12*A*), relative to other black shales of the Lisburne Group, are consistent with this interpretation because analyses of these KRA samples fall off the inverse trend in P_2O_5 versus Ce/Ce* shown by samples from other localities in the Brooks Range (fig. 13*D*). In contrast, all other black shales in our study display large negative Ce anomalies that follow the inverse trend towards the larger negative Ce anomalies of the granular phosphorites (average Ce/Ce*=0.11±0.03; table 3). Coeval, variably phosphatic black shales of the Kuna Formation show a similar trend (fig. 8*F* in Slack and others, 2004a). Possible effects of high concentrations of C_{org} and inferred organic complexation on Ce anomalies in the black shales, as shown by experimental data (Davranche and others, 2005), apparently are unimportant because our C_{org}-rich samples lack evidence for suppression of Ce anomalies.

In modern oceans, very large negative Ce anomalies (<0.15) occur in seawater only at or below water depths of ~400 m (for example, German and others, 1995; Alibo and Nozaki, 1999). Assuming that the redox profiles of Carboniferous oceans were similar to those of today (excluding time periods of global ocean anoxia; Arthur and Sageman, 1994), the Ce anomalies of the granular phosphorites could reflect deposition at water depths of ≥400 m. A similar model was proposed by Bonnot-Courtois and Flicoteaux (1989) and Baturin and Yushina (1998) for Late Cretaceous to early Tertiary phosphorite deposition, based on REE patterns and Ce data. Elderfield and Pagett (1986) and Grandjean and others (1987) found analogous contrasts in the Ce anomalies of modern fish remains from shallow shelf versus deep-sea settings. Based on these data and related sedimentological evidence, we present two models for the depositional setting and redox evolution of the Lisburne Group phosphorites and associated black shales.

Depositional Models

The first model involves suboxic deposition under relatively deep-water (≥400 m) conditions. Projection of the inverse trend in P_2O_5 versus Ce/Ce* for the black shales (fig. 13*D*) implies that these C_{org}-rich strata also were deposited under the same depth constraints as the granular phosphorites.

This interpretation is based on the assumption that the REE contents and Ce anomalies are contained mainly in minor apatite; several samples having <5 weight percent P_2O_5 do not follow this trend, probably due to influence by REE-rich detrital minerals such as monazite and xenotime (for example, Lev and others, 1999), and (or) to later diagenetic effects. However, uniformly low contents of MnO and consistent data for V, Cr, Mo, and Re (figs. 10, 11) preclude their formation in fully oxic seawater, instead suggesting deposition chiefly under suboxic conditions, in agreement with models proposed by numerous other workers (Arning and others, 2009b, and references therein). This model is supported by the nature of Ce anomalies in Quaternary and Recent phosphorites, which typically display small negative to small positive anomalies in samples from present water depths of ≤353 m (avg Ce/Ce* = 0.99 ± 0.09, n = 29; Piper and others, 1988; Watkins and others, 1995; Rao and others, 2000, 2002; Baturin, 2005), whereas large negative anomalies like those in many of the Lisburne Group phosphorites (avg Ce/Ce* = 0.11 ± 0.03; table 3) occur in samples from modern seamounts at water depths of 1,400 and 2,000 m (avg Ce/Ce* = 0.10 ± 0.10, n = 3; Bau and others, 1996).

A major problem with this deep-water model is the presence, several tens of meters below and above the phosphorites at Skimo and Tiglukpuk creeks, of sedimentary features (thick- and cross-bedded grainstones) and faunal components (foraminifers, algae, micritized bioclasts) that indicate midramp or shallower depositional settings (Dumoulin and others, 2008). Such settings occur above storm wave base at water depths of 100–200 m or less (for example, Wilson and Jordan, 1983). Thus, water-depth fluctuations of several hundred meters would be implied both before and after deposition of the phosphorites. Eustatic effects of Gondwanan glaciation were felt in Laurussia by late Visean time (Smith and Read, 2000), roughly coeval with Lisburne phosphogenesis, and extensional faulting affected northern Alaska throughout much of the Mississippian (Young, 2004). However, relative sea-level changes of several hundred meters seem unlikely, even if both eustatic and tectonic factors are invoked.

A second, preferred model involves suboxic deposition of the phosphorites and black shales under shallower water depths of ~100–200 m. This model is supported by the sedimentologic and faunal data outlined above and is consistent with settings of modern sedimentary phosphate deposits forming in suboxic bottom waters on the Namibian and Peruvian shelves (Kuypers and others, 2005; Piper and Perkins, 2011). However, the model does not explain the lowest Ce/Ce* values (<0.1) of the phosphorites, which, based on modern settings, imply deposition at or below a water depth of 400 m. To our knowledge, no REE data are available for suboxic seawater in a modern, open-ocean ramp or shelf environment, thus redox-based analogs to the Lisburne Group are unknown. Nevertheless, some data are consistent with this model, such as the low Ce/Ce* values that occur at and near the upper oxic-suboxic interface off the northeast coast of Oman in the Northwest Indian Ocean (German and Elderfield, 1990). Especially important is the likelihood of a large spike in oxygenation of the Permo-Carboniferous ocean (Holland, 2006), owing to its equilibrium with a highly oxygenated atmosphere that developed following the evolution of large vascular land plants and concomitant burial of organic carbon (Berner and Canfield, 1989; Berner, 2006). This inferred major oxygenation of the ocean would have greatly decreased Ce concentrations and Ce/Ce* values in seawater due to increased scavenging of Ce by Mn oxides and oxyhydroxides (for example, Byrne and Sholkovitz, 1996; Ohta and Kawabe, 2001) that likely precipitated during this time period. Piper and others (2007) first proposed this model in order to explain the large negative Ce anomalies of phosphorites in the Permian Phosphoria Formation of southeastern Idaho and western Wyoming. We suggest that the model also applies to the uniformly large negative Ce anomalies of phosphorites in the mainly Carboniferous Lisburne Group (fig. 12*B*) and in the Mississippian Deseret Limestone and Woodman Formation of eastern Nevada and western Utah (Jewell and others, 2000).

Both abiotic and biotic processes have been proposed for the precipitation of marine phosphate deposits (for example, Föllmi, 1996). Abiotic processes are constrained by kinetic limitations. A growing consensus argues for microbial activity as the predominant mechanism for phosphate precipitation (Nathan and others, 1993; Schulz and Schulz, 2005; Arning and others, 2009a). Recent experimental work by Goldhammer and others (2010) indicates that apatite is sequestered preferentially by sulfur bacteria in anoxic pore fluids, especially those in iron-limited sediments that lack sufficient Fe for authigenic pyrite formation. Within subsurface pore fluids, such iron-limited sediments generate abundant H_2S and, as a result, increased amounts of sulfur bacteria that mediate apatite precipitation. This bacteriogenic model is consistent with the apparently iron-limited nature of Lisburne Group black shales (avg Fe/Ti=5.12) and related low S/C_{org} ratios (fig. 8), and it also explains their low median C_{org}/P ratio of 25.3 relative to those of black shales of Carboniferous age elsewhere (range of median C_{org}/P ratios 36–176; Algeo and Ingall, 2007).

Diagenetic Effects

The redox signatures of the black shales and phosphorites of the Lisburne Group also could have been affected by interaction with pore fluids during diagenesis. In modern marine sediments having appreciable organic-carbon contents, such pore fluids vary in redox state from suboxic to anoxic to locally sulfidic. Reactions among oxygen-depleted pore fluids, organic carbon, and sedimentary minerals in these settings may produce diagenetic growth of new phases and different redox signatures including, for example, formation of Mn carbonates and (or) Fe sulfides, higher mineral and bulk $Fe^{2+}/(Fe^{3+}+Fe^{2+})$ ratios, and higher Ce/Ce* values. Possible changes in Ce anomalies during diagenesis

are especially important because such anomalies serve as important monitors of paleoredox history; we thus focus here on Ce anomalies for evaluating possible diagenetic effects on redox signatures. Excluding the three samples from the KRA, all of the Lisburne Group black shales have similar Ce anomalies (Ce/Ce*=0.16–0.34; figs. 12*A*, 13*D*), thus suggesting either minimal influence by pore fluids or similar and pervasive overprinting during diagenesis. The former explanation is favored here because Ce/Ce* values in the phosphorites and P-rich (>7 weight percent P_2O_5) black shales all are ≤0.21, in contrast to values of >0.5 inferred for partial to complete equilibration with anoxic pore fluids, which in modern marine sediments have Ce/Ce* values mainly in the range of ~0.7–1.1 (Elderfield and Sholkovitz, 1987; Haley and others, 2004). However, we cannot rule out some diagenetic mobility of REE (Lev and others, 1999), especially for the low-P (<4 weight percent P_2O_5) black shales that fall off the inverse trend in Ce/Ce* versus P_2O_5 as defined by other samples from the Lisburne Group (fig. 13*D*), and for the four black shales that plot within the anoxic field on the Mo versus Re discrimination diagram (fig. 11).

Unlike massive granular phosphorites that generally are believed to form on or close to the sea floor coeval with sedimentation, discrete phosphorite nodules are viewed as products of subsurface diagenesis (for example, Jarvis and others, 1994; Cook and Shergold, 2005). The three phosphorite nodules in our Lisburne Group database show small, negative Ce anomalies (Ce/Ce*=0.61–0.79) that contrast with the much larger negative anomalies of the P-rich black shales and phosphorites (fig. 12). These smaller Ce anomalies are consistent with phosphate precipitation from anoxic pore fluids, based on similar ranges shown by anomalies that occur in the modern examples described above; however, diagenetic growth of the nodules within suboxic pore fluids cannot be ruled out. The mostly flat patterns of the MREE within the nodules (fig. 12*C*) differ greatly from the typical concave-downward, "hump-type" patterns that occur in many phosphate nodules elsewhere, owing to preferential mobility of MREE during diagenesis (for example, Jarvis and others, 1994; Kidder and others, 2003; Jiang and others, 2007).

Redox Conditions during Deposition of the Kuna Formation

Slack and others (2004a) interpreted whole-rock geochemical data for black shales of the Kuna Formation as recording deposition mainly in anoxic bottom waters, based on low MnO contents of <0.01 weight percent (with several exceptions) and generally high Cr and V concentrations; however, in their study, marine fractions of V, Cr, and Mo were not calculated for discriminating anoxic and suboxic conditions of bottom waters during Kuna sedimentation. Using this approach yields mostly high V_{MF}/Mo_{MF} and Cr_{MF}/Mo_{MF} ratios like those shown by the coeval Lisburne Group phosphorite-related black shales (fig. 10). These new data suggest, therefore, that the Kuna Formation black shales were deposited chiefly in suboxic, not anoxic, bottom waters.

Sources of Metal Concentrations in the Black Shales

Metalliferous black shales have been studied for decades, but the sources of metal concentrations within them have remained controversial. Four principal sources have been identified (for example, Piper, 1994): terrigenous (detrital), biogenic, hydrogenous (seawater), and hydrothermal. A detailed quantitative evaluation of these possible sources is beyond the scope of the present study; herein, we focus on the overall metal concentrations and qualitatively evaluate their origins. Highlighted for 17 Lisburne Group black shales are the average contents (table 3) of Cu (144±72 ppm), Zn (1,112±1,081 ppm), Cd (52.5±48.6 ppm), Ni (283±137 ppm), Ag (13.4±12.3 ppm), and Tl (2.1±3.3 ppm), which are higher than those of most black shales worldwide (for example, Yudovich and Ketris, 1997). Ratios of these averages for Zn/Cu, Cd/Cu, and Ni/Cu are similar to ratios of these metals in modern plankton (fig. 1 in Piper, 1994), as are the trends of Zn versus Cu, Cd versus Cu, and Ni versus Cu for the majority of our black shale samples, thus suggesting that these metals were derived largely from biogenic sources. However, a few samples have Zn and Cd contents (up to 4,670 ppm and 142 ppm, respectively) and Zn/Cd ratios that are much higher than those of modern plankton, consistent with an additional hydrothermal component. We propose that this component was derived from the giant stratiform Zn-Pb-Ag deposits of the Red Dog district (Slack and others, 2004b) and (or) the coeval Drenchwater Zn-Pb-Ag deposit (fig. 1; Graham and others, 2009) which, like similar deposits worldwide, formed by synsedimentary-hydrothermal processes (for example, Leach and others, 2005). In our model, metal-rich hydrothermal fluids vented (exhaled) into bottom waters of the Kuna Basin were transported by upwelling currents to outer ramp settings, and precipitated metals syngenetically (from seawater) during deposition of Lisburne Group phosphorites and black shales.

Some of the phosphorite-related black shales also have high contents of Tl, including four samples that contain 3.5–12.3 ppm; for comparison, Tl contents of 49 unaltered and unmineralized black shales of the coeval Kuna Formation are ≤1.1 ppm (Slack and others, 2004a, d). Relative to this threshold value, most sulfide ores and hydrothermally-altered black shales of the Red Dog district have very high Tl concentrations of up to 313 ppm and 110 ppm, respectively (Slack and others, 2004b), as does the Drenchwater deposit (Graham and others, 2009). We infer that the locally high Tl contents in the phosphorite-related black shales reflect a hydrothermal component derived from one or more sedimentary-exhalative (sedex) systems within the Red Dog district and (or) the Drenchwater area. The high Ag contents (up to 43.5 ppm) that characterize the majority of the phosphorite-related black shales similarly may reflect contributions from these distal

sedex-type hydrothermal systems. A more detailed, quantitative evaluation of the sources of metals in the Lisburne Group black shales will be the focus of a future study.

Environmental Synthesis

Phosphorites and associated black shales of the Lisburne Group likely accumulated in middle to outer ramp settings. Geochemical data, in concert with paleogeographic reconstructions, imply that the black shales in the phosphorite interval were deposited when suboxic, denitrifying bottom water upwelled from the Kuna Basin onto the margins of adjacent carbonate platforms. Lithologic and paleontologic data indicate similar, coeval incursions in the Ikpikpuk-Umiat Basin. Sedimentologic and faunal evidence suggest that these upwelling pulses were linked to relative sea-level rise, which in turn reflected eustatic and (or) tectonic changes (Dumoulin and others, 2008); sea-level rise commonly is associated with phosphogenesis (for example, Föllmi, 1996).

Upwelling systems, due to cool-water intrusion, high nutrient loads, enhanced productivity, and related dysoxic conditions, can reduce carbonate production and lead to carbonate-platform drowning (Hallock and Schlager, 1986; Whalen, 1995). Many workers have noted the abundance of upwelling-influenced, heterozoan-dominated carbonate ramps during the Carboniferous (for example, Wright, 1994; James, 1997). The Lisburne ramp also appears to have been influenced and partially drowned by an associated upwelling system. Schematic reconstructions of continental margin upwelling zones (Parrish, 1982; James, 1997; Parrish and others, 2001) provide insight into the distribution of upwelling-related lithofacies in the Lisburne Group (fig. 15). Decay of organic matter in the most productive part of the upwelling zone forms a belt of organic-rich sediment beneath oxygen-depleted water, with phosphate precipitation favored on the landward margin of this zone (Parrish and others, 2001). Organic-rich black shale, fine-grained limestone, and phosphorite were deposited along the ramp in the transition between these two zones; phosphate likely precipitated within suboxic bottom waters at and just below the sediment-water interface (Föllmi, 1996; Piper and Perkins, 2011). Glauconite formation is favored further landward in more oxygenated water. Less-phosphatic Lisburne Group strata that contain up to 40 volume percent glauconite may have formed in this more shoreward setting; these strata are not interbedded with organic-rich rocks. All highly glauconitic facies in the Lisburne Group are older or younger than the phosphorites, however, forming prior to or after the period of most intense primary productivity and suboxia. Because the formation of glauconite (Fe^{3+}-rich mica) requires a source of iron in local sediments, its abundance in the glauconitic facies suggests that iron-limited conditions largely were restricted to the phosphorite and interbedded black shale sequence. A corollary of this interpretation is that iron-limited detritus was contributed intermittently to the Lisburne depositional system, mainly during late Meramecian to early Chesterian time.

The inability of carbonate platforms in the western Brooks Range to recover from the early Chesterian drowning episode, in contrast to platforms to the east and north, suggests that upwelling and consequent nutrification were more intense to the west (for example, Whalen, 1995; Caplan and others, 1996). Additionally, or alternatively, tectonically enhanced rates of sea-level rise may have been higher to the west; this hypothesis is supported by abundant evidence for Late Mississippian extensional faulting in the Red Dog district (Young, 2004; Kelley and others, 2004a). Downdropping of parts of the central Brooks Range (eastern EMA) along reactivated extensional structures is a likely cause of final drowning of the Lisburne platform in this area during the early Morrowan. Nutrification appears to have been less important in this drowning as it is associated only with minor phosphatization and deposition of much less organic-rich shale (Whalen and others, 2006; Dumoulin and others, 2008).

Paleogeography

Development of a Carboniferous upwelling system in northern Alaska requires specific paleogeographic and paleoceanographic conditions. Wind-driven, ocean-surface currents must parallel the coastline, induce offshore Ekman transport, and drive either meridional or zonal coastal upwelling (Parrish, 1982). Parrish (1982) did not predict upwelling in northern Alaska during Carboniferous time, but the Paleozoic position of northern Alaska in the global reconstructions that formed the basis for her predictions was poorly constrained. More recent paleogeographic reconstructions (Lawver and others, 2002; Colpron and Nelson, 2009) are consistent with Carboniferous upwelling in northern Alaska, but differ in the type of upwelling expected.

Lawver and others (2002) suggested that Arctic Alaska formed a roughly east-trending, peninsular extension of Laurussia that was situated at about 30°N during the Late Mississippian (fig. 16). This model is compatible with zonal marine upwelling along Arctic Alaska, produced by circum-polar easterly currents that generated northerly-directed Ekman transport and southerly-directed upwelling. The modern Antarctic circum-polar current reaches north to latitudes of approximately 40°S; development of zonal upwelling along the Arctic Alaska continental margin would require a circum-polar current that reached a paleolatitude of about 30–40°N.

Colpron and Nelson (2009) showed Arctic Alaska as a north-trending peninsula of Laurussia that lay between ~30° and 40°N in Late Mississippian time; this reconstruction is consistent with meridional marine upwelling along the west side of Arctic Alaska, analogous to that found along the modern Pacific margin of the northwestern United States. Meridional upwelling also was favored by Kelly and others (2007) to explain deposition of Triassic phosphorites in northern Alaska.

Paleoenvironmental data suggest that meridional upwelling better explains phosphorite deposition in the Lisburne Group. The climate in northern Alaska became increasingly

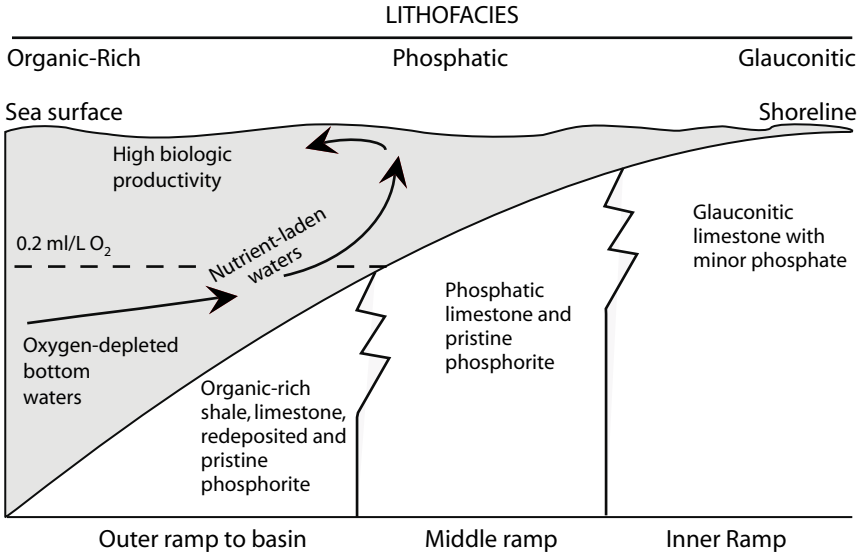

Figure 15. Schematic reconstruction of lithofacies and water circulation perpendicular to the paleoshoreline along the northern side of the Kuna Basin during deposition of Lisburne Group phosphorites, after Burchette and Wright (1992), James (1997), and Parrish and others (2001); maximum water depth on left side of the figure is likely ~300 m. Lisburne Group phosphorite-bearing strata formed in the transition zone between organic-rich and phosphatic facies. Less-phosphatic limestones, with as much as 40 volume percent glauconite, were deposited further shoreward in the transition between phosphatic and glauconitic facies; such limestones are observed only locally and mostly are older or younger than the phosphorites.

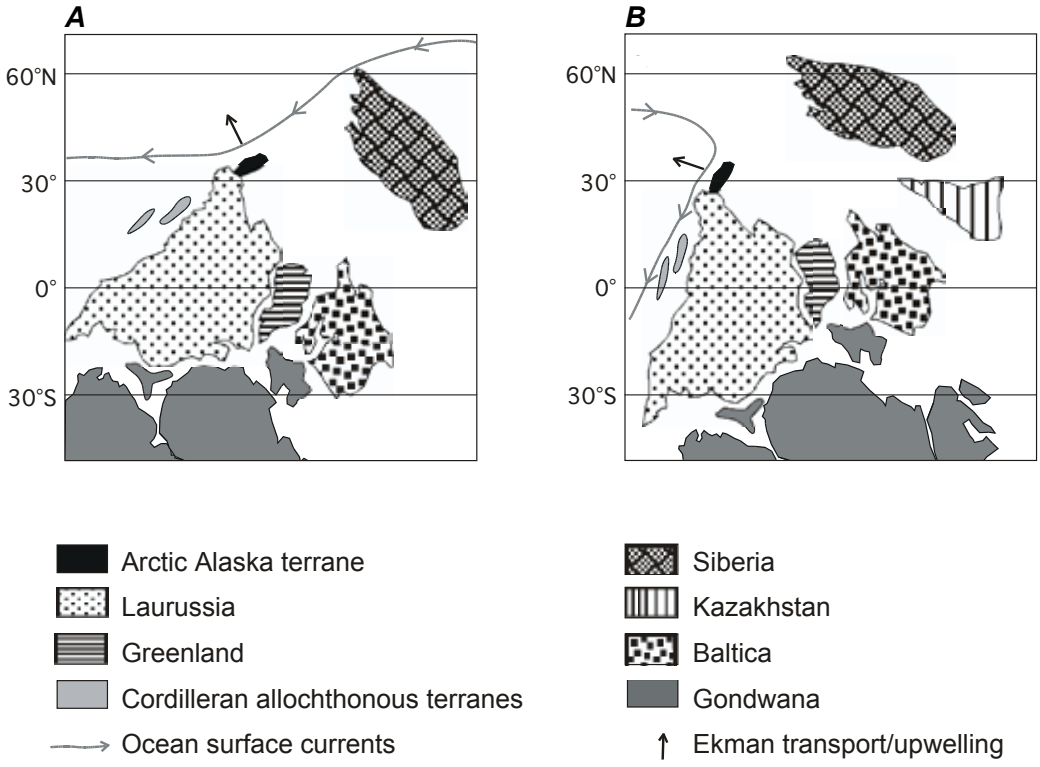

Figure 16. Recent reconstructions of Mississippian paleogeography. *A*, In the model of Lawver and others (2002), northern Alaska is shown as a roughly east-trending peninsular extension of Laurussia. A zonal marine upwelling system along Arctic Alaska could have been produced by circum-polar easterly currents that generated northerly-directed Ekman transport and southerly-directed upwelling. *B*, In the model of Colpron and Nelson (2009), northern Alaska is shown as a roughly north-trending peninsular extension of Laurussia. Meridional marine upwelling, analogous to that found along the modern Pacific margin of the northwestern United States, could have developed under this paleogeographic arrangement.

arid during Late Mississippian (late Meramecian-Chesterian) time (Dumoulin and Bird, 2001; Dumoulin and others, 2004). Aridity is associated with many meridional upwelling regimes (for example, present-day Peru, Namibia, and California; Permian Phosphoria Formation), but is less common in zonal upwelling environments (for example, present-day Venezuela).

Development of phosphatic rocks on opposing sides of the Kuna Basin presents a paleoceanographic conundrum. A modern analog for this distribution may be the Gulf of Mexico, where the loop current (Hofmann and Worley, 1986) sets up a system of circulation that generates upwelling along opposing continental shelves. The Gulf of Mexico loop current is a clockwise flow northward into the Gulf of Mexico (Hofmann and Worley, 1986); recent upwelling associated with loop-current dynamics has been documented on both the eastern margin of the Yucatan Peninsula (Merino, 1997) and along the west Florida shelf (Li and Weisberg, 1999; Weisberg and others, 2000). Detailed paleogeography and paleoceanography of the Kuna Basin is poorly understood, but circulation involving a loop current similar to that in the modern Gulf of Mexico could explain the development of upwelling and concomitant phosphatic deposits on both sides of the basin.

Formation of less-phosphatic strata within the Lisburne Group also may be linked to upwelling. Such facies are coeval, older, and younger than Lisburne Group phosphorites. Those of late Meramecian-early Chesterian age may have formed along parts of the Lisburne platform that were less intensely and (or) less consistently affected by upwelling than were the areas of phosphorite formation. Older (Early Mississippian) and younger (latest Mississippian-Pennsylvanian) less-phosphatic strata bracket the time of Lisburne phosphorite deposition, commonly contain notable glauconite, and are not associated with organic-rich facies. These relations suggest that weaker and (or) more intermittent upwelling prevailed during waxing and waning of the main episode of Lisburne phosphogenesis, and that phosphate accumulated at these times in a more oxygenated (and landward) environment (phosphate-glauconite transition zone of Parrish and others, 2001; fig. 15).

Acknowledgments

We thank the Mineral Resources and Energy Resources Programs of the USGS for financial support of this study, the Alaska Division of Geological and Geophysical Surveys and Petro-Canada Oil and Gas for logistical support of fieldwork in the central Brooks Range, and Mike Kunz (U.S. Bureau of Land Management) for providing camp facilities at Ivotuk and Utukok River. We particularly acknowledge Robert Burruss, Craig Johnson, and Karen Kelley (USGS), Ellen Harris and Paige Delaney (Alaska Division of Geological and Geophysical Surveys), Gil Mull (Alaska Division of Oil and Gas), and Jeff Bever, Jeff Lukasic, and Mike McDonough (Petro-Canada Oil and Gas) for their help and discussions in the field and office. Thanks also to Erin Marsh and Theresa Taylor of the USGS for assistance with the figures and to Ken Bird and David Piper (USGS) for thorough reviews of an early version of the manuscript. Comments by Kurt Grimm, Joe Macquaker, Gene Rankey, Peir Pufahl, and an anonymous referee are appreciated.

References Cited

Adams, K.E., 1991, Permian sedimentation in the northcentral Brooks Range, Alaska—Implications for tectonic reconstructions: Fairbanks, University of Alaska, master's thesis, 122 p.

Algeo, T.J., and Ingall, E., 2007, Sedimentary C_{org}:P ratios, paleocean ventilation, and Phanerozoic atmospheric pO_2: Palaeogeography, Palaeoclimatology, Palaeoecology, v. 256, p. 130–155.

Algeo, T.J., and Lyons, T.W., 2006, Mo-total organic carbon covariation in modern anoxic marine environments—Implications for analysis of paleoredox and paleohydrographic conditions: Paleoceanography, v. 21, 23 p.

Algeo, T.J., and Maynard, J.B., 2004, Trace-element behavior and redox facies in core shales of Upper Pennsylvanian Kansas-type cyclothems: Chemical Geology, v. 206, p. 289–318.

Algeo, T.J., and Maynard, J.B., 2008, Trace-metal covariation as a guide to water-mass conditions in ancient anoxic marine environments: Geosphere, v. 4, p. 872–887.

Alibo, D.S., and Nozaki, Y., 1999, Rare earth elements in seawater—Particle association, shale-normalization, and Ce oxidation: Geochimica et Cosmochimica Acta, v. 63, p. 363–372.

Armstrong, A.K., 1970, Mississippian dolomites from Lisburne Group, Killik River, Mount Bupto region, Alaska: American Association of Petroleum Geologists Bulletin, v. 54, p. 251–264.

Armstrong, A.K., and Mamet, B.L., 1977, Carboniferous microfacies, microfossils, and corals, Lisburne Group, Arctic Alaska: U.S. Geological Survey Professional Paper 849, 129 p.

Armstrong, A.K., and Mamet, B.L., 1978, Microfacies of the Carboniferous Lisburne Group, Endicott Mountains, Arctic Alaska, *in* Stelck, C.R., and Chatterton, B.D.E., eds., Western and Arctic Canadian biostratigraphy: Geological Association of Canada Special Paper 18, p. 333–394.

Armstrong, A.K., Mamet, B.L., and Dutro, J.T., Jr., 1970, Foraminiferal zonation and carbonate facies of Carboniferous (Mississippian and Pennsylvanian) Lisburne Group, central and eastern Brooks Range, Arctic Alaska: American Association of Petroleum Geologists Bulletin, v. 54, no. 5, p. 687–698.

Arning, E.T., Birgel, D., Brunner, B., and Peckman, J., 2009a, Bacterial formation of phosphatic laminites off Peru: Geobiology, v. 7, p. 295–307.

Arning, E.T., Lückge, A., Breuer, C., Gussone, N., Birgel, D., and Peckman, J., 2009b, Genesis of phosphorite crusts off Peru: Marine Geology, v. 262, p. 68–81.

Arthur, M.A., and Sageman, B.B., 1994, Marine black shales: Depositional mechanisms and environments of ancient deposits: Annual Review of Earth and Planetary Sciences, v. 22, p. 499–551.

Baturin, G.N., 2005, Geochemistry of rare earth elements in phosphorites from the Namibian shelf: Geochemistry International, v. 43, p. 973–987.

Baturin, G.N., and Dubinchuk, V.T., 2005, Authigenic minerals of uranium and rare earth elements in oceanic phosphorites: Oceanology, v. 45, p. 857–866.

Baturin, G.N., and Yushina, I.G., 1998, Rare-earth elements in phosphorites from the Pacific seamounts and the depth of phosphorite formation: Oceanology, v. 38, p. 556–565.

Bau, M., Koschinsky, A., Dulski, P., and Hein, J.R., 1996, Comparison of the partitioning behaviours of yttrium, rare earth elements, and titanium between hydrogenetic marine ferromanganese crusts and seawater: Geochimica et Cosmochimica Acta, v. 60, p. 1,709–1,725.

Berner, R.A., 2006, GEOCARBSULF—A combined model for Phanerozoic atmospheric O_2 and CO_2: Geochimica et Cosmochimica Acta, v. 70, p. 5,653–5,664.

Berner, R.A., and Canfield, D.E., 1989, A new model for atmospheric oxygen over Phanerozoic time: American Journal of Science, v. 289, p. 333–361.

Bird, K.J., 2001, Framework geology, petroleum systems, and play concepts of the National Petroleum Reserve-Alaska, *in* Houseknecht, D.W., ed., NPRA core workshop; petroleum plays and systems in the National Petroleum Reserve-Alaska: SEPM (Society for Sedimentary Geology) Core Workshop no. 21, p. 5–17.

Blome, C.D., Reed, K.M., and Harris, A.G., 1998, Radiolarian and conodont biostratigraphy of the type section of the Akmalik Chert (Mississippian), Brooks Range, Alaska, *in* Gray, J.E., and Riehle, J.R., eds., Geologic studies in Alaska by the U.S. Geological Survey, 1996: U.S. Geological Survey Professional Paper 1595, p. 51–69.

Bonnot-Courtois, C., and Flicoteaux, R., 1989, Distribution of rare-earth and some trace elements in Tertiary phosphorites from the Senegal Basin and their weathering products: Chemical Geology, v. 75, p. 311–328.

Bowsher, A.L., and Dutro, J.T., Jr., 1957, The Paleozoic section in the Shainin Lake area, central Brooks Range, Alaska: U.S. Geological Survey Professional Paper 303-A, 39 p.

Brosgé, W.P., and Armstrong, A.K., 1977, Lithologic logs of Lisburne Group in Lawrence Livermore Laboratory Drill Holes 1 and 2, Confusion Creek, Chandler Lake quadrangle, northern Alaska: U.S. Geological Survey Open-File Report 77-26, 11 p.

Brosgé, W.P., and Reiser, H.N., 1951, Selected sections of Lisburne Limestone, Brooks Range, Alaska, *in* Geological investigations of Naval Petroleum Reserve No. 4: U.S. Geological Survey Open-File Report 40, 18 p.

Brumsack, H.-J., 2006, The trace metal content of recent organic carbon-rich sediments—Implications for Cretaceous black shale formation: Palaeogeography, Palaeoclimatology, Palaeoecology, v. 232, p. 344–361.

Burchette, T.P., and Wright, V.P., 1992, Carbonate ramp depositional systems: Sedimentary Geology, v. 79, p. 3–57.

Byrne, R.H., and Sholkovitz, E.R., 1996, Marine chemistry and geochemistry of the lanthanides, *in* Gschneidner, K.A., Jr., and Eyring, L., eds., Handbook on the physics and chemistry of the rare earths: Amsterdam, Elsevier Ltd., v. 23, p. 497–593.

Caplan, M.L., Bustin, R.M., and Grimm, K.A., 1996, Demise of a Devonian-Carboniferous carbonate ramp by eutrophication: Geology, v. 4, p. 715–718.

Cole, F., Bird, K.J., Toro, J., Roure, F., O'Sullivan, P.B., Pawlewicz, M., and Howell, D.G., 1997, An integrated model for the tectonic development of the frontal Brooks Range and Colville Basin 250 km west of the Trans-Alaska Crustal Transect: Journal of Geophysical Research, v. 102, no. B9, p. 20,685–20,708.

Colpron, M., and Nelson, J.L., 2009, A Palaeozoic northwest passage—Incursion of Caledonian, Baltican and Siberian terranes into eastern Panthalassa, and the early evolution of the North American Cordillera, *in* Cawood, P., and Kröner, A., eds., Earth accretionary systems in space and time: Geological Society of London Special Publication 318, p. 273–307.

Cook, P.J., and Shergold, J.H., 2005, Phosphorite deposits of the world—Proterozoic and Cambrian phosphorites: Cambridge, U.K., Cambridge University Press, Cambridge Earth Science Series, v. 1, 408 p.

Coveney, R.M., Jr., 2003, Metalliferous Paleozoic black shales and associated strata, *in* Lentz, D.R., ed., Inorganic geochemistry of sediments and sedimentary rocks—Evolutionary considerations to mineral deposit-forming environments: Geological Association of Canada, GeoText 4, p. 135–144.

Creaney, S., and Passey, Q.R., 1993, Recurring patterns of total organic carbon and source rock quality within a sequence stratigraphic framework: American Association of Petroleum Geologists Bulletin, v. 77, p. 386–401.

Crusius, J., Calvert, S., Pederson, T., and Sage, D., 1996, Rhenium and molybdenum enrichments in sediments as indicators of oxic, sub-oxic and sulfidic conditions of deposition: Earth and Planetary Science Letters, v. 145, p. 67–78.

Curtis, S.M., Ellersieck, I., Mayfield, C.F., and Tailleur, I.L., 1984, Reconnaissance geologic map of southwestern Misheguk Mountain quadrangle, Alaska: U.S. Geological Survey Miscellaneous Investigations Series Map I-1502, 2 sheets, scale 1:63,360.

Curtis, S.M., Ellersieck, I., Mayfield, C.F., and Tailleur, I.L., 1990, Reconnaissance geologic map of the De Long Mountains A-1 and B-1 quadrangles and part of the C-1 quadrangle, Alaska: U.S. Geological Survey Miscellaneous Investigations Series Map I-1930, 2 sheets, scale 1:63,360.

Daessle, L.W., and Carriquiry, J.D., 2008, Rare earth and metal geochemistry of land and submarine phosphorites in the Baja California Peninsula, Mexico: Marine Georesources and Geotechnology, v. 26, p. 340–349.

Davranche, M., Pourret, O., Gruau, G., Dia, A., and Le Coz-Bouhnik, M., 2005, Adsorption of REE(III)-humate complexes onto MnO_2—Experimental evidence for cerium anomaly and lanthanide tetrad effect suppression: Geochimica et Cosmochimica Acta, v. 69, p. 4,825–4,835.

Desborough, G.A., and Poole, F.G., 1983, Metal concentrations in some marine black shales of the United States, *in* Shanks, W.C., III, ed., Cameron volume on unconventional mineral deposits: New York, American Institute of Mining, Metallurgical, and Petroleum Engineers, Inc., p. 99–110.

Dover, J.H., Tailleur, I.L., and Dumoulin, J.A., 2004, Geologic and fossil locality maps of the west-central part of the Howard Pass quadrangle and part of the adjacent Misheguk Mountain quadrangle, western Brooks Range, Alaska: U.S. Geological Survey Miscellaneous Field Studies Map MF-2413, 2 sheets with 25 p. of explanatory text, scale 1:100,000.

Dumoulin, J.A., and Bird, K.J., 2001, Stratigraphy and lithofacies of Lisburne Group carbonate rocks (Carboniferous-Permian) in the National Petroleum Reserve-Alaska, *in* Houseknecht, D.W., ed., NPRA core workshop; petroleum plays and systems in the National Petroleum Reserve-Alaska: SEPM (Society for Sedimentary Geology) Core Workshop no. 21, p. 141–166.

Dumoulin, J.A., and Bird, K.J., 2002, Lithofacies and stratigraphy of the Lisburne and Etivluk Groups in the Lisburne 1 well and adjacent outcrops, central Brooks Range, Alaska [abs.]: AAPG Program and Abstracts, Pacific Section, p. 71.

Dumoulin, J.A., and Harris, A.G., 1993, Lithofacies and conodonts of Carboniferous strata in the Ivotuk Hills, western Brooks Range, Alaska, *in* Dusel-Bacon, C., and Till, A.B., eds., Geologic studies in Alaska by the U.S. Geological Survey during 1992: U.S. Geological Survey Bulletin 2068, p. 31–47.

Dumoulin, J.A., Harris, A.G., Blome, C.D., and Young, L.E., 2004, Depositional settings, correlation, and age of Carboniferous rocks in the western Brooks Range, Alaska: Economic Geology, v. 99, p. 1,355–1,384.

Dumoulin, J.A., Harris, A.G., Blome, C.D., and Young, L.E., 2006a, Conodont and radiolarian data from the De Long Mountains quadrangle and adjacent areas: U.S. Geological Survey Open-File Report 2006-1068, accessed January 24, 2011, at http://pubs.usgs.gov/of/2006/1068/.

Dumoulin, J.A., Harris, A.G., and Schmidt, J.M., 1993, Deep-water lithofacies and conodont faunas of the Lisburne Group, western Brooks Range, Alaska, *in* Dusel-Bacon, C., and Till, A.B., eds., Geologic studies in Alaska by the U.S. Geological Survey during 1992: U.S. Geological Survey Bulletin 2068, p. 12–30.

Dumoulin, J.A., Harris, A.G., Slack, J.F., and Whalen, M.T., 2006b, Phosphatic rocks of the Lisburne Group in the southern NPRA and adjacent areas [abs.]: Alaska Miners Association Annual Convention Abstracts, p. 12–14.

Dumoulin, J.A., Watts, K.F., and Harris, A.G., 1997, Stratigraphic contrasts and tectonic relationships between Carboniferous successions in the Trans-Alaska Crustal Transect corridor and adjacent areas, northern Alaska: Journal of Geophysical Research, v. 102, no. B9, p. 20,709–20,726.

Dumoulin, J.A., Whalen, M.T., Harris, A.G., and Slack, J.F., 2006c, Paleogeographic and metallogenic implications of phosphatic rocks in the Lisburne Group (Permian-Carboniferous), northern Alaska [abs.]: Geological Society of America Abstracts with Programs, v. 38, no. 5, p. 85.

Dumoulin, J.A., Whalen, M.T., and Harris, A.G., 2008, Lithofacies, age, and sequence stratigraphy of the Carboniferous Lisburne Group in the Skimo Creek area, central Brooks Range, *in* Haeussler, P.J., and Galloway, J.P., eds., Studies by the U.S. Geological Survey in Alaska, 2006: U.S. Geological Survey Professional Paper 1739-B, 64 p., accessed January 24, 2011, at http://pubs.usgs.gov/pp/pp1739/b/.

Dunham, R.J., 1962, Classification of carbonate rocks according to depositional texture, *in* Ham, W.E., ed., Classification of carbonate rocks—A symposium: American Association of Petroleum Geologists Memoir 1, p. 108–121.

Dutro, J.T., Jr., 1987, Revised megafossil biostratigraphic zonation for the Carboniferous of northern Alaska, *in* Tailleur, I.L., and Weimer, P., eds., Alaskan North Slope geology: Society of Economic Geologists and Mineralogists, Pacific Section, Book 50, v. 1, p. 359–364.

Dutro, J.T., Jr., and Silberling, N.J., 1988, Megafossil biostratigraphy of some of the deep test wells, National Petroleum Reserve in Alaska, *in* Gryc, G., ed., Geology and exploration of the National Petroleum Reserve in Alaska, 1974–1982: U.S. Geological Survey Professional Paper 1399, p. 667–686.

Elderfield, H., and Pagett, R., 1986, Rare earth elements in ichthyoliths—Variations with redox conditions and depositional environment: Science of the Total Environment, v. 49, p. 175–197.

Elderfield, H., and Sholkovitz, E.R., 1987, Rare earth elements in the pore waters of reducing nearshore sediments: Earth and Planetary Science Letters, v. 82, p. 280–288.

Embry, A.F., III, and Klovan, J.E., 1972, Absolute water depth limits of Late Devonian paleoecological zones: Geologische Rundschau, v. 61, p. 672–686.

Föllmi, K.B., 1996, The phosphorus cycle, phosphogenesis and marine phosphate-rich deposits: Earth-Science Reviews, v. 40, p. 55–124.

German, C.R., and Elderfield, H., 1990, Rare earth elements in the NW Indian Ocean: Geochimica et Cosmochimica Acta, v. 54, p. 1,929–1,940.

German, C.R., Masuzawa, T., Greaves, M.J., Elderfield, H., and Edmond, J.M., 1995, Dissolved rare earth elements in the Southern Ocean—Cerium oxidation and the influence of hydrography: Geochimica et Cosmochimica Acta, v. 59, p. 1,551–1,558.

Goldhammer, T., Brüchert, V., Ferdelman, T.G., and Zabel, M., 2010, Microbial sequestration of phosphorous in anoxic upwelling sediments: Nature Geoscience, v. 3, p. 557–561.

Gordon, M., Jr., 1957, Mississippian cephalopods of northern and eastern Alaska: U.S. Geological Survey Professional Paper 283, 61 p.

Graham, G.E., Kelley, K.D., Slack, J.F., and Koenig, A.E., 2009, Trace elements in Zn-Pb-Ag deposits and related stream sediments, Brooks Range Alaska, with implications for Tl as a pathfinder element: Geochemistry—Exploration, Environment, Analysis, v. 9, p. 19–37.

Grandjean, P., Cappetta, H., Michard, A., and Albarède, F., 1987, The assessment of REE patterns and $^{143}Nd/^{144}Nd$ ratios in fish remains: Earth and Planetary Science Letters, v. 84, p. 181–196.

Gromet, L.P., Dymek, R.F., Haskin, L.A., and Korotev, R.L., 1984, The "North American shale composite"—Its compilation, major and trace element characteristics: Geochimica et Cosmochimica Acta, v. 48, p. 2,469–2,482.

Haley, B.A., Klinkhammer, G.P., and McManus, J., 2004, Rare earth elements in pore waters of marine sediments: Geochimica et Cosmochimica Acta, v. 68, p. 1,265–1,279.

Hallock, P., and Schlager, W., 1986, Nutrient excess and the demise of coral reefs and carbonate platforms: Palaios, v. 1, p. 389–398.

Hofmann, E.E., and Worley, S.J., 1986, An investigation of the circulation of the Gulf of Mexico: Journal of Geophysical Research, v. 91, no. C12, p. 14,221–14,236.

Holland, H.D., 2006, The oxygenation of the atmosphere and oceans: Philosophical Transactions of the Royal Society, B, v. 361, p. 903–915.

Hubbard, R.J., Edrich, S.P., and Rattey, R.P., 1987, Geologic evolution and hydrocarbon habitat of the 'Arctic Alaska Microplate,' *in* Tailleur, I.L., and Weimer, Paul, eds., Alaskan North Slope geology: Bakersfield, Calif., Pacific Section SEPM and Alaska Geological Society, v. 2, p. 797–830.

James, N.P., 1997, The cool-water carbonate depositional realm, *in* James, N.P., and Clarke, J.A.D., eds., Cool-water carbonates: Society of Economic Paleontologists and Mineralogists, Special Publication 56, p. 1–20.

Jarvis, I., Burnett, W., Nathan, Y., Almbaydin, F.S.M., Attia, A.K.M., Castro, L.N., Flicoteaux, R., Hilmy, M.E., Husain, V., Qutawnah, A.A., Serjani, A., and Zanin, Y.N., 1994, Phosphorite geochemistry—State-of-the-art and environmental concerns: Eclogae Geologicae Helvetiae, v. 87, p. 643–700.

Jewell, P.W., Silberling, N.J., and Nichols, K.M., 2000, Geochemistry of the Mississippian Delle phosphatic event, eastern Great Basin, U.S.A.: Journal of Sedimentary Research, v. 70, p. 1,222–1,233.

Jiang, S.-Y., Zhao, H.-X., Chen, Y.-Q., Yang, T., Yang, J.-H., and Ling, H.-F., 2007, Trace and rare earth element geochemistry of phosphate nodules from the Lower Cambrian black shale sequence in the Mufu Mountain of Nanjing, Jiangsu Province, China: Chemical Geology, v. 244, p. 584–604.

Johnsson, M.J., Evans, K.R., and Marshall, H.A., 1999, Thermal maturity of sedimentary rocks in Alaska; digital resources: U.S. Geological Survey Digital Data Series DDS-54, CD-ROM, accessed January 24, 2011, http://pubs.usgs.gov/dds/dds-54/.

Kelley, K.D., and Jennings, S., 2004, Barite and Zn-Pb-Ag deposits in the Red Dog district, western Brooks Range, northern Alaska; preface: Economic Geology, v. 99, p. 1,267–1,280.

Kelley, K.D., Dumoulin, J.A., and Jennings, S., 2004a, The Anarraaq Zn-Pb-Ag and barite deposit, northern Alaska—Evidence for replacement of carbonate by barite and sulfides: Economic Geology, v. 99, p. 1,577–1,591.

Kelley, K.D., Leach, D.L., Johnson, C.A., Clark, J.L., Fayek, M., Slack, J.F., Anderson, V.M., Ayuso, R.A., and Ridley, W.I., 2004b, Textural, compositional, and sulfur isotope variations in sulfide minerals in the Red Dog Zn-Pb-Ag deposits—Implications for ore formation: Economic Geology, v. 99, p. 1,509–1,532.

Kelley, K.D., and Mull, C.G., 1995, Maps showing areas of potential for mineral resources in the Killik River 1° x 3° quadrangle, Alaska: U.S. Geological Survey Miscellaneous Field Studies Map 2225-A, 25 p., 1 sheet, scale 1:250,000.

Kelly, L.N., Whalen, M.T., McRoberts, C.A., Hopkin, E., and Tomsich, C.S., 2007, Sequence stratigraphy and geochemistry of the upper Lower through Upper Triassic of northern Alaska—Implications for paleoredox history, source rock accumulation, and paleoceanography: Alaska Division of Geological and Geophysical Surveys Report of Investigations 2007-1, 50 p.

Kidder, D.L., Krishnaswamy, R., and Mapes, R.H., 2003, Element mobility in phosphatic shales during concretion growth and implications for provenance analysis: Chemical Geology, v. 198, p. 335–353.

Kurtak, J.M., Hicks, R.W., Werdon, M.B., Meyer, M.P., and Mull, C.G., 1995, Mineral investigations in the Colville mining district and southern National Petroleum Reserve in Alaska: U.S. Bureau of Mines Open-File Report 8-95, 217 p.

Kuypers, M.M.M., Lavik, G., Woebken, D., Schmid, M., Fuchs, B.M., Amann, R., Jorgensen, B.B., and Jetten, M.S.M., 2005, Massive nitrogen loss from the Benguela upwelling system through anaerobic ammonium oxidation: Proceedings of the National Academy of Sciences, v. 102, p. 6,478–6,483.

Lanci, L., Kent, D.V., and Miller, K.G., 2002, Detection of Late Cretaceous and Cenozoic sequence boundaries on the Atlantic coastal plain using core log integration of magnetic susceptibility and natural gamma ray measurements at Ancora, New Jersey: Journal of Geophysical Research, v. 107(B10), 2216, doi:10.1029/2000JB000026.

Lawver, L.A., Grantz, A., and Gahagan, L.M., 2002, Plate kinematic evolution of the present Arctic region since the Ordovician, *in* Miller, E.L., Grantz, A., and Klemperer, S.L., eds., Tectonic evolution of the Bering Shelf-Chukchi Sea-Arctic margin and adjacent landmasses: Geological Society of America Special Paper 360, p. 333–358.

Leach, D.L., Sangster, D.F., Kelley, K.D., Large, R.R., Garven, G., Allen, C.R., Gutzmer, J., and Walters, S., 2005, Sediment-hosted lead-zinc deposits—A global perspective, *in* Hedenquist, J.W., Thompson, J.F.H., Goldfarb, R.J., and Richards, J.P., eds., Economic Geology one hundredth anniversary volume, 1905-2005: Littleton, Colo., Society of Economic Geologists, Inc., p. 561–607.

Legg, G.W., 1983, Geological report on the Lisburne Test Well No. 1: Husky Oil NPR Operations, Inc., 17 p. plus appendices.

Lev, S.M., McLennan, S.M., and Hanson, G.N., 1999, Mineralogic controls on REE mobility during black-shale diagenesis: Journal of Sedimentary Research, v. 69, p. 1,071–1,082.

Li, Z., and Weisberg, R.H., 1999, West Florida shelf response to upwelling favorable wind forcing—Kinematics: Journal of Geophysical Research, v. 104, no. C6, p. 13,507–13,527.

Loutit, T.S., Hardenbol, J., Vail, P.R., and Baum, G.R., 1988, Condensed sections—The key to age dating and correlation of continental margin sequences, *in* Wilgus, C.K., and others, eds., Sea-level changes—An integrated approach: SEPM Special Publication 42, p. 183–213.

Mayfield, C.F., Tailleur, I.L., and Ellersieck, I., 1988, Stratigraphy, structure, and palinspastic synthesis of the western Brooks Range, northwestern Alaska, *in* Gryc, G., ed., Geology and exploration of the National Petroleum Reserve in Alaska, 1974-1982: U.S. Geological Survey Professional Paper 1399, p. 143–186.

McArthur, J.M., and Walsh, J.N., 1984, Rare-earth geochemistry of phosphorites: Chemical Geology, v. 47, p. 191–220.

McLennan, S.M., 1989, Rare earth elements in sedimentary rocks—Influence of provenance and sedimentary processes, *in* Lipin, B.R., and McKay, G.A., eds., Geochemistry and mineralogy of rare earth elements: Reviews in Mineralogy, v. 21, p. 169–200.

Merino, M., 1997, Upwelling on the Yucatan Shelf—Hydrographic evidence: Journal of Marine Systems, v. 13, p. 101–121.

Mull, C.G., Moore, T.E., Harris, E.E., and Tailleur, I.L., 1994, Geologic map of the Killik River Quadrangle, Brooks Range, Alaska: U.S. Geological Survey Open-File Report 94-679, 1 sheet, 1:125,000.

Nathan, Y., Bremner, J.M., Loewenthal, R.E., and Monteiro, P., 1993, Role of bacteria in phosphorite genesis: Geomicrobiology Journal, v. 11, p. 69–76.

Ohta, A., and Kawabe, I., 2001, REE(III) adsorption onto Mn dioxide (δ-MnO_2) and Fe oxyhydroxide—Ce(III) oxidation by δ-MnO_2: Geochimica et Cosmochimica Acta, v. 65, p. 695–703.

Parrish, J.T., 1982, Upwelling and petroleum source beds, with reference to the Paleozoic: American Association of Petroleum Geologists Bulletin, v. 66, p. 750–774.

Parrish, J.T., Droser, M.L., and Bottjer, D.J., 2001, A Triassic upwelling zone—The Shublik Formation, Arctic Alaska, U.S.A.: Journal of Sedimentary Research, v. 71, p. 272–285.

Patton, W.W., Jr., and Matzko, J.J., 1959, Phosphate deposits in northern Alaska: U.S. Geological Survey Professional Paper 302-A, 17 p.

Peacor, D.R., Coveney, R.M., Jr., and Zhao, G., 2000, Authigenic illite and organic matter—The principal hosts of vanadium in the Mecca Quarry Shale at Velpen, Indiana: Clays and Clay Minerals, v. 48, p. 311–316.

Perkins, R.B., Piper, D.Z., and Mason, C.E., 2008, Trace-element budgets in the Ohio/Sunbury shales of Kentucky—Constraints on ocean circulation and primary productivity in the Devonian-Mississippian Appalachian Basin: Palaeogeography, Palaeoclimatology, Palaeoecology, v. 265, p. 14–29.

Piper, D.Z., 1994, Seawater as a source of minor elements in black shales, phosphorites, and other sedimentary deposits: Chemical Geology, v. 114, p. 95–114.

Piper, D.Z., 2001, Marine chemistry of the Permian Phosphoria Formation and basin, southeast Idaho: Economic Geology, v. 96, p. 599–620.

Piper, D.Z., Baedecker, P.A., Crock, J.G., Burnett, W.C., and Loebner, B.J., 1988, Rare earth elements in phosphatic-enriched sediment of the Peru Shelf: Marine Geology, v. 80, p. 269–285.

Piper, D.Z., and Calvert, S.E., 2009, A marine biogeochemical perspective on black shale deposition: Earth-Science Reviews, v. 95, p. 63–96.

Piper, D.Z., and Perkins, R.B., 2011, Geochemistry of marine phosphate deposits: Signposts to phosphogenesis, *in* Scott, S.D., ed., Geochemistry of mineral resources: Amsterdam, Elsevier, Treatise on Geochemistry, v. 12 (in press).

Piper, D.Z., Perkins, R.B., and Rowe, H.D., 2007, Rare-earth elements in the Permian Phosphoria Formation—Paleo proxies of ocean geochemistry: Deep-Sea Research II, v. 54, p. 1,396–1,413.

Piper, D.Z., Skorupa, J.P., Presser, T.S., Hardy, M.A., Hamilton, S.J., Huebner, M., and Gulbrandsen, R.A., 2000, Phosphoria Formation at the Hot Springs mine in southeast Idaho—A source of selenium and other trace elements to surface water, ground water, vegetation, and biota: U.S. Geological Survey Open-File Report 2000-50, 82 p.

Porter, S.C., 1966, Stratigraphy and deformation of Paleozoic section at Anaktuvuk Pass, central Brooks Range, Alaska: American Association of Petroleum Geologists Bulletin, v. 50, p. 952–980.

Posamentier, H.W., and Allen, G.P., 1999, Siliciclastic sequence stratigraphy—Concepts and applications: SEPM Concepts in Sedimentology and Paleontology, v. 7, 210 p.

Pufahl, P.K., and Grimm, K.A., 2003, Coated phosphate grains—Proxy for physical, chemical, and ecological changes in seawater: Geology, v. 31, p. 801–804.

Rao, V.P., Michard, A., Naqvi, S.W.A., Böttcher, M.E., Krishnaswamy, R., Thamban, M., Natarajan, R., and Borole, D.V., 2002, Quaternary phosphorites off the southeast coast of India: Chemical Geology, v. 182, p. 483–502.

Rao, V.P., Naqvi, S.W.A., Kumar, M.D., Cardinal, D., Michard, A., Borole, D.V., Jacobs, E., and Natarajan, R., 2000, A comparative study of Pleistocene phosphorites from the continental slope off western India: Sedimentology, v. 47, p. 945–960.

Rimmer, S.M., 2004, Geochemical paleoredox indicators in Devonian–Mississippian black shales, central Appalachian basin (USA): Chemical Geology, v. 206, p. 373–391.

Ripley, E.M., Shaffer, N.R., and Gilstrap, M.S., 1990, Distribution and geochemical characteristics of metal enrichment in the New Albany Shale (Devonian-Mississippian), Indiana: Economic Geology, v. 85, p. 1,790–1,807.

Ross, D.J.K., and Bustin, R.M., 2009, Investigating the use of sedimentary geochemical proxies for paleoenvironment interpretation of thermally mature organic-rich strata—Examples from the Devonian-Mississippian shales, western Canadian sedimentary basin: Chemical Geology, v. 260, p. 1–19.

Sageman, B.B., Murphy, A.E., Werne, J.P., Ver Straeten, C.A., Hollander, D.J., and Lyons, T.W., 2003, A tale of shales—The relative roles of production, decomposition, and dilution in the accumulation of organic-rich strata, Middle-Upper Devonian, Appalachian Basin: Chemical Geology, v. 195, p. 229–273.

Sanford, R.F., Pierson, C.T., and Crovelli, R.A., 1993, An objective replacement method for censored geochemical data: Mathematical Geology, v. 25, p. 59–80.

Schieber, J., Southard, J., and Thaisen, K., 2007, Accretion of mudstone beds from migrating floccule ripples: Science, v. 318, p. 1,760–1,763.

Schulz, N.H., and Schulz, H.D., 2005, Large sulfur bacteria and the formation of phosphorite: Science, v. 307, p. 416–418.

Shields, G., Stille, P., and Brasier, M.D., 2000, Isotopic records across two phosphorite giant episodes compared—The Precambrian-Cambrian and the Late Cretaceous-Recent, *in* Glenn, C.R., Prevot-Lucas, L., and Lucas, J., eds., Marine authigenesis—From global to microbial: SEPM (Society for Sedimentary Geology) Special Publication 66, p. 103–115.

Siok, J.P., 1985, Geologic history of the Siksikpuk Formation on the Endicott Mountains and Picnic Creek allochthons, north-central Brooks Range, Alaska: Fairbanks, University of Alaska, master's thesis, 253 p.

Slack, J.F., Dumoulin, J.A., Schmidt, J.M., Young, L.E., and Rombach, C.S., 2004a, Paleozoic sedimentary rocks in the Red Dog Zn-Pb-Ag district and vicinity, western Brooks Range, Alaska—Provenance, deposition, and metallogenic significance: Economic Geology, v. 99, p. 1,385–1,414.

Slack, J.F., Kelley, K.D., Anderson, V.M., Clark, J.L., and Ayuso, R.A., 2004b, Multistage hydrothermal silicification and Fe-Tl-As-Sb-Ge-REE enrichment in the Red Dog Zn-Pb-Ag district, northern Alaska—Geochemistry, origin, and exploration applications: Economic Geology, v. 99, p. 1,481–1,508.

Slack, J.F., Kelley, K.D., and Clark, J.L., 2004c, Whole rock geochemical data for altered and mineralized rocks, Red Dog Zn-Pb-Ag district, western Brooks Range, Alaska: U.S. Geological Survey Open-File Report 2004-1372, accessed January 24, 2011, at http://pubs.usgs.gov/of/2004/1372/.

Slack, J.F., Schmidt, J.M., and Dumoulin, J.A., 2004d, Whole rock geochemical data for Paleozoic sedimentary rocks of the western Brooks Range, Alaska: U.S. Geological Survey Open-File Report 2004-1371, accessed January 24, 2011, at http://pubs.usgs.gov/of/2004/1371/.

Smith, L.B., Jr., and Read, J.F., 2000, Rapid onset of late Paleozoic glaciation on Gondwana—Evidence from Upper Mississippian strata of the Midcontinent, United States: Geology, v. 28, p. 279–282.

Taylor, S.R., and McLennan, S.M., 1985, The continental crust—Its composition and evolution: Oxford, U.K., Blackwell Scientific Publications, 312 p.

Till, A.B., Dumoulin, J.A., Harris, A.G., Moore, T.E., Bleick, H.A., and Siwiec, B., 2008, Bedrock geologic map of the southern Brooks Range, Alaska, and accompanying conodont data: U.S. Geological Survey Open-File Report 2008-1149, 88 p., 2 sheets, sheet 1-scale 1:500,000, sheet 2-scale 1:600,000.

Trappe, J., 1998, Phanerozoic phosphorite depositional systems—A dynamic model for a sedimentary resource system: Berlin, Springer-Verlag, Lecture Notes in Earth Sciences, v. 76, 316 p.

Vallini, D., Rasmussen, B., Krapež, B., Fletcher, I.R., and McNaughton, N.J., 2002, Obtaining diagenetic ages from metamorphosed sedimentary rocks—U–Pb dating of unusually coarse xenotime cement in phosphatic sandstone: Geology, v. 30, p. 1,083–1,086.

Watkins, R.T., Nathan, Y., and Bremner, J.M., 1995, Rare earth elements in phosphorite and associated sediment from the Namibian and South African continental shelves: Marine Geology, v. 129, p. 111–128.

Weisberg, R.H., Black, B.D., and Li, Z., 2000, An upwelling case study on Florida's west coast: Journal of Geophysical Research, v. 105, no. C5, p. 11,459–11,469.

Whalen, M.T., 1995, Barred basins—A model for eastern ocean basin carbonate platforms: Geology, v. 23, p. 625–628.

Whalen, M.T., Dumoulin, J.A., Lukasic, J.J., and White, J.G., 2006, Simultaneous carbonate platform progradation and drowning, Lisburne Group, eastern and central Brooks Range, Alaska [abs.]: Geological Society of America Abstracts with Programs, v. 38, no. 5, p. 86.

Wilson, J.L., and Jordan, C., 1983, Middle shelf, *in* Scholle, P.A., Bebout, D.G., and Moore, C.H., eds., Carbonate depositional environments: American Association of Petroleum Geologists Memoir 33, p. 297–344.

Wright, V.P., 1994, Early Carboniferous carbonate systems—An alternative to the Cainozoic paradigm: Sedimentary Geology, v. 93, p. 1–5.

Wright, V.P., and Burchette, T.P., 1998, Carbonate ramps; an introduction: Geological Society of London Special Publication 149, 465 p.

Young, L.E., 2004, A geologic framework for mineralization in the western Brooks Range, Alaska: Economic Geology, v. 99, p. 1,281–1,306.

Yudovich, Ya.E., and Ketris, M.P. 1997, Geochemistry of black shales, Part I—Outline: Syktyvkar, Russia, Russian Academy of Sciences, Komi Science Centre, 52 p. [in English].

Tables 1–3

Table 1. Phosphorite localities in the Lisburne Group, northern Alaska.

[Localities listed from most allochthonous (Kelly River Allochthon) to parautochthonous; within each structural level, localities listed from west to east. In Chandler Lake quadrangle, Skimo thrust sheet localities listed first, followed by Tiglukpuk thrust sheet, and then thrust sheets south of Skimo thrust sheet. Column 1: numbered localities are shown in figure 1; field numbers in bold indicate localities investigated for this study, or older stations that yielded samples analyzed for this study. Other field numbers from references in Column 9. Collectors (all with U.S. Geological Survey unless stated otherwise): ABe, W. Brosgé; ABo, A. Bowsher; AD, J. Dumoulin; AGr, G. Gryc; AKa, K. Adams (University of Alaska, Fairbanks); AKe, B. Kent; AMu, C. Mull (Alaska Division of Geological and Geophysical Surveys [ADGGS]); APa, W. Patton; ASi, J. Siok (University of Alaska, Fairbanks); (A)Tr, I. Tailleur; CMD, J. Kurtak and co-workers (U.S. Bureau of Mines); JS, J. Slack; My, B. Murchey; PP, Paige Peapples (now Delaney; ADGGS). Column 3: EMA, Endicott Mountains Allochthon; KRA, Kelly River Allochthon; distance below top of Lisburne is to top of phosphorite and black shale or chert interval. Column 5 [and 6-9]: CO, conodont sample; GX, geochemical sample; MS, measured section (of entire exposed Lisburne Group, unless stated otherwise); TS, thin section. Rock types are BS, black shale; G, grainstone; GP, granular phosphorite; M, mudstone; P, packstone; PG, packstone-grainstone; PL, phosphatic limestone; PN, phosphorite nodule; PR, phosphate rock; W, wackestone; WP, wackestone-packstone. Column 6: Thin section data from J. Dumoulin unless stated otherwise in column 9. Column 7: Conodont data from Anita Harris; radiolarian data from Paula Noble; other data from listed sources. CAI, conodont color alteration index. Conodont data sources: (1), Dumoulin and others (2006a); (2), unpublished fossil report; (3), Dumoulin and others, 2008. Column 8: values are maxima for each rock type analyzed from locality; see Appendix table A1 for complete geochemical data for sample numbers in bold; other geochemical data from Patton and Matzko (1959); C_{org}, total organic carbon. Column 9, CHMC, conodont heavy mineral concentrate]

1 Locality no., name (field no.)	2 Quadrangle, latitude N., longitude W. (Sec., T, R)	3 Structural and stratigraphic setting	4 Thickness and characteristics of phosphate zone	5 Data base	6 Thin section features
Loc. 1 **(00AD04, JS-00-02)**	De Long Mtns. B-3 68°17.370' 163°22.040'	KRA (Wulik Peaks plate); uppermost Lisburne Group.	~3 m of recessive black shale contains radiolarian-bearing phosphorite nodules 3-4 cm in diameter.	1 CO 2 GX (BS, PN; see table A1) 2 TS (BS with small PN, PN)	PN: radiolarians, siliceous and calcareous sponge spicules, minor barite.
Loc. 2 **(03AD27, JS-04-23)**	De Long Mtns. B-1 68°23.662' 162°27.326'	KRA (Amphitheatre plate); uppermost Lisburne Group.	<15 m of carbonaceous black shale interbedded with phosphatic limestone that grades to limy phosphate rock; phosphorite nodules to 15 cm in diameter.	1 MS (phosphorite zone only, 03AD27) 2 CO (1 barren) 5 GX (BS, PN; see table A1) 11 TS (BS, PL, PN, PR)	PN: radiolarians, sponge spicules, phosphatic clasts, minor barite. PR, PL: phosphatic peloids > composite grains, ooids; phosphatic crust?; bored bioclasts.
Loc. 3 **(03AD38)**	Misheguk Mtn. B-5 68°27.627' 161°58.391'	KRA (Kelly plate); uppermost Lisburne Group.	≤10 m of carbonaceous black shale interbedded with phosphatic limestone that grades to phosphate rock.	1 MS (phosphorite zone only, 03AD38) 1 CO 3 GX (BS, PL, PR; see table A1) 10 TS (BS, PL, PR)	PL, PR: phosphatic peloids, a few ooids?, partly phosphatized and bored bioclasts (some borings filled with phosphate).
Loc. 4 Mt. Bupto North side **(90AD54, 05AD56, JS-05-93**; 50ATr160 near here) Top (south) **(92AD32-34)**	Howard Pass C-3 North side: 68°31.154' 157°30.188' Top (south): 68°30.660' 157°30.920'	EMA (Ivotuk plate); uppermost Lisburne Group.	~5-20 m of thinly interbedded mudstone, chert, and dolostone; all lithologies are black, phosphatic, and intergradational. 50Tr160 is slumped cutbank of calcareous phosphate rock interbedded with black, bituminous shale, sooty chert, and fine-grained, fetid limestone.	1 MS (92AD33) 2 CO 2 GX (BS; see table A1) 12 TS (BS; also chert, dolostone, and mudstone that contain 1-2% P_2O_5)	Chert, dolostone, and mudstone contain small PN, phosphatic peloids and coated grains (with 1 or 2 layers), radiolarians, spicules.
Loc. 5 Lisburne Ridge West side **(65Tr75, 92AD31, CMD 5803**; 50ATr61) East side **(92AD16)**	Howard Pass C-2 West side: CMD, TR: 68°38.070' 156°44.526' 92AD31: 68°37.967' 156°43.750' East side: 68°37.400' 156°37.080'	EMA (Ivotuk plate); uppermost Lisburne Group.	~1.5-2.4 m of thinly interbedded dolostone, chert, black shale, and granular phosphorite; at least 2 discrete phosphorite intervals, ~10-15 cm thick, made up of 2- to 5- cm-thick beds.	2 MS (92AD16; Armstrong, 1970) 3 CO 4 GX (BS, GP; see table A1) 14 TS (BS, GP; also chert, dolostone, partly silicified WP)	GP: phosphatic peloids, ooids + pisoids (30-50% of some samples, 2 >8 layers), notable radiolarians, quartz silt; matrix is dolomite and organic(?) material. WP: bored bioclasts.

7 Age control, biofacies, CAI	8 Geochemical data		9 Remarks
	P_2O_5 wt %	C_{org} wt %	
Conodonts (from skeletal P just below phosphorite zone): probable Mississippian age; CAI >2 to 3.5-4 (1).	30.91 (**00AD4A**, PN) 9.51 (**JS-00-02**, BS)	4.41 (**JS-00-02**, BS) 2.76 (**00AD4A**, PN)	Loc. 1, Dumoulin and others (2004); loc. 5, Dumoulin and others (2006a).
Conodonts (from skeletal WP ~5 m below top of phosphorite zone): early Chesterian (late Late Mississippian); CAI 2-2.5 (1).	26.22 (**03AD27L**, PN) 10.12 (**JS-04-23A**, BS)	3.04 (**03AD27A**, BS) 1.50 (**03AD27C**, PN)	Loc. 15, Dumoulin and others (2004); loc. 94, Dumoulin and others (2006a). CHMC mainly phosphatic clasts and lesser phosphatized and phosphatic bioclasts.
Conodonts (from skeletal WP ~1 m below top of phosphorite zone): early Chesterian; CAI 2-2.5 (1). Radiolarians (basal 2 m of overlying Etivluk Gp.): late Atokan-Artinskian (middle Pennsylvanian-late Early Permian)(2).	14 (03AD38A, PR) 1.5 (03AD38K, PL) 0.92 (**03AD38C**, BS)	7.68 (**03AD38C**, BS) 1.25 (03AD38K, PL)	Loc. 17, Dumoulin and others (2004); loc. 116, Dumoulin and others (2006a); GX data for 38A, 38K are from J. Dumoulin and J. Slack, unpub. data. CHMC mainly phosphatic and phosphatized rock fragments, minor phosphatic brachiopod fragments, and rare glauconitic grains.
Conodonts (from calcareous radiolarite interbedded with slightly phosphatic chert and dolostone): likely early Chesterian; normal marine, gnathodid biofacies; CAI 1-1.5 (2).	13.7 (50Tr160, PR) 1.42 (**JS-05-93**, BS)	4.47 (**JS-05-93**, BS)	50ATr160 (GX) in Patton and Matzko (1959). See loc. 71, Dover and others (2004) for conodont data from MS. CHMC mainly phosphatic grains and bioclasts; some fluorite.
Conodonts (from dolostone at top of 1.5-m interval of BS, GP): late Meramecian-earliest Chesterian; relatively deep water gnathodid biofacies; CAI 1-1.5 (2; revised by A. Harris 10/04).	26.02 (**65Tr75**, GP) 7.69 (**92AD31H**, BS)	15.90 (**92AD31A**, BS; 20.15 wt % C_{org} from split of this sample analyzed by USGS lab in Denver, CO) 3.84 (**65Tr75,** GP)	See Armstrong (1970) for MS; see locs. 1-3 (Dumoulin and others, 1993) for more conodont data. See Kurtak and others (1995) for more phosphorite geochemistry and discussion of resource potential. 50Tr61 (GX, TS) in Patton and Matzko (1959) contains large dolomite rhombs (confirmed by x-ray analysis) that partly replace some phosphatic peloids; many rhombs have ragged edges due to solution.

Table 1. Phosphorite localities in the Lisburne Group, northern Alaska.—Continued

1 Locality no., name (field no.)	2 Quadrangle, latitude N., longitude W. (Sec., T, R)	3 Structural and stratigraphic setting	4 Thickness and characteristics of phosphate zone	5 Data base	6 Thin section features
Loc. 6 Ivotuk Hills West South outcrop (**90AD59**) North outcrop (**JS-05-82, 05AD44** [also see table 2])	Killik River B-5 South outcrop: 68°28.833' 155°42.750' North outcrop: 68°28.906' 155°42.703'	EMA (Ivotuk plate); upper Lisburne Group (probably ≤10 m below top); north outcrop is folded, structurally complex repeat of upper part of main Lisburne section to south.	North outcrop: ≤3 m (tectonically thickened?) of interbedded phosphorite and dark gray shale that overlies black fetid dolostone; at least 3 normally graded phosphorite beds, 2-8 cm thick; phosphatic clasts (to 2 cm in diameter) in shale, dolostone.	2 MS (90AD59; 05AD44 of phosphorite zone only) 2 CO (1 barren) 3 GX (BS, GP; see table A1) 9 TS (GP, BS, phosphatic dolostone)	GP: phosphatic peloids dominant, many with "wormy" (bored?) texture; <5-30% ooids (2-7 layers); minor composite grains, quartz silt, radiolarians, spicules; dolomite (± calcite?) cement, phosphatic(?) mud. Dolostone: phosphatic peloids, ooids.
Loc. 7 Lisburne 1 well (**7,450-15,350 ft** [also see table 2]))	Killik River B-5 68°29.133' 155°41.417'	EMA (Ivotuk plate; 5 distinct thrust sheets); uppermost Lisburne Group.	Clasts of granular phosphorite seen in cuttings ~7-21 m (24-70 ft) below top of Lisburne Group (as located in Legg, 1983) in plates 1, 2, 4, and 5.	5 TS (cuttings) with GP [7,450-80 ft (2 ts); 9,710-40 ft; 13,760-90 ft; 15,320-50 ft (#2)]	GP: phosphatic peloids, coated grains (1-2 layers), composite grains, spicules, radiolarians.
Ivotuk Hills East (**05AD42**)	Killik River B-5 68°28.423' 155°33.642'	EMA (Ivotuk plate); upper Lisburne Group.	~1-2 m total section; fine rubble of granular phosphorite, phosphatic dolostone, and radiolarian chert in grassy tundra, between exposures of main Lisburne section and overlying Siksikpuk Formation.	4 TS (GP, phosphatic dolostone; also radiolarian chert, silicified skeletal P)	GP: phosphatic peloids, ~5% ooids (≤4 layers); spicules, radiolarians; phosphatic mud matrix and phosphatic cement.
Loc. 8 Akmalik Creek East (**05AD65,** ~85AMu2 [also see table 2]))	Killik River B-2 68°22.055' 154°10.401'	EMA (Killik River sequence of Mull and others, 1994); upper Lisburne Group (~15-20 m below top).	~17-20 m of black shale, platy limestone, and phosphorite (C.G. Mull; unpub. field notes, 1985); phosphorite layer at least 40 cm thick.	1 MS (C. Mull) 1 CO 2 GX (GP) 5 TS (GP)	GP: phosphatic peloids, ooids (≤80%); bored hardground(?); radiolarians; calcite and phosphatic cement.
Okpikruak River (85ASi18; Petro-Canada section)	Killik River C-1 Siok section: 68°32.300' 153°28.500' PC section: 68°32.355' 153°27.783'	EMA (Okpikruak River sequence of Mull and others, 1994); upper Lisburne Group (~10-20 m below top); section here <50 m thick (fault at base).	~15 m of interbedded black sooty shale, lime mudstone, peloidal phosphorite, and chert (chert beds thin and decrease upward); local carbonate concretions contain radiolarians.	1 CO 1 GX (BS)	No TS data available.
Loc. 9 Monotis Creek (**05AD6, 7; CMD 4518**)	Chandler Lake B-5 05AD6: 68°22.900' 152°51.490'-530' 05AD7: 68°22.800' 152°50.915'	EMA (Skimo thrust sheet); top of shale and phosphorite unit is ~185 ft (~56 m) below top of Lisburne Group (Patton and Matzko, 1959).	Three distinct phosphorite occurrences here: on both sides of an anticline and at a 2nd locality to the south. ~7-10 m of interbedded granular phosphorite, black shale, and fine-grained carbonate (beds and concretions [60 cm max diam]); 2-4 phosphatic zones, 30 cm-3.4 m thick. Beds cannot be correlated across 600 m (Patton and Matzko, 1959).	8 MS (Brosgé and Reiser 1951; Patton and Matzko; 1959; Kurtak and others, 1995) 1 CO 2 GX (BS, GP; see table A1) 8 TS (BS, GP; also chert, dolostone, lime M)	GP: phosphatic peloids> ooids, composite grains; phosphatic crust(?); radiolarians, spicules, quartz silt; silica> carbonate cement. BS: abundant phosphatic peloids.
Little Chandler Lake (45AGr21; locs. in Brosgé and Reiser, 1951)	Chandler Lake B-5 (several sites, approximately located, in T13S, E part R3W and W part R2W)	EMA (Skimo thrust sheet and 2 others to south); ~35 m below top of Lisburne Group.	Black, medium- to coarse-grained oolitic phosphatic rock, in float and possibly in place.	2 MS (Brosgé and Reiser 1951) 1 GX (GP) 1 TS (GP)	GP: phosphatic peloids, ooids (0.5–1.4 mm diam) in matrix of calcite, dark (organic?) material, and purple fluorite.
Siksikpuk River (**05PP63**)	Chandler Lake B-4 68°19.015' 152°20.216'	EMA (Skimo thrust sheet); likely ~60-110 m below top of Lisburne Group.	Small phosphorite outcrop in cutbank on east side unnamed fork of Siksikpuk River, associated with large carbonate concretions.	1 CO 2 GX (GP, see table A1) 1 TS (GP)	GP: phosphatic peloids, minor coated grains (1 layer); abundant quartz silt; rare spicules, radiolarians.

7 Age control, biofacies, CAI	8 Geochemical data		9 Remarks
	P_2O_5 wt %	C_{org} wt %	
Conodonts (from dolostone 2 m above GP at north outcrop): early Chesterian; CAI 1-1.5 (2). See Dumoulin and Harris (1993) for conodont data from south outcrop (90AD59).	31.56 (**JS-05-82B,** GP) 2.42 (**JS-05-82C,** BS)	17.36 (**JS-05-82C,** BS) 3.22 (**JS-05-82B,** GP)	North outcrop: Kelley and Mull (1995) show phosphorite here. See Kurtak and others (1995) for more phosphorite geochemistry and discussion of mineralogy, extent, and resource potential of phosphorite; these authors interpreted host unit as Otuk Formation, but conodont data disprove this. South outcrop: Slump swale on south-facing dip slope exposes upper 5 m of Lisburne Group, which is thinly interbedded black limestone, chert, and phosphorite (C.G. Mull, written commun., 2005).
Foraminifers indicate an age of late Meramecian-early Chesterian (Mamet Zone 14-16) for the phosphatic interval in all 4 plates (Legg, 1983).			GP grains in plates 1, 2, and 5 have a matrix of phosphatic(?) mud and dolomite cement; those in plate 4 have a matrix of spiculitic chert.
			GP here contains 5-10% glauconite grains, and several clasts of glauconitic spiculitic siltstone.
Conodonts (from ~5-8 above top of phosphorite interval): early Chesterian; relatively shallow to moderately deep biofacies; CAI 2.5 (2).	36.98 (**05AD65K2**, GP)	1.52 (**05AD65K2**, GP)	85AMu2 in C.G. Mull, unpub. field notes, 1985. Kelley and Mull (1995) show phosphorite here, and suggest "considerable" lateral extent for the phosphorite in the Killik River quadrangle.
Conodonts (from highest exposed Lisburne Group): no older than earliest Morrowan (Early Pennsylvanian) with redeposited Chesterian forms; CAI 1-1.5 (2).		8.84 (BS, J. Lukasic, written commun., 2005)	85ASi18 in J. Siok, unpub. field notes, 1985; other information from J. Lukasic and M. McDonough, Petro-Canada Oil and Gas Co., 2005. Structurally, rocks are ~on trend with (just north of) Tiglukpuk thrust sheet to east and Ivotuk plate to west. Lithologically, they resemble rocks of the Killik River sequence of Mull and others (1994).
Conodonts (from 8x30 cm concretion of carbonaceous lime M with radiolarians and spicules; GP beds occur 1-2 m above and below): early Chesterian; deep, anoxic biofacies; CAI 1-1.5 (3). Earliest Chesterian cephalopods from phosphatic interval at several localities near here (Gordon, 1957).	19.35 (**CMD4518**, GP) 7.91 (**05AD6E**, BS)	15.0 (**05AD6E**, BS) 1.48 (**CMD4518**, GP)	Loc. 5, Dumoulin and others (2008). See Kurtak and others (1995) for 5 MS and data on phosphorite geochemistry, mineralogy, extent, and resource estimate; see Patton and Matzko (1959) for 2 MS and Brosgé and Reiser (1951) for 1 MS. Conodonts in concretion abundant (>500 specimens) but low diversity; many pristine, delicate forms, suggesting deposition via fecal pellets.
	25.6 (45AGr21, GP)		Phosphatic interval occurs in lower Kiruktagiak member of Lisburne Group of Brosgé and Reiser (1951), who map it in 3 thrust sheets here and show it in 2 MS; 45AGr21 (GX and TS) in Patton and Matzko (1959).
Conodonts (from 05PP59C, bioclastic G slightly SE of 63, near top of Lisburne Group): Chesterian; CAI 1.5-2 (3).	20.57 (**05PP63CG,** GP) 13.36 (**05PP63FG,** GP)	3.52 (**05PP63CG**, GP) 2.25 (**05PP63FG**, GP)	Close to loc. 8 (05PP59C, Dumoulin and others, 2008). Note lower $P_2O_5 + C_{org}$ content in more loosely packed rock with calcite cement (63FG) versus tightly packed rock with silica cement (63CG).

Table 1. Phosphorite localities in the Lisburne Group, northern Alaska.—Continued

1 Locality no., name (field no.)	2 Quadrangle, latitude N., longitude W. (Sec., T, R)	3 Structural and stratigraphic setting	4 Thickness and characteristics of phosphate zone	5 Data base	6 Thin section features
Loc. 10 Confusion Creek (**04AD9, CCP** [J. Dumoulin section]; Petro-Canada section)	Chandler Lake B-4 68°17.500' 152°01.061'	EMA (Skimo thrust sheet); ~110 m below top of Lisburne Group (J. Lukasic, written commun., 2003).	Ten discrete phosphorite intervals (4-40 cm thick) in 8.25-m-thick zone within 12 m section of upper part of shale and phosphorite unit; phosphorites typically cap cycles of shale grading up into lime mudstone ± chert. Local chert and lime mudstone concretions; abundant radiolarians, especially in lower part of section.	2 MS (Petro-Canada; CCP [J. Dumoulin] of phosphorite zone only) 1 CO 15 GX (6 BS, 9 GP; see table A1) 39 TS: 6 BS, 11 GP, 15 lime M, 7 chert	GP: phosphatic peloids (some with quartz silt, radiolarians, spicules, bioclasts), lesser ooids (≤10 layers), composite grains, nodules. Calcite cement in most samples; local quartz, fluorite, dolomite cement.
Loc. 11 Skimo Creek (**03AD2; SKB** [J. Dumoulin, M. Whalen section], **SKBo**; see Remarks for other sections)	Chandler Lake B-4 SKB: 68°17.735' 151°54.869' SKBo: 68°17.773' 151°54.609'	EMA (Skimo thrust sheet); ~170 m below top of Lisburne Group.	Shale and phosphorite unit is ~30 m thick; contains 5 phosphorite intervals (10-40 cm thick, in upper 9-12 m of unit) that cap cycles of shale grading up into lime mudstone. Locally abundant carbonate and chert concretions contain radiolarians and sponge spicules.	5 MS (see Remarks) 3 CO 6 GX (4 BS [3 C_{org} only], 2 GP; see table A1) 21 TS (4 BS, 6 GP, 2 PL, 4 lime M, 4 carbonate and chert concretions, 1 P)	GP: phosphatic peloids (quartz silt), lesser ooids (≤10 layers), composite grains, nodules (to 1 cm diam), ?crusts; local radiolarians. Matrix: calcite, quartz, minor fluorite cement; minor phosphatic mud.
South Tiglukpuk Creek (**04AD8**; **CMD 4617,** 75Tr1, and 80My7-10 near here)	Chandler Lake B-4 68°18.180' 151°50.400'	EMA (Skimo thrust sheet); ~160 m below top of Lisburne Group.	9.8 m of oolitic to pisolitic phosphorite interbedded with black shale and limestone; 5 phosphorite beds ~5-35 cm thick and several thinner beds. Local phosphorite nodules (to 2 cm max diam); zone of siliceous concretions (to 0.5 x 3 m) ~6 m below main phosphorite interval.	2 MS near here (section SC3 in Kurtak and others, 1995, and section 2 in Patton and Matzko, 1959) 6 CO (Tr, My) 2 GX (GP; see table A1) 3 TS (GP)	GP: phosphatic peloids, ooids (1-50%, ≤7 layers), composite grains; some layers normally graded. Radiolarians, elongate shells. Cement: quartz, dolomite [8D]; calcite, phosphatic mud [CMD].
Akmagolik Creek (**03AD10**; 50AKe279 near here)	Chandler Lake B-3 68°17.860' 151°42.660'	EMA (Skimo thrust sheet); probably ~150 m below top of Lisburne Group.	25-30 m of interbedded black shale, lime mudstone, and phosphorite (several beds, ≤40 cm thick; nodules to 0.5 cm). Minor chert beds and nodules; abundant carbonate concretions (10-30 cm max diam).	2 GX (GP; see table A1) 3 TS (GP, lime M)	GP: phosphatic peloids (some contain abundant quartz silt), lesser ooids (2->4 layers); calcite, minor fluorite cement.
Anaktuvuk River West (50ABo76; loc. in Brosgé and Reiser, 1951)	Chandler Lake B-3 (secs. 13 and (or) 24, T13S, R2E)	EMA (Skimo thrust sheet); ~150->170 m below top of Lisburne Group.	Phosphatic rock similar to that at Anaktuvuk River East locality but from dipslope on opposite side of river.	1 MS (Brosgé and Reiser, 1951) 1 GX (PR?) 1 TS (PR?)	PR?: phosphatic peloids (with abundant quartz) and ooids in calcite matrix with fluorite and carbonaceous matter.
Anaktuvuk River East (50ABo78; near Petro-Canada loc.)	Chandler Lake B-3 (secs. 28 and (or) 33, T13S, R3E)	EMA (Skimo thrust sheet?); ≥150 m below top of Lisburne Group.	Phosphorite is thin stringers in calcareous shale with chert and limestone nodules (concretions?); ~13 m above base of black chert and shale member and >800 m above base of Lisburne Group.	1 GX (GP) 1 TS (GP)	GP: phosphatic peloids (with abundant quartz) and ooids in calcite matrix with fluorite and carbonaceous matter.
Lawrence Livermore Drillholes (Brosgé and Armstrong, 1977)	Chandler Lake B-4 (sec. 26, T12S, R1W; 2 drillholes, 170 m apart; DH 1 [west] and DH 2 [east])	EMA (likely Tiglukpuk thrust sheet); ~100-120 m below top of Lisburne Group.	Peloidal phosphorite occurs near base of ~20 m of black shaly limestone with chert nodules; phosphorite in layers 1-1.5 m thick (1 layer in DH1, 2 in DH2).	Lithology and geochemistry of cuttings reported in Brosgé and Armstrong (1977)	GP: black phosphatic peloids to 1 mm.
West Tiglukpuk anticline (**05AD2**)	Chandler Lake B-4 68°22.595' 151°57.078'	EMA (Tiglukpuk thrust sheet); ~110 m below top of Lisburne Group.	Rubble of phosphorite, phosphatic limestone, spiculitic chert, and lime mudstone (10 cm thick bed) overlie skeletal supportstone (with bored bioclasts seen in TS).	1 CO 1 GX (GP; see table A1) 13 TS (GP, PL, also spiculitic chert, lime M, peloidal-skeletal PG)	GP: phosphatic peloids, ooids (≤7 layers), nodules (≤7 mm diam); spicules, radiolarians. Matrix: quartz and calcite cement, lime and phosphatic mud.

7 Age control, biofacies, CAI	8 Geochemical data		9 Remarks
	P_2O_5 wt %	C_{org} wt %	
Conodonts (from skeletal PG ~40 m above top of shale and phosphorite unit): early Chesterian; high energy, near- shoal biofacies; CHMC has abundant phosphatic clasts and bioclasts; CAI 1.5-2 (3).	25.67 (**CCP-4.85**, GP) 11.54 (**CCP-3.4**, BS)	9.43 (**CCP-3.4**, BS; C_{org} values in BS increase up section, then decrease) 6.73 (**04AD9H**, GP)	Loc. 4, Dumoulin and others (2008). MS from J. Lukasic and M. McDonough, Petro-Canada Oil and Gas Co., 2003. Some phosphorite layers reversely graded; others normally graded. Ooids most abundant (30-50%) near middle of section; composite grains most notable in upper half of section. One TS from this locality is a complex granular phosphorite with 4 distinct layers that differ in composition and grain size.
Conodonts (from within, and ~38 m above, GP zone): earliest Chesterian; sample from lime M in GP zone is a winnow into relatively deep water; CAI 1 or 1.5-2 (3). Early Chesterian cephalopods from just above phosphatic zone (Gordon, 1957).	23.84 (**03AD2B**, GP) 0.5 (**SKBo25**, BS)	5.32 (**SKBo25**, BS; see Dumoulin and others, 2008 for C_{org} data from 3 BS in SKB) 3.78 (**03AD2B**, GP);	Loc. 1, Dumoulin and others (2008). See Patton and Matzko (1959) and Kurtak and others (1995) for MS and more on phosphorite chemistry, extent, and resource estimate; MS also in Brosgé and Reiser (1951), Armstrong and others (1970), and Armstrong and Mamet (1977, 1978). Black shales examined in TS from this locality contain abundant phosphatic peloids and nodules. Also see table 2.
Conodonts all from limestone beds in shale and phosphorite unit; most restricted age (80My7C) is early Chesterian; CAIs are 1.5, 1-5-2, and 2 (2).	22.04 (**CMD 4617-1**, GP) 30 (GP, Patton and Matzko, 1959) 9-15.5 (BS, Kurtak and others, 1995)	3.57 (**04AD8D**, GP)	Loc. 7, Dumoulin and others (2008). See Patton and Matzko (1959) and Kurtak and others (1995) for MS and more on phosphorite chemistry, extent, and resource estimate. Ro and T_{max} data from upper Lisburne Group near here in Johnsson and others (1999) and K. Bird, written commun., (2002).
	28.62 (**03AD 10B,** GP) 27.9 (50AKe 279, GP)	1.21 (**03AD 10B,** GP)	Loc. 3, Dumoulin and others (2008); local brachiopods, notable nautiloid cephalopods here. 50AKe279 (GX) in Patton and Matzko (1959) from ~1-1.5 mi north (3 mi south of Natvakruak Lake).
	± 15 (50ABo76, PR?)		50ABo76 (GX, TS) in Patton and Matzko (1959); MS in Brosgé and Reiser (1951).
Late Mississippian (~late Meramecian) cephalopods (Gordon, 1957) from 86 m (282 ft) below top of black chert and shale member.	21.4 (50ABo78, GP)		50ABo78 (GX, TS) in Patton and Matzko (1959); Petro-Canada locality a few mi to east (secs. 35 and (or) 36, T13S, R3E; written commun., Paige Peapples, 2005).
Foraminifers from nearby outcrops suggest a Meramecian-early Chesterian age for these rocks (Brosgé and Armstrong, 1977).	9.41 (DH2, sample 36)		Brosgé and Armstrong (1977); P_2O_5 values from testing with ammonium molybdate; other samples in DH2 had values of 0.74, 2.14, and 5.92 wt % P_2O_5.
Conodonts (from peloidal-skeletal PG, likely just below GP): early Chesterian; abundant (>700) and represent a winnow; CAI 1.5-2 (3).	21.35 (**05AD2C**, GP)	1.84 (**05AD2C**, GP)	Loc. 11, Dumoulin and others (2008); similar rocks occur 2 km SW at loc. 12. One TS from this locality is a complex granular phosphorite with 4-6 unconformably bounded layers that differ in grading, matrix composition, and phosphatic particle types and sizes. CHMC contains glauconite and pyrite.

Table 1. Phosphorite localities in the Lisburne Group, northern Alaska.—Continued

1 Locality no., name (field no.)	2 Quadrangle, latitude N., longitude W. (Sec., T, R)	3 Structural and stratigraphic setting	4 Thickness and characteristics of phosphate zone	5 Data base	6 Thin section features
North Tiglukpuk Creek (**TNC** [M. Whalen, J. Dumoulin section])	Chandler Lake B-4 68°21.870' 151°52.440'	EMA (Tiglukpuk thrust sheet); ~110 m below top of Lisburne Group. Main phosphorite at TNC 191.6 m; phosphatic limestone from 189.3-199 m.	Rubble of lime mudstone and granular phosphorite (beds ≤5 cm thick; interval ≤1-2 m), overlain by graded skeletal-peloidal supportstone (bioclasts variously micritized and phosphatized), underlain by lime mudstone and spiculitic chert.	1 MS [TNC; part of TN] 1 CO 1 GX (GP, see table A1) 8 TS (GP, PL)	GP: phosphatic peloids, many ooids and pisoids (100 μ-4 mm diam, ≤6 layers); notable quartz silt, some bioclasts; cement: silica, minor calcite and fluorite.
Loc. 12 Shainin Lake (**KW91V** [K. Watts, J. Dumoulin section]; Bowsher and Dutro, 1957)	Chandler Lake B-2 KW91V, 105.6 m: 68°20.3' 151°00.6'	EMA (Tiglukpuk thrust sheet, or a structural level between the Skimo and Tiglukpuk sheets, W. Wallace, pers. commun., 2006); ~26 m below top of Lisburne Group (Dumoulin and others, 1997).	Black chert and shale member of Bowsher and Dutro (1957) is ~11-15 m thick and contains 2 intervals, 0.75-1 m thick, of interbedded grayish brown, calcareous, carbonaceous shale and black phosphorite(?) in thin beds and nodules.	3 MS (Bowsher and Dutro, 1957; Armstrong and Mamet, 1977; Dumoulin and others, 1997) 1 CO 1 TS (skeletal P)	No TS data available on phosphorite. Skeletal P that yielded conodonts contains bored bioclasts; some bioclasts have micritic rims.
East and West of Anaktuvuk Pass (Porter, 1966)	Chandler Lake A-3 (SW ¼ T14S, R2E; NW ¼ T15S, R3E)	EMA (unnamed thrust sheets south of Skimo thrust sheet); ~243 m below top of Lisburne Group.	Middle member of Alapah (75-83 m thick) consists of dark, recessive, calcareous shale, chert, platy limestones, and argillaceous phosphorite.		No TS data available.
"Agiak Lake" (51APa52, 53; 51ABe92, 93)	Wiseman D-6 (southern third T37N, R23W; north of Agiak Creek)	EMA (south of Toyuk thrust fault); at top of Lisburne Group.	Grainy phosphate interval ≤3 m thick overlies massive black chert (~5 m thick) above ~30 m of black, locally calcareous shale.	1 MS (Brosgé, unpub. field notes)	No TS data available.
Ekokpuk Creek (78ABe232, 233; 84AKa15)	Chandler Lake A-5 AKa15: 68°4.000' 152°45.700'	EMA (south of Toyuk thrust fault); near top of Lisburne Group (78ABe 232); ~15 m below top (78ABe233).	232: ~15 m of black laminated chert and sooty limestone with two phosphatic, fluoritic intervals. 233: ~15 m of shale with scattered phosphate grains; underlies 15 m of black limestone and overlies 15-30 m of black chert.	3 MS (2 in W. Brosgé, unpub. field notes; 1 [upper Lisburne Gp. only] in Adams, 1991).	No TS data available on phosphorite. TS from associated lithologies (from K. Adams) are spiculite, chert, dolostone.
"Ekokpuk Mt." (75Tr15.2)	Chandler Lake A-4 (sec 2, T17S, R2W [loc. approximate, near confluence of John River and Ekokpuk Creek])	EMA (south of Toyuk thrust fault); 45 m below top of Lisburne Group.	~10 m of peloidal phosphorite interbedded with dark limestone (with local phosphatic peloids, bioclasts) and chert; 2 or 3 graded(?) phosphatic zones (5-20 cm thick) ~3-6 m above base of interval have phosphatic peloids to 1.5 cm diam.	1 MS (I. Tailleur, unpub. field notes) 2 CO	No TS data available.
Till Creek (Armstrong and Mamet, 1978; A. Armstrong, unpub. notes)	Wiseman D-4 (NW ¼ sec. 11, T36N, R19W)	EMA (>2 thrust sheets south of Soakpak Mtn.; south of Toyuk thrust fault); ~140 m below top of Lisburne Group.	5-10 m of interbedded chert and lime mudstone with abundant blue-gray phosphatic pisolites above 32 m of thinly interbedded black shale, radiolarian chert, and argillaceous, spiculitic, locally phosphatic lime mudstone.	1 MS and TS data (Armstrong and Mamet, 1978; A. Armstrong, unpub. notes)	GP (235, 237 m in MS): phosphatic peloids (≤2 mm diam) in sparry calcite matrix. PL (213, 209 m in MS): 10-30% phosphatic peloids (50-150μ).
Tinayguk River (Armstrong and Mamet, 1978; A. Armstrong, unpub. notes; 84AKa1)	Wiseman D-3 (NE ¼ sec. 35, T37N, R16W)	EMA (thrust sheet south of sheet that contains Alapah Mt; south of Toyuk thrust fault); ~168 m below top of Lisburne Group.	~30 m of phosphatic lime mudstone to skeletal packstone, interbedded with black shale and spiculitic limestone; megafossils include mollusks, cephalopods, pelecypods, and brachiopods.	2 MS (Armstrong and Mamet, 1978; K. Adams, unpub. notes) 1 CO 10 TS (PL, lime M, WP, PG from K. Adams)	PL ± PN at 345, 354, 356, 372 in MS (A. Armstrong, unpub. notes); PL [TS from K. Adams]: phosphatic nodules (3-7 mm diam.), radiolarians.

7 Age control, biofacies, CAI	8 Geochemical data		9 Remarks
	P_2O_5 wt %	C_{org} wt %	
Conodonts (from PL just above GP): early Chesterian; abundant (>2000) and represent a winnow; CAI 1.5-2 (3).	20.62 (**TNC 191.6F**, GP)	2.25 (**TNC 191.6F**, GP)	Loc. 2, Dumoulin and others (2008); chert and phosphorite unit ≥35 m thick. Phosphatic peloids here contain notable quartz silt and aggregate grains. Skeletal PG just above GP (TNC 208.6 m) contains some calcareous ooids. CHMC contains abundant phosphatized rock fragments and bioclasts.
Conodonts (from skeletal P ~6 m above base of black chert and shale member), foraminifers, and goniatite cephalopods (*G. americanus* [was *G. crenistria*]): late Meramecian-early Chesterian; CAI 2 (2).			MS, description of phosphorite, cephalopod data: Bowsher and Dutro (1957); MS, foraminifer data: Armstrong and others (1970), Armstrong and Mamet (1977); additional cephalopod data: Dutro (1987); MS: Dumoulin and others (1997). Diverse conodont assemblage indicates normal-salinity, open-marine setting (A. Harris, unpub. fossil report).
			Porter (1966, pp. 956 [map], 967 [lithologic description]).
			W. Brosgé, unpub. notes; unpub. MS provided by K. Bird. Lisburne Group here ~110 m thick; underlies Siksikpuk Fm. (yellow clay at base), overlies Kayak Shale; consists of ~70 m of black shale and chert above ~40 m of limestone.
Phosphatic intervals at 78ABe 232, 233 yielded goniatite cephalopod *G. americanus* (late Meramecian-early Chesterian) (W. Brosgé, unpub. notes).			W. Brosgé, unpub. field notes (1978); unpub. MS provided by K. Bird. At 232, ≤21 m of Lisburne Group underlies Siksikpuk Fm.; lower 6 m is radiolarian chert; base of section is a fault. Uppermost Lisburne yielded middle Chesterian foraminifers (Mamet Zone 18) at 232 and latest Chesterian goniatites at AKa15 (Dutro, 1987).
GP interval yielded late Meramecian-early Chesterian brachiopods but also Osagean conodonts (reworked?); Mid. Devonian-Early Mississippian conodonts occur ~25-50 m below GP; CAI 5, 5.5 (2).			I. Tailleur, unpub. field notes (1975); unpub. MS provided by K. Bird. Lisburne Group here ~150-155 m thick; underlies Siksikpuk Fm. (orange-weathering at base), above Kayak Shale (contact covered); consists of ~45 m of limestone above a 10-m-thick phosphatic zone above 95 m of cherty limestone, chert, and dolostone.
Foraminifers of early Chesterian (Mamet Zone 16s) age 40 m above top of GP interval (Armstrong and Mamet, 1978).			Thickness, lithologies, and microfacies of phosphatic zone here, as described by Armstrong and Mamet (1978), sound very similar to that of phosphatic zone at Skimo Creek (loc. 11 above).
Phosphatic interval yields late Meramecian foraminifers (Armstrong and Mamet, 1978) and late Meramecian-early Chesterian conodonts; CAI 4-4.5 (2).			MS, TS descriptions from Armstrong and Mamet (1978) and A. Armstrong, unpub. notes; MS (phosphatic zone only), TS (examined by J. Dumoulin) from K. Adams. Uncertain if these strata are phosphorites or less-phosphatic rocks. Phosphatic nodules in AKa TS made up mostly of phosphatic peloids and bioclasts.

Table 1. Phosphorite localities in the Lisburne Group, northern Alaska.—Continued

1 Locality no., name (field no.)	2 Quadrangle, latitude N., longitude W. (Sec., T, R)	3 Structural and stratigraphic setting	4 Thickness and characteristics of phosphate zone	5 Data base	6 Thin section features
Lisburne Peninsula (Section 68A-9; Armstrong and Mamet, 1977)	Point Hope C-2 (NW ¼ sec. 33, T8S, R60W; S side of Cape Lewis)	Parautochthonous (Young, 2004) or EMA (Lisburne Hills sequence; Mayfield and others, 1988); ~792-914 m (2,600-3,000 ft) below top of Lisburne Group.	Phosphatic nodules in shale, limestone, and sandstone ~30-60 m (100-200 ft) and 182 m (600 ft) above base of Lisburne Group, in lower part of Nasorak Fm.	1 MS and TS data (Armstrong and Mamet, 1977)	TS data (in Armstrong and Mamet, 1977) indicates phosphatic rocks are interbedded with glauconitic P and spiculite.
Loc. 13 Ikpikpuk 1 well (**14,600-650 ft**)	Teshekpuk B-3 70°27.333' 154°19.883'	Arctic Slope parautochthon (Young, 2004); ~990.6 m (3,250 ft) below top of Lisburne Group.	Phosphatic grains in cuttings from 14,600-14,650 ft (~15 m thick zone) associated with dark mudstone, spiculite, and muddy skeletal packstone.	4 TS (cuttings) with GP [14,600 ft, 14,610 ft, 14,630 ft, and 14,640 ft]	GP: peloids, ooids(?), rare quartz sand and bioclasts; calcite cement.

Table 2. Less-phosphatic localities in the Lisburne Group, northern Alaska.

[All samples were analyzed for this study unless stated otherwise in column 9. Samples included have ≥1 wt % P_2O_5, and (or) contain visible phosphate in thin section and (or) conodont heavy mineral concentrates. Samples grouped by age and then structural level (structurally highest [Kelly River Allochthon] to lowest [parautochthonous]); within these groupings, listed from west to east. Diamond drill hole localities from Red Dog district listed in increasing numeric order. Column 1: numbered localities are shown in figure 1. Collectors (all with U.S. Geological Survey unless stated otherwise): ACh, R. Chapman; AD, J. Dumoulin; AKa, K. Adams (University of Alaska, Fairbanks); ALS, A. Strauch (Alaska Division of Geological and Geophysical Surveys [ADGGS]); AMu, C. Mull (ADGGS); ASi, J. Siok (University of Alaska, Fairbanks); DDH, diamond drill core samples from deposits in the Red Dog district, collected by J. Slack; JS (1991-94), J. Schmidt; JS (2003-05), J. Slack; KE, K. Evans; PP, Paige Peapples (now Delaney; ADGGS). MS, measured section (of entire exposed Lisburne Group unless stated otherwise). Column 3: EMA, Endicott Mountains Allochthon; PCA, Picnic Creek Allochthon; KRA, Kelly River Allochthon; distance below top of Lisburne Group is to top of phosphatic interval. Akmalik Chert, Kuna Formation, and Tupik Formation are formations of the Lisburne Group. Column 5 [and 6-9]: For most localities, only phosphatic GX and TS samples are listed; other GX and TS samples of non-phosphatic lithologies may have been taken at these stations. CHMC, conodont heavy mineral concentrate; CO, conodont sample; GX, geochemical sample; TS, thin section. Rock types are BS, black shale; G, grainstone; M, mudstone; P, packstone; PBS, phosphatic black shale; PG, packstone-grainstone, PL, phosphatic limestone; PW, packstone-wackestone. Other abbreviations: abt, abundant; ph, phosphatic. Column 6: Thin section data from J. Dumoulin unless stated otherwise in column 9. Column 7 (and 9): Conodont data from Anita Harris; other data from listed sources. CAI, conodont color alteration index. Data sources: (1), unpublished USGS fossil report; (2), Dumoulin and Harris (1993); (3), Dumoulin and others (2006a); (4), Dover and others (2004); (5), Dumoulin and others (1993); (6), Dumoulin and others (2008); (7), Dumoulin and others (1997); (8) Till and others (2008). Column 8: n.a., not available]

1 Locality no., name (field no.)	2 Quadrangle, latitude N., longitude W.	3 Structural and stratigraphic setting	4 Thickness and characteristics of phosphatic strata	5 Data base	6 Evidence for and (or) details of phosphate
					Phosphatic strata of known or probable
(06AD22)	Misheguk Mt. C-5 68°32.778' 161°48.181'	PCA?; position within Lisburne Group uncertain.	Phosphatic, skeletal grainstone (1- to 8-cm thick platy beds); forms 1-m-thick lens in section of thinly interbedded carbonate and non-carbonate mudstone.	1 CO (22B) 1 TS (22B: PL)	CHMC: Very abt ph clasts and >1500 conodonts. TS: few-5% ph peloids (200µ-1.5 mm diam).
Loc. 6 Ivotuk Hills West (90AD59 [MS], 91JS39 [also see table 1])	Killik River B-5 68°28.906' 155°42.703'	EMA (Ivotuk plate); lower Lisburne Group (Dumoulin and Bird, 2002; these rocks called Kayak Shale by Dumoulin and Harris, 1993).	45 m of black shale and mudstone, subordinate beds of chert, spiculite, and dolostone. Basal 2.1 m has 2 intervals of supportstone (lower is 1.5 m thick, upper is 0.5 m thick, 5-to 10-cm-thick beds) that contain tracks and possible mud cracks.	1 CO (59C) 2 GX (39B, C: both BS) 3 TS (59A: lower PG [PL]; 59C, CC: upper PG [PL])	TS: lower PG has minor ph patches; upper PG (hardground?) has 5-25% ph bioclasts > clasts (irregular peloids, ooids?, ≤5 mm diam).
Loc. 7 Lisburne 1 well (7,450-15,350 ft [also see table 1])	Killik River B-5 68°29.133' 155°41.417'	EMA (Ivotuk plate; 5 distinct thrust sheets); lower Lisburne Group (unit I of Legg, 1983).	Interval of shale, mudstone, quartz siltstone to sandstone, and limestone that is locally glauconitic and phosphatic; found in plates 1, 3, 4, and 5; interval thickness varies from 9 m (plate 4) to ≤45 m (plate 3).	6 TS (cuttings) contain PL with ph grains; 2 in plate 3 (12,390-420, 510-540 ft) and 4 in plate 5 (16,270-310 ft). Additional cuttings data in Legg (1983).	TS (cuttings) from unit I in plates 3 and 5 contain skeletal P, G with notable phosphatic bioclasts and clasts (like those in 90AD59C described above).

7 Age control, biofacies, CAI	8 Geochemical data		9 Remarks
	P_2O_5 wt %	C_{org} wt %	
Foraminifers indicate an age of early Chesterian (Mamet Zone 16) for both phosphatic zones.			Armstrong and Mamet (1977; see plates 40, 41). Uncertain if these strata are phosphorites or less-phosphatic rocks. Stratigraphic position near base of Lisburne Group is like that of phosphorite in Ikpikpuk well.
Foraminifers indicate an age of early Chesterian (Mamet Zone 16) for the phosphatic interval (Dumoulin and Bird, 2001).			Phosphatic interval occurs near top of lower limestone unit of Dumoulin and Bird (2001, p. 148).

7 Age control, biofacies, CAI	8 Geochemical data		9 Remarks
	P_2O_5 wt %	C_{org} wt %	
Osagean (late Early Mississippian) age			
Conodonts (from 22B): middle Osagean (*Sc. anchoralis-D. latus* Zone); mixed biofacies; CAI 2.5-3 (1).			Grainstone layer may be a turbidite; highly irregular shape of some ph clasts suggests they may have been deposited while semi-lithified; some ph clasts contain quartz silt.
Conodonts (from upper PG): early Osagean; derived from a range of shelf environments; fauna has mix of traits characteristic of both Kuna Formation and Kayak Shale; CAI 1.5 (1, 2).	No GX from phosphatic rocks.	39B: 1.38 39C: 1.31	Conodont data (Dumoulin and Harris, 1993) suggest possible unconformity between early Osagean strata (called Kayak Shale by these authors) and overlying late Meramecian strata (lower unit of Lisburne Group of these authors). 39C GX data are intermediate between those typical of Kayak Shale and Kuna Formation.
Foraminifers indicate that this interval in all plates is of Mamet Zone 12/13 age (Osagean-Meramecian boundary; Legg, 1983).			These rocks may be low-stand deposits (above an unconformity) and may represent a hardground and (or) exposure surface. Core 18 spans the unit I/J boundary; the mixed age fauna from this core (Dutro and Silberling, 1988) may reflect older forms reworked along the unconformity.

Table 2. Less-phosphatic localities in the Lisburne Group, northern Alaska.—Continued

1 Locality no., name (field no.)	2 Quadrangle, latitude N., longitude W.	3 Structural and stratigraphic setting	4 Thickness and characteristics of phosphatic strata	5 Data base	6 Evidence for and (or) details of phosphate
Phosphatic strata of known or probable middle or late Meramecian-early Chesterian (Late Mississippian) age;					
(04AD39)	De Long Mts. A-3 68°13.725' 163°13.020'	KRA (?Wulik Peaks plate); uppermost Lisburne Group.	At least several meters of crinoidal-brachiopod packstone-wackestone, locally dolomitic, glauconitic, and phosphatic.	1 CO (39A) 3 TS (39A, D, E: all PL).	CHMC: abt ph bioclasts. TS (PL): ≤15% ph bioclasts (some bored), clasts, nodules (≤2 mm).
(06AD21)	Misheguk Mt. C-5 68°32.447' 161°41.036'	KRA (Kelly plate); highest exposed Lisburne Gp. (rubble), overlain by 2 m of grassy cover, then rubble of Siksikpuk Fm.	2 rubbly layers, each several dm thick, of crinoidal supportstone (in irregular, 5-cm-thick beds) with ≤5% black phosphatic grains.	1 CO (21C) 4 TS (21C-E, CC: all PL)	PL (4 TS) contains ph peloids, rare composite ph grains, and partly ph bioclasts.
(99AD19)	De Long Mts. B-2 68°21.933' 162°49.908'	PCA (Wulik plate); highest carbonate bed in Lisburne Group; underlies grassy swale with float of black silicified mudstone.	0.5-m-thick irregular outcrop of crinoidal grainstone with 3- to 4-mm-long black mud clasts; many bioclasts partly or totally replaced by phosphate.	1 CO (19D) 1 TS (19D: PL)	CHMC: ph composite grains, bioclasts, and steinkerns. TS (PL): 10-25% ph clasts, bioclasts, patches (≤1.7 mm diam).
Stack barite deposit (05AD50)	Howard Pass C-3 50F: 68°36.056' 157°30.160' 50L: 68°36.031' 157°36.032'	PCA; Akmalik Chert.	Layer (~0.5 m thick) of distinctive, lightweight, silver-weathering, phosphatic "oil shale" (interbedded with radiolarian chert, calcareous radiolarite); underlies barite.	1 CO (91TR23) 2 TS (50F, L: both "oil shale")	"Oil shale" in TS: ph clasts (60-300µ, ovoid to elongate) are 10-15% in 50F, few % in 50L.
Bion barite deposit (05AD51, 91JS31)	Howard Pass C-3 68°37.032' 157°30.160'	PCA; Akmalik Chert.	Distinctive, lightweight, silver-weathering, phosphatic "oil shale" (interbedded with radiolarian chert and calcareous radiolarite) in rubble and subcrop; underlies barite.	1 CO (91Tr17) 1 GX (31D: "oil shale") 2 TS (31D, 51C: both "oil shale")	"Oil shale" in TS: ph clasts (60-200µ, ovoid to elongate) are 10-20% in 31D and abt in 51C.
(94JS17)	Howard Pass C-5 68°33.132' 158°44.316'	EMA (Key Creek-Aniuk plates); near top of Kuna Formation.	Platy black shale (beds <5 cm thick, laminae <1 mm), yellow bloom on weathering surface.	1 GX: (17T: PBS)	GX only; no TS data.
(94JS19)	Howard Pass C-5 68°33.636' 158°38.586'	EMA (Key Creek-Aniuk plates); Kuna Formation.	Black siliceous mudstone without obvious coarser-grained layers.	1 GX (19A: PBS)	GX only; no TS data.
(94JS7)	Howard Pass B-4 68°20.484' 158°09.666'	EMA (Key Creek-Aniuk plates); Kuna Formation above Kayak Shale.	Black sooty shale (laminae ≤5 mm thick).	1 GX (7A: PBS)	GX only; no TS data.
(92AD74, JS-05-96)	Howard Pass B-3 68°19.500' 157°43.830'	EMA (Key Creek-Aniuk plates); Kuna Fm. (74: near top of formation; 96: position unknown).	74 is black, platy, silty mudstone 8 m below contact with Siksikpuk Fm.; 96 is black mudstone from lower(?) in section.	2 GX (74C, 96: both PBS) 1 TS (74C: PBS)	74C TS: abt quartz silt, ≤10% ph bioclasts and clasts (most irregular, silt-sized).
(94JS9)	Howard Pass B-3 68°26.286' 157°40.632'	EMA (Key Creek-Aniuk plates); upper part of Kuna Formation.	H, K: spiculitic, cherty mudstone interbedded with bioturbated limestone ~5 m below top of Lisburne Group; L: chert ≥20 m lower.	3 GX (9H, K, L: all PBS)	GX only; no TS data.
(JS-05-94, 05AD57)	Howard Pass C-3 68°31.000' 157°35.695'	EMA (Key Creek-Aniuk plates); Kuna Formation.	Black sooty shale (94) interbedded with dolostone (57A) and chert (57D).	1 GX (94; no TS match) 2 TS (57A, D)	57A TS: few % ph clasts and bioclasts to 2 mm diam.
(93JS7)	Howard Pass B-2 68°19.668' 156°55.536'	EMA (Key Creek-Aniuk plates); Kuna Formation above Kayak Shale.	Black, sooty, laminated shale associated with gray bioturbated limestone.	2 GX (7C, J: both PBS)	GX only; no TS data.

7 Age control, biofacies, CAI	8 Geochemical data		9 Remarks
	P_2O_5 wt %	C_{org} wt %	
some samples from Kuna Formation could be older (Osagean?, late Early Mississippian)			
Conodonts (from PL): late Meramecian-early Chesterian; outer shelf or deeper; CAI 2 (3).			Loc. 8, Dumoulin and others (2006a). 39A from uppermost Lisburne Gp. (beds 10-30 cm thick); D, E from distinctive yellow-weathering interval, with platy beds (1-2 cm thick), 2-4 m lower in section.
Conodonts (from PL): Mississippian (likely Late Mississippian); CAI 2.5-3 (1).			Grassy zone may be underlain by shale. CHMC is chiefly phosphatized composite grains, crinoid columnals, and tube fillings, plus phosphatic shell fragments.
Conodonts (PL): early Chesterian or younger (with re-worked Osagean forms); lag concentrate with mix of mostly outer-shelf to off-shelf forms; CAI 2.5 (3).			Loc. 35, Dumoulin and others (2006a). In TS, see one composite grain made of smaller phosphatic peloids, at least some of which are coated grains (1-2 layers).
Conodonts (from calcareous radiolarite layer in the barite body): late Osagean-Meramecian (probably middle Meramecian); CAI 1.5-2 (4).			Loc. 40, Dover and others (2004).
Conodonts (from limy layer in barite): Mississippian; CAI 1.5-2 (4).	31D: 1	31D: 22	Loc. 30, Dover and others (2004); Slack and others (2004d). Ph bioclasts? (≤1 mm diam) in 31D TS; trace glauconite? in 51C TS. Chert (25 m above 91Tr17) contains Late Mississippian-Early Pennsylvanian radiolarians (4).
No age control here, but sample from upper part of Kuna Fm.	1.38	n.a.	Slack and others (2004d). Drenchwater area.
No age control here.	1.02	n.a.	Slack and others (2004d). Drenchwater area.
No age control here.	3.68	n.a.	Slack and others (2004d).
Conodonts (8 m below top of nearby section 92AD35): late Osagean-Meramecian; CAI 3 (4).	74C: 5.59 96: 3.36	74C: 8.4 96: 5.41	Type section of Kuna Fm., loc. 146, Dover and others (2004); Slack and others (2004d). Other TS from beds a few meters above and below 74C are mudstone with silt, radiolarians, and (or) spicules.
No age control here.	H: 5.60 K: 1.31 L: 1.68	n.a.	Slack and others (2004d).
91Tr05b near here: Silurian-Permian conodonts; CAI 1.5-2) (4).	1.24	11.02	J. Slack, unpub. GX data (2008).
No age control here.	7C: 3.15 7J: 2.69	7C: 6.38 7J: 6.58	Slack and others (2004d). Near Kuna Basin-carbonate platform transition.

Table 2. Less-phosphatic localities in the Lisburne Group, northern Alaska.—Continued

1 Locality no., name (field no.)	2 Quadrangle, latitude N., longitude W.	3 Structural and stratigraphic setting	4 Thickness and characteristics of phosphatic strata	5 Data base	6 Evidence for and (or) details of phosphate
(92AD9)	Howard Pass C-2 68°36.666' 156°45.414'	EMA (Key Creek-Aniuk plates); Kuna Formation.	Sooty mudstone with dolostone beds (and concretions?).	2 GX (9B, C: [P]BS) 2 TS (9B, C: [P]BS)	9B TS: mudstone with ≤10% orange ph clasts (200-400μ diam).
(91JS19)	Howard Pass B-1 68°20.682' 156°06.336'	EMA (Key Creek-Aniuk plates); Kuna Formation.	Sooty, platy, locally phosphatic black shale; stratigraphic position within Lisburne Group uncertain.	1 GX (19B: PBS) 1 TS (19B: PBS)	TS is spiculitic shale with few % ph bioclasts and clasts.
(91JS20)	Howard Pass B-1 68°21.300' 156°03.834'	EMA (Key Creek-Aniuk plates); Kuna Formation.	Cherty section with rare shaly, locally phosphatic? laminae (1-3 mm thick).	1 GX (20C: PBS)	GX only; no TS data.
(91AD1 [MS], 91JS4)	Killik River B-5 68°19.800' 155°30.916'	EMA (Key Creek-Aniuk plates); Kuna Formation (23.5 m above Kayak Sh., upper contact of Kuna Fm. not exposed here.)	Siliceous, phosphatic mudstone with thin, clast-rich layers; local spicules, radiolarians, and evidence of bioturbation.	2 CO 2 GX (1B-3.0, 4G: both PBS) 2 TS	No TS match GX, but TS from ~0.4 m below, and 1.7 m above, 1B-3.0 have abt ph? mud clasts (0.3-1 mm diam).
Oolamnagavik River (50ACh55)	Killik River B-3 (NW ¼ T11S, R11W)	EMA (Key Creek-Aniuk plates); Kuna(?) Formation.	~9 m of black shaly siltstone with beds and concretions (0.3-1 m diam) of petroliferous limestone.	1 GX (55) 1 TS (55)	TS: quartz siltstone with carbonaceous cement and a few ph nodules.
(99AD4 [MS]; near 98AD10)	De Long Mts. A-2 68°14.340' 162°54.85'	EMA (Red Dog plate); Kuna Formation (chert-rich upper part of Ikalukrok unit).	≥15 m of interbedded chert, siliceous mudstone, and carbonate rocks (including calcareous radiolarite).	2 CO (98AD10A, 8-16-83C) 1 GX (4L) 1 TS (4L)	TS: siliceous mudstone with crystalline apatite, minor spicules and radiolarians.
Shear Creek (JS03-1B, 03AD20)	De Long Mts. A-2 68°08.073' 162°47.85'	EMA (Red Dog plate); Kuna Formation (Ikalukrok unit).	Black shale.	1 GX (JS03-1B)	GX only; no TS data.
(DDH 551A, 88.5 ft)	De Long Mts. A-2 68°04.609' 162°50.320'	EMA (Red Dog plate); Kuna Fm. (Ikalukrok unit); Aqqaluk deposit.	Siliceous black shale with fluorapatite and pyrite laminae.	1 GX (88.5 ft)	GX only; no TS data.
(DDH 552, 624.5 ft)	De Long Mts. A-2 68°04.644' 162°49.706'	EMA (Red Dog plate); Kuna Fm. (Ikalukrok unit); Aqqaluk deposit.	Black shale with pyrite laminae, minor sphalerite and galena.	1 GX (624.5 ft)	GX only; no TS data.
(DDH 806, 1,866.5, 2,305 ft)	De Long Mts. A-2 68°09.688' 162°57.344'	EMA (Red Dog plate); Kuna Fm. (Ikalukrok unit); Anarraaq deposit.	1866.5: siliceous black shale; 2305: black shale with pyrite and fluorapatite.	2 GX (1,866.5, 2,305 ft)	GX only; no TS data.
(DDH 809, 2,006-2,427 ft)	De Long Mts. A-2 68°09.688' 162°57.745'	EMA (Red Dog plate); Kuna Fm. (Ikalukrok unit); Anarraaq deposit.	2,006, 2,275.5: black shale with pyrite and minor sphalerite; 2,079: calcareous lithic turbidite; 2,288, 2,295: black shale; 2,363.5: black shale with abundant pyrite, minor sphalerite, and fluorapatite; 2,427: black shale with pyrite, sphalerite, galena, and fluorapatite.	7 GX (2,006, 2,079, 2,275.5, 2,288, 2,295, 2,363.5, 2,427 ft) 1 TS (2,079 ft)	TS from lithic turbidite (2079 ft) contains notable phosphatic clasts.
(DDH 812, 1,981 ft)	De Long Mts. A-2 68°09.583' 162°58.533'	EMA (Red Dog plate); Kuna Fm. (Ikalukrok unit); Anarraaq deposit.	Calcareous lithic turbidite.	1 GX (1,981 ft)	No TS match GX, but see Remarks.
(DDH 924, 2,169.5, 2,197.5 ft)	De Long Mts. A-2 68°09.810' 162°57.544'	EMA (Red Dog plate); Kuna Fm. (Ikalukrok unit); Anarraaq deposit.	2,169.5: black shale with pyrite and sphalerite; 2,197.5: siliceous, semi-massive pyrite with fluorapatite.	2 GX (2,169.5, 2,197.5 ft)	GX only; no TS data.

7 Age control, biofacies, CAI	8 Geochemical data		9 Remarks
	P_2O_5 wt %	C_{org} wt %	
No age control here.	9B: 1.20	9B: 5.39 9C: 4.84	Slack and others (2004d). Near Kuna basin-carbonate platform transition. 9B TS much like samples from Mt. Bupto (loc. 4, table 1) and 91JS31D (Bion barite deposit, above).
Conodont sample here (19A) was barren.	4.68	5.54	Loc. 10, Dumoulin and others (1993); Slack and others (2004d). Near Kuna Basin-carbonate platform transition.
No age control here.	2.73	4.55	Slack and others (2004d). Near Kuna Basin-carbonate platform transition; chert beds near GX sample contain minor radiolarians and spicules.
Conodonts (from 12.25 m and 21 m above base of section): Osagean-Meramecian; CAI 3 (5).	1B-3.0: 3.89 4G: 1.58	1B-3.0: 5.01 4G: 3.98	Loc. 14, Dumoulin and others (1993); Slack and others (2004d). 1B-3.0 from ~20 m below top of Kuna Fm.; 4G from "upper Kuna Formation." Locality is close to Kuna Basin-carbonate platform transition.
No age control here.	1.4		TS and GX from Patton and Matzko (1959); location approximate.
Combination of conodont and radiolarian data here restricts age to early Chesterian; CAI~3, 4 (3).	2.25	1.37	Loc. 3, Dumoulin and others (2004); loc. 41, Dumoulin and others (2006a); Slack and others (2004d).
No age control on Ikalukrok unit here.	2.91	3.96	Slack and others (2004d).
No age control here.	1.51	1.01	Slack and others (2004c); see also fig. 8, Slack and others (2004b).
No age control here.	1.06	7.49	Slack and others (2004c); see also fig. 9, Slack and others (2004b).
No age control here.	1,866.5: 1.24 2,305: 2.44	1,866.5: 3.98 2,305: 5.42	Slack and others (2004c); see also fig. 10, Slack and others (2004b).
No age control here.	2,006: 1.09 2,079: 1.43 2,275.5: 1.02 2,288: 1.18 2,295: 1.01 2,363.5: 5.44 2,427: 6.11	2,006: 2.73 2,079: 0.96 2,275.5: 2.71 2,288: 1.88 2,295: 1.72 2,363.5: 3.15 2,427: 1.53	Slack and others (2004c); see also fig. 11, Slack and others (2004b).
No age control here.	1.63	2.26	J. Slack, unpub. data (2004). TS from similar turbidite <1 m higher (1.978.5 ft) has phosphatic clasts (≤1 mm diam) that contain radiolarians.
No age control here.	2,169.5: 1.19 2,197.5: 2.78	2,169.5: 3.77 2,197.5: 3.20	Slack and others (2004c).

Table 2. Less-phosphatic localities in the Lisburne Group, northern Alaska.—Continued

1 Locality no., name (field no.)	2 Quadrangle, latitude N., longitude W.	3 Structural and stratigraphic setting	4 Thickness and characteristics of phosphatic strata	5 Data base	6 Evidence for and (or) details of phosphate
(DDH 942, 1,912.5 ft)	De Long Mts. A-2 68°09.891' 162°57.736'	EMA (Red Dog plate); Kuna Fm. (Ikalukrok unit); Anarraaq deposit.	Calcareous gray shale.	1 GX (1912.5 ft)	No TS match GX, but see Remarks.
(KE98-25)	De Long Mts. A-2 68°07.000' 163°08.600'	EMA (Wolverine Creek plate; Rok window); top of Lisburne Group.	Dolomitic, silicified skeletal grainstone with local vugs that contain dead oil.	1 CO (25A)	CHMC: Abt ph composite grains and bioclasts.
(00AD21)	De Long Mts. A-2 68°05.900' 163°06.950'	EMA (Wolverine Creek plate; Rok window); ~10 m below top of Lisburne Group.	Dolostone with chert and relict crinoidal debris.	1 CO (21A)	CHMC: notable ph bioclasts and steinkerns.
(KE98-27)	De Long Mts. A-2 68°12.598' 162°52.800'	EMA (Wolverine Creek plate; Mt. Raven window); position within Lisburne Group uncertain.	Partly silicified dolostone with local vugs that contain dead oil.	1 CHMC (27) 1 TS (27: dolostone)	CHMC: ph bioclasts. TS: minor intercrystalline ph(?) material.
(99AD13)	De Long Mts. A-2 68°13.470' 162°50.473'	EMA (Wolverine Creek plate; Mt. Raven window); highest carbonate bed in Lisburne Group.	Carbonate bed is fine-grained, organic-rich dolostone with peloids and rare bioclasts; underlies a few meters of black chert.	1 CO (13I) 1 TS (13I: phosphatic dolostone)	CHMC: abt ph peloids, composite grains, and steinkerns. TS: few % ph clasts.
			Phosphatic strata of known or probable late early-late Chesterian (late Late		
(06AD27)	Misheguk Mt. C-4 68°33.120' 161°12.200'	KRA; uppermost Lisburne Group (uppermost Tupik Formation).	35-cm-thick layer of phosphatic crinoidal supportstone is highest exposed Lisburne Group here.	1 CO (27L) 5 TS (27 G, H, I, J, L: all are GP with minor ph)	CHMC: abt conodonts, (>900), ph bioclasts. TS: minor ph, bored bioclasts, micritic clasts.
(05AD64)	Killik River B-3 68°122.839' 154°12.404'	PCA; basal unit of Imnaitchiak Chert (unit F of Siok, 1985) just above Akmalik Chert.	Silicified oncolitic grainstone, with local phosphate, glauconite, and barite; layer ≤50 cm thick; oncolites ≤11 cm in diam.	2 TS (64D, 04ADonc: both are oncolitic G with ph)	TS: minor ph as clasts (≤4 mm), matrix, and replacing and filling radiolarian tests.
Loc. 6 Ivotuk Hills West (top of south section) (85ASi14-18, 92AD41, 05AD58 [see table 1])	Killik River B-5 68°28.600' 155°42.500'	EMA (Ivotuk plate); uppermost Lisburne Group.	10 m of outcrop (dipslope; ~4? m section) of bioturbated siliceous spiculite interbedded with siltstone and silty mudstone, beds even to nodular, 2-15 cm thick; overlies 30-50 m of cover above top of main Ivotuk section (90AD59); Siksikpuk Formation exposed in nearby scarp.	2 CO (Si14-18; 41A) 8 TS (41A-C, AA; 58A-D)	TS: minor ph clasts, bioclasts (and glauconite clasts) in silty mudstone (58A), siliceous and (or) calcareous spiculite (41A, AA, 58B-D), and quartz-carbonate siltstone (41B).
Loc. 6 Ivotuk Hills West (top of north section) (05AD44 [see table 1])	Killik River B-5 68°28.906' 155°42.703'	EMA (Ivotuk plate); uppermost Lisburne Group.	Uppermost 6-10 m of section are green-gray, glauconitic, carbonate siltstone in undulatory beds 1-40 cm thick; abundant trace fossils include *Zoophycus*.	1 CO (44N) 12 TS (44S, W: ph dolostone; 44E, K, L, N, P, R, T; Ivo-0, -3, -4: slightly ph dolostone [44N has spicules; 44P, Ivo-4 have quartz silt])	TS: 5-25% ph peloids, ≤15% glauconite in 44S, W; others have minor ph and glauconite; a few ph ooids in 44L, S; ph nodules (>1.3 cm diam) in 44T.

7 Age control, biofacies, CAI	8 Geochemical data		9 Remarks
	P_2O_5 wt %	C_{org} wt %	
No age control here.	1.16	0.85	Slack and others (2004c). TS (1,908.8 ft) from 1.5-m-thick turbidite that begins immediately above this shale contains notable (≤5%) phosphatic clasts.
Conodonts (from dolomitic G): Chesterian; outer shelf or deeper; CAI 2.5 (3).			Loc. 14, Dumoulin and others (2004); loc. 73, Dumoulin and others (2006a).
Conodonts (from dolostone): very early Chesterian; shallow-water, near high-energy setting; CAI 3.5-4 (3).			Loc. 15, Dumoulin and others (2004); loc. 75, Dumoulin and others (2006a).
Conodont sample from this locality was barren (3).			Loc. 44, Dumoulin and others (2006a).
Conodonts (from ph dolostone): late Meramecian-early Chesterian; slope setting; CAI 4 (3).			Loc. 4, Dumoulin and others (2004); loc. 42, Dumoulin and others (2006a). Ph clasts and bioclasts in TS mostly 140-400 μ diam; clasts rounded to ovoid.
Mississippian) and (or) very earliest Morrowan (early Early Pennsylvanian) age			
Conodonts (27L): late Chesterian-middle Morrowan (with redeposited late Early and early Late Mississippian forms); CAI 3-3.5 (1).			
Akmalik Chert is Early-Late Mississippian (Blome and others, 1998).			Radiolarians of Meramecian-Chesterian age occur below unit F; radiolarians of Morrowan (to Chesterian?) age occur above unit F (Siok, 1985).
Conodonts (Si14-18, "gray-black micrite to sparite, 11 m below top of Lisburne," J. Siok unpub. notes, 1985): latest Chesterian; CAI 1.5 (2).			41A (siliceous spiculite with minor glauconite, matrix of mud and carbonate, 1 m below top of outcrop) yielded conodont fragments of indeterminate age, CAI 1-1.5; CHMC is chiefly fluorite, phosphatized composite grains, and probable pyrite. Lithologies here similar to SKA 219-221 (Skimo Creek section; see below) but conodonts are older.
Conodonts (from dolostone 2 m above ph rocks): early Chesterian? (if single element of *B. utahensis* in this fauna is reworked, sample could be of younger Chesterian age); CAI 1-1.5 (1).			Lithologies here resemble those of SKA 187, 219-221 (Skimo Creek section), suggesting late early Chesterian (or younger) age. CHMC contains abundant phosphatized composite grains (including some bioclasts) as well as phosphatic brachiopod fragments.

Table 2. Less-phosphatic localities in the Lisburne Group, northern Alaska.—Continued

1 Locality no., name (field no.)	2 Quadrangle, latitude N., longitude W.	3 Structural and stratigraphic setting	4 Thickness and characteristics of phosphatic strata	5 Data base	6 Evidence for and (or) details of phosphate
Loc. 8 Akmalik Creek East (05AD65 ~85AMu2 [see table 1])	Killik River B-2 68°22.055' 154°10.401'	EMA (Killik River sequence of Mull and others, 1994); ~5-6 m below top of Lisburne Group.	4-5 m of dark-weathering skeletal packstone-wackestone, beds 5-25 cm thick; uppermost ≥10 cm of this interval contains notable glauconite and phosphate.	1 CO (Mu2-10) 4 TS (65D: glauconitic P; 65E: glauconitic ph quartz sandstone (hardground?); 65F, G: glauconitic ph PW)	TS: 65E (highest) has 30-40% glauconite, 20-30% ph clasts (peloids, a few ooids) and nodules; 65F, G have ≤5% ph clasts and bioclasts.
(05AD8; 05PP22 very near here)	Chandler Lake B-4 68°16.905' 152°11.621'	EMA (unnamed thrust sheet just south of Skimo thrust sheet); upper Lisburne Group.	35-cm-thick bed of crinoidal supportstone (with ≤10% glauconite) overlain by 6-8 m of dark, laminated mudstone.	1 CO (8C) 2 TS (8C, 22: PL)	TS: minor ph grains (8C); 2 partly ph nodules (≤2 mm diam; 22).
Northwest Soakpak Mt. (04AD13)	Chandler Lake A-4 68°11.728' 151°53.967'	EMA (unnamed thrust sheet south of Skimo thrust sheet); upper Lisburne Group.	Outcrop and rubble of skeletal supportstone and wackestone and quartz-carbonate sandstone; all lithologies bioturbated, and contain notable phosphate and glauconite.	1 CO (13A) 5 TS (13A, AA, E: ph PG; D: ph W; F: ph quartz-carbonate sandstone)	TS: ph bioclasts, pore fillings, patches in A, AA; ph bioclasts, clasts (≤2 mm diam; contain spicules, silt) in D-F.
Northwest Soakpak Mt. (04AD12)	Chandler Lake A-4 68°11.998' (to 11.881') 151°51.953' (to 51.509')	EMA (unnamed thrust sheet south of Skimo thrust sheet); upper Lisburne Group.	Subcrop and rubble of bioturbated, phosphatic skeletal supportstone (with glauconite, quartz, pyrite) and variously phosphatic and glauconitic quartz and (or) carbonate siltstone.	6 TS (12B, C, H: ph PG; 12F, G, J: ph siltstone).	TS: ph peloids (≤3.5 mm diam), bioclasts in all; ph ≤7-10% in 12H, J, minor in others; silt, spicules in ph clasts in 12J; ph nodule (1 cm diam) in 12B.
West Soakpak Mt. area (84/85AKa16 [MS, plate 5 in Adams, 1991])	Chandler Lake A-4 68°12.25' 151°51.35'	EMA (unnamed thrust sheet south of Skimo thrust sheet); uppermost Lisburne Group.	Crinoidal limestone with notable glauconite, phosphatic clasts and nodules, and pyrite; some bioclasts bored and (or) partly phosphatized; directly underlies Siksikpuk Fm. (contact is sharp and undulatory).	1 CO (16-1) 1 TS (16-1: PL)	TS: skeletal PW-M with ph nodule (>1cm diam; cut by borings?), few % ph peloids and bioclasts, and ≤5% glauconite; may be a hardground.
East side of Soakpak Mt. (SOAK-TOP)	Chandler Lake A-3 ~68°13' 151°40' (location approximate)	EMA (unnamed thrust sheet south of Skimo thrust sheet); uppermost Lisburne Group.	Pelmatozoan-bryozoan grainstone with notable ph clasts + bioclasts.	1 CO 1 TS [both from same bed]	TS: few % ph bioclasts (some only partly replaced) and rounded ph peloids (200-400μ diam).
Gray Mt. (84AKa17 [MS, plate 2 in Adams, 1991])	Wiseman D-3 67°56.300' 151°15.200'	EMA (south of Toyuk thrust fault); uppermost Lisburne Group.	Uppermost Lisburne Group is calcareous siltstone; basal Siksikpuk Formation is sandy siltstone with phosphatic pebbles (≤5 cm diam).	Lithologic description in Adams (1991).	Adams reports pyrite-rimmed ph? clasts (≤2 cm diam.) in uppermost Lisburne Group.
Siksikpuk River (05PP59)	Chandler Lake B-4 68°18.664' 152°19.981'	EMA (Skimo thrust sheet); upper Lisburne Group.	Crinoid-bryozoan grainstone (59C) overlain by silty mudstone (59A) and siliceous spiculite (59Y, Z).	1 CO (59C) 4 TS (59A, C, Y, Z)	TS: minor ph patches (59C), ph bioclasts and clasts (59A), and 2 ph nodules (≤ 2 mm; 59Y).
Loc. 11 Skimo Creek (SKA 178-187 [Dumoulin, Whalen MS]; also see table 1)	Chandler Lake B-4 ~68°17.840' 151°55.070'	EMA (Skimo thrust sheet); ~34 m below top of Lisburne Group.	SKA 178-186: brachiopod supportstone, overlain by calcareous shale and mudstone. SKA187: 45-cm-thick interval (omission surface?) of bioturbated skeletal grainstone with notable ph clasts, glauconite, lesser quartz sand; some bioclasts bored.	2 CO (SKA 178, 187) 2 GX (C_{org} only: SKA 180.5, 183.5; both BS) 5 TS with ph and (or) glauconite (SKA 180.5, 181: BS; 186.75, 187.05, 187.1C: ph G)	TS: ?ph nodule (1x2cm) in SKA 181 (BS); ph bioclasts in SKA 186.75, 187.05, 187.1C; rounded ph clasts in SKA 187.1C.
Encampment Creek (05AD9 [MS, upper Lisburne Group only])	Chandler Lake B-4 68°22.592' 152°06.565'	EMA (Tiglukpuk thrust sheet); upper Lisburne Group.	Poorly exposed interval (1-2 m thick) of bioturbated, muddy, calcareous siltstone, with 5-10% glauconite and pyrite, and a few phosphatic clasts and nodules.	1 CO (9I) 3 TS (9I, J, K: all ph muddy siltstone)	TS: I, J, K have minor rounded to irregular ph clasts (≤300μ diam); ph bioclasts and nodules (to 800μ diam) in I.

7 Age control, biofacies, CAI	8 Geochemical data		9 Remarks
	P_2O_5 wt %	C_{org} wt %	
Conodonts: very abundant; Chesterian; moderate water depth or deeper; CAI 2.5 (1). CHMC: abt ph bioclasts, including crinoid, ostracode, and bryozoan fragments (1).			65E likely correlates with SKA 187 (Skimo Creek section); 65D, F, G may correlate with ~SKA 181. Additional TS data: 65D has fitted fabric, ≤10% glauconite. 65E has 10-20% quartz sand, ≤10% pyrite, silica cement; some ph peloids contain abt spicules. Bored bioclasts in 65D, F.
Conodonts (8C): Chesterian, CAI 1.5-2 (6).			Loc. 9, Dumoulin and others (2008). 8C may correlate with SKA 187 (Skimo Creek section). Bored bioclasts (8C, 22?); CHMC yielded glauconite-filled radiolarians(?) and ph steinkerns.
Conodonts (from 13A): Chesterian (not earliest); CAI 1.5-2; CHMC chiefly ph clasts and bioclasts (6).			Loc. 14, Dumoulin and others (2008). 13A, AA may correlate with ~SKA 178 (Skimo Creek section); 13D-F correlate with SKA 187. Additional TS data: most abt, biggest ph grains in F (≤7%); some bored bioclasts (and ph clasts?) in E.
No age control here.			Close to K. Adams measured section 84/85AKa16. Glauconite ≤10-20% in 12H, J, ≤5% in others. 12B, C, could correlate with SKA 178 (Skimo Creek section); 12H, J, very similar to SKA 187; 12F, G could correlate with SKA 219-221, or 05AD9 siltstone (Encampment Creek, see below).
Conodonts: latest Mississippian-earliest Pennsylvanian (no younger than lower *D. noduliferus* Zone); CAI 2.5-3 (6).			Loc. 15, Dumoulin and others (2008). K. Adams (unpub. field notes) describes "phosphatic clasts" (≤1 cm diam) near top of Lisburne Group here; her MS of upper Lisburne Group only. TS (from K. Adams, examined by J. Dumoulin) contains some bioclasts with phosphate-filled borings.
Conodonts: very late Chesterian; lag concentrate; CAI 2.5-3 (6).			Loc. 18, Dumoulin and others (2008); sample collected by geologists from Petro-Canada Oil and Gas Co. CHMC: mostly ph brachiopod fragments, lesser phosphatized lithic and crinoid fragments.
No age control here; regional relations suggest upper Lisburne Group is late Late Mississippian.			Adams (1991); MS of upper Lisburne Group only.
Conodonts: abt (>500); Chesterian; relatively shallow water, high energy setting; CAI 1.5-2 (6).			Loc. 8, Dumoulin and others (2008). 59C likely correlates with SKA 178 (Skimo Creek section); 59C TS contains some partly ph bioclasts. Glauconite minor in 59C; 5-30% in Y and Z.
Conodonts (from both): Chesterian; CAI 1.5. Conodonts (from SKA 187): not earliest Chesterian; drowned lag concentrate (6).		180.5: 1.79 183.5: 1.68	Loc. 1, Dumoulin and others (2008). Conodonts in SKA 187 fairly abundant (>180); CHMC mainly pyritic, glauconitic, ph carbonate rock fragments, with minor ph bioclasts and fluorite crystals. CHMC from SKA 178 contains glauconite.
Conodonts (from 9I): early Chesterian; CAI 1.5-2 (6).			Loc. 13, Dumoulin and others (2008). This interval may correlate with SKA 187 (Skimo Creek section).

Table 2. Less-phosphatic localities in the Lisburne Group, northern Alaska.—Continued

1 Locality no., name (field no.)	2 Quadrangle, latitude N., longitude W.	3 Structural and stratigraphic setting	4 Thickness and characteristics of phosphatic strata	5 Data base	6 Evidence for and (or) details of phosphate
Erratic Creek (PP 03 026, 27)	Chandler Lake B-2 68°21.552' 150°47.663'	EMA (thrust sheet uncertain); upper Lisburne Group.	Crinoidal supportstone with minor phosphatic bioclasts.	1 CO (27) 1 TS (26: ph PG) [both from same bed]	TS: minor ph bioclasts and glauconite.
Atigun Gorge West (90KW H [Dumoulin, Watts MS, upper Lisburne Group])	Philip Smith Mts. B-5 (NW ¼ sec. 25, T12S, R10E)	EMA (unnamed thrust sheet); upper Lisburne Group.	Uppermost 7.5 m of Lisburne Group is bryozoan wackestone (with lenses of supportstone) that contains rare to minor phosphate, most notably in the upper 1 m of section. Overlying Siksikpuk Fm. is heterogeneous, ranging from lime mudstone to pebbly sandstone.	3 CO 51 TS (43 from Lisburne Group; 8 from Siksikpuk Formation)	TS: minor ph bioclasts, rounded ph clasts, and ph skeletal pore fillings.
Atigun Gorge East (90KW F [Dumoulin, Watts]; AKa21 [Adams]; both are MS, upper Lisburne Gp.)	Philip Smith Mts. B-4 KW F: 68°29.25' 149°08.833' AKa21: 68°27.583' 149°16.0'	EMA (unnamed thrust sheet); upper Lisburne Group.	Uppermost 15 m of Lisburne Group consists of several cycles of skeletal grainstone grading up into wackestone and (or) packstone; overlying Siksikpuk Fm. is quartz siltstone and sandstone. Minor phosphate and glauconite in uppermost Lisburne and lower Siksikpuk.	2 CO 23 TS (Lisburne Group: 7 from KW F, 11 from AKa21; Siksikpuk Formation: 5 from KW F)	TS: minor rounded ph and glauconite clasts in KW F, with possible ph hardground ≥10 m below top of Lisburne Group. Ph nodules (≤6 mm diam) and bioclasts in AKa TS.
					Phosphatic strata of early (but not earliest)
Loc. 8 Akmalik Creek East (05AD65, ~85AMu2 [see table 1])	Killik River B-2 68°22.055' 154°10.401'	EMA (Killik River sequence of Mull and others, 1994); uppermost Lisburne Group.	Highest exposed Lisburne Gp., <1-2 m below exposed base of Siksikpuk Fm., is 3.5 m of gray, skeletal supportstone (with black phosphatic grains) in 40-cm-thick beds.	1 CO (Mu2-9) 1 TS (65B)	TS: 10-25% ph clasts (including ooids with >15 layers); some clasts contain silt, radiolarians; notable bored bioclasts.
05ALS15	Chandler Lake B-4 68°16.058' 152°03.320'	EMA (sheet just south of Skimo thrust sheet); upper Lisburne Group.	Interbedded muddy siltstone to very fine grained sandstone and spiculitic mudstone.	1 TS (15B: bioturbated silty ph M with spicules and glauconite)	TS: Few % ph clasts and bioclasts, rounded to irregular, ≤200μ diam.
Loc. 11 Skimo Creek (SKA 210-221 [Dumoulin, Whalen MS])	Chandler Lake B-4 ~68°17.864' 151°54.952'	EMA (Skimo thrust sheet); uppermost 2 m of Lisburne Group.	Lime mudstone with 5- to 15-cm-thick, more resistant, partly bioturbated intervals of dark shale that contain lenses (≤ a few cm thick) of glauconitic, phosphatic, silty to muddy spiculite.	2 CO (219, 221) 8 TS (SKA 210, 210.5, 210.5A, 219A, 219AA 221, 221A, 221B: all ph spiculite with quartz silt, ≤5% glauconite)	TS: 5-20% ph peloids (≤600 μ diam) > bioclasts in all 221 TS; minor ph (mostly bioclasts ≤200 μ diam) in all 210 and 219 TS.
Bombardment Creek (89AD44, 45 [MS upper Lisburne Group])	Wiseman D-2 44:68°55.467' 150°42.667' 45: 68°54.917' 150°40.333'	Parautochthonous (e.g., Young, 2004) [Doonerak antiform]; uppermost Lisburne Group.	Upper 5 m of Lisburne Group is skeletal supportstone; basal 80 cm of overlying Echooka Fm. is quartz-carbonate siltstone to very fine grained sandstone. Notable phosphate ~4.4 m below top of Lisburne and in basal Echooka.	5 CO (44C, Z; 45F; AKa4-1, 4-3) 31 TS (Lisburne Group: 10 from 44, 10 from 45, 2 from AKa4; Echooka Formation: 3 from 44, 1 from 45).	TS: in 44K (4.4 m below top of Lisburne Gp.) ≤10% ph material, mostly filling bryozoan pores, lesser clasts (≤ 800μ diam; 1 ?composite grain).

7 Age control, biofacies, CAI	8 Geochemical data		9 Remarks
	P_2O_5 wt %	C_{org} wt %	
Conodonts: abt (>500); Chesterian (likely very late Chesterian); CAI 2-3 (6).			Loc. 19, Dumoulin and others (2008). Samples taken ~5 m below base of Siksikpuk Formation.
Conodonts (from ≤7.5 m below top of Lisburne Group): latest Chesterian; shallow-water biofacies (lowest sample, shallow to moderate water depths; others, high-energy settings); CAI 2-2.5 (1, 7).			Loc. 3, Dumoulin and others 1997. TS from Siksikpuk Fm. contain locally abt clasts of phosphate and glauconite.
Conodonts (from 1 and 8 m below top of Lisburne Group): Chesterian, possibly late Chesterian; relatively shallow-water biofacies; CAI 2-2.5 (1, 7).			90KW F is loc. 2, Dumoulin and others (1997); AKa21 data from plate 7, Adams (1991) and K. Adams, unpub. field notes (thin sections provided by Adams and examined by J. Dumoulin). Several AKa TS contain ≤5% ph clasts and 30-70% glauconite clasts and resemble SKA 187 (Skimo Creek section). TS from Siksikpuk Fm. contain locally abt clasts of phosphate and glauconite.
Morrowan (Early Pennsylvanian) or younger age			
Conodonts (from 0.5 below top of Lisburne Group): late Morrowan or younger, with redeposited Chesterian forms; CAI 3 (1).			65B taken <1 m below top of highest Lisburne Gp. exposure, and <1-2 m below basal Siksikpuk Fm. [grassy covered zone lies between]; 65B likely from same bed as 2-9. Strata here are slightly younger, and a different lithology, than SKA 221 (Skimo Creek section).
No age control here.			Loc. 10, Dumoulin and others (2008). Lithologies here most like SKA 219-221 (Skimo Ck. section) but could also correlate with SKA 187.
Conodonts: abundant (>300 in SKA 219; >550 in SKA 221); early (but not earliest) Morrowan; CAI 1.5-2 (6).			Loc. 1, Dumoulin and others (2008). CHMC from SKA 221 contains phosphatic clasts and bioclasts. 221B TS contains a 1-mm-wide burrow(?) filled with ph peloids (20-80 μ in diam). Also see table 1.
Tightest ages from conodonts: from 44C (highest Lisburne Gp.), early (not earliest) Morrowan; from 44Z (10 m lower), very latest Chesterian-very earliest Morrowan; CAI 4.5-5 (1, 8).			Near MS 74-1 (Armstrong and Mamet, 1978) and 84AKa4 (Adams, 1991; MS of upper Lisburne Gp. only). TS from Echooka Formation: ≤5% ph clasts (≤4 mm diam) and bioclasts in 44A, 10-30% ph clasts in 44D (filling burrow or boring on top of Lisburne Group).

Table 3. Compositions of black shales, phosphorites, and phosphorite nodules from the Lisburne Group, northern Alaska.

[For statistical calculations the censured values (<x.xx) are assigned one-half the analytical detection limit (Sanford and others, 1993). REE anomalies are calculated by shale normalization (SN) using data for PAAS (Taylor and McLennan, 1985): $Ce/Ce^*_{(SN)} = 2Ce_{SN}/(La_{SN}+Pr_{SN})$; $Eu/Eu^*_{(SN)} = 2Eu_{SN}/(Sm_{SN}+Gd_{SN})$. MF, calculated marine fraction (see text)]

Component	Black Shales (*n*=17)		Phosphorite (*n*=24)		Phosphorite Nodules (*n*=3)	
	Mean S.D.	Range	Mean S.D.	Range	Mean S.D.	Range
SiO_2 (wt %)	41.50±18.57	11.91-67.12	18.88±16.91	1.99-46.89	18.69±4.66	13.31-21.43
TiO_2	0.256±0.131	0.017-0.510	0.011±0.006	<0.001-0.027	0.024±0.010	0.018-0.036
Al_2O_3	4.88±2.35	0.46-9.27	0.35±0.18	0.11-0.88	1.24±0.71	0.49-1.89
Fe_2O_3	1.65±0.52	0.70-2.62	0.26±0.24	0.07-1.25	0.52±0.16	0.35-0.67
MnO	0.042±0.054	0.005-0.190	0.013±0.031	0.001-0.148	0.025±0.009	0.017-0.035
MgO	1.81±2.21	0.53-9.90	0.68±1.13	0.03-4.70	1.23±1.02	0.06-1.90
CaO	19.66±14.55	4.22-47.21	40.76±9.42	24.85-53.72	42.42±2.05	40.92-44.76
Na_2O	0.32±0.21	0.09-0.84	0.17±0.07	<0.01-0.32	0.17±0.18	0.06-0.38
K_2O	1.32±0.74	0.13-2.72	0.09±0.05	<0.01-0.22	0.09±0.06	0.04-0.13
P_2O_5	4.20±3.61	0.54-11.54	23.49±4.56	17.63-36.98	27.6±2.84	25.80-30.91
LOI	23.49±8.52	8.12-36.06	11.65±6.07	3.98-21.49	6.66±0.34	6.26-6.87
F	0.76±0.60	0.17-2.01	4.29±1.51	1.95-7.63	5.07±1.18	4.28-6.43
Total C	10.71±3.97	3.20-17.10	4.72±1.94	2.05-8.28	2.65±0.47	2.11-3.00
C_{org}	7.53±5.15	1.34-17.36	3.01±1.30	1.21-6.73	1.69±0.99	0.81-2.76
CO_2	12.41±11.93	0.53-33.40	8.47±6.61	0.9-18.10	3.52±2.26	0.92-4.90
S	0.89±0.59	0.28-2.60	0.45±0.16	0.25-0.90	0.49±0.18	0.30-0.66
SO_4	0.70±0.63	0.05-2.10	1.01±0.50	0.12-1.90	0.42±0.03	0.40-0.45
Li (ppm)	17.5±13.2	2.4-43.7	2.5±1.8	1.1-10.5	1.4±0.4	1.1-1.8
Be	2±2	<1-6	1±1	<1-3	<1	<1
B	45±27	10-104	9±4	5-23	8±3	5-11
Sc	7.5±3.9	2.5-19.3	2.1±1.0	0.6-3.9	8.2±1.6	6.8-9.9
Zr	75±27	26-120	19±7	8-39	26±9	16-35
Hf	2.0±0.9	0.7-3.5	0.4±0.2	0.1-1.0	0.8±0.3	0.5-1.0
Nb	3.6±1.8	1.2-8.7	0.5±0.4	<0.2-1.4	1.3±0.7	0.7-2.0
Ta	0.26±0.16	<0.01-0.57	<0.01	<0.01-0.43	0.05±0.01	<0.01-0.06
Cr	759±561	39-1,690	117±54	35-297	31±8	23-38
V	881±767	55-2,831	371±161	79-763	26±7	21-34
Co	4.8±3.1	1.4-12.8	0.8±0.3	0.6-1.7	2.0±1.5	0.8-3.7
Ni	283±137	87-551	50±21	20-110	20±3	16-23
Cu	144±72	28-312	39±58	<10-300	57±72	13-140
Zn	1,112±1,081	<30-4,670	283±149	90-710	115±112	32-242
Cd	52.5±48.6	1.01-142	21.5±13.1	5.74-61.0	0.55±0.19	0.42-0.77
Mo	56.5±35.1	15.8-135	8.77±5.08	2.25-21.0	4.62±1.15	3.74-5.92
Re	0.299±0.225	0.084-0.855	0.138±0.088	0.033-0.326	0.034±0.011	0.022-0.043
Au (ppb)	5.49±14.7	<0.5-58.7	<0.5	<0.5	<0.5	<0.5
Ag	13.4±12.3	<0.5-43.5	0.9±0.5	<0.5-2.48	<0.5	<0.5
Tl	2.08±3.26	<0.05-12.3	0.76±1.28	<0.05-5.94	<0.05	<0.05-0.09
Pb	9.79±4.37	3.79-19.6	4.82±1.74	2.51-10.1	3.64±0.86	2.89-4.58
Ga	3.85±2.16	0.58-8.67	0.23±0.19	<0.02-0.60	0.79±0.55	0.32-1.39
Ge	2.3±2.6	<0.5-10	<0.5	<0.5-2.3	<0.5	<0.5
Rb	40±22	2.5-88	3±2	<1-7	3±2	<1-4
Sr	315±267	67-1,010	688±133	457-969	1,930±147	1,800-2,090

Table 3. Compositions of black shales, phosphorites, and phosphorite nodules from the Lisburne Group, northern Alaska.—Continued

Component	Black Shales (*n*=17)		Phosphorite (*n*=24)		Phosphorite Nodules (*n*=3)	
	Mean S.D.	Range	Mean S.D.	Range	Mean S.D.	Range
Sn	<1	<1-4	<1	<1-5	<1	<1
W	1.1±0.8	<0.5-3.5	<0.5	<0.5-1.9	<0.5	<0.5
Th	3.86±1.73	0.93-7.18	0.47±0.65	0.11-3.36	1.36±1.33	0.34-2.86
U	37.0±25.5	9.47-118	93.3±35.0	45.2-166	91.4±32.3	60.2-125
As	29.0±18.1	9.8-77.9	4.6±7.9	<0.5-33.4	6.1±4.0	2.1-10
Sb	8.8±4.8	2.4-19.0	1.7±1.9	0.5-9.9	1.0±0.2	0.9-1.3
Te	0.33±0.17	0.15-0.67	0.06±0.03	<0.02-0.12	0.10±0.03	0.08-0.14
Se	45.2±24.2	22.7-111	12.2±6.00	4.60-27.2	11.9±4.47	8.30-16.9
Ba	899±2,090	83.0-8,770	595±1,159	37-4,060	3,707±627	3,140-4,380
Y	139±92.6	26.1-340	232±202	72.7-1030	216±110	94.4-308
La	70.2±40.4	26.4-150	113±103	35.9-517	82.5±40.6	40.9-122
Ce	32.3±14.7	12.3-68.4	21.5±25.8	5.20-132	124±73.4	55.4-201
Pr	11.6±6.39	4.26-25.3	13.7±16.7	3.56-82.8	19.3±10.3	8.05-28.3
Nd	47.1±27.1	16.1-117	49.7±60.1	11.6-298	86.9±47.5	34.5-127
Sm	9.06±4.92	2.87-21.0	9.18±11.7	2.17-58.5	22.4±12.8	8.58-33.8
Eu	2.215±1.231	0.619-4.978	2.288±2.856	0.560-14.30	6.157±3.432	2.319-8.932
Gd	10.5±6.19	2.50-26.1	12.7±15.0	3.46-75.6	24.7±13.4	9.41-34.7
Tb	1.79±0.99	0.47-3.89	2.00±2.25	0.51-11.3	4.45±2.39	1.78-6.40
Dy	11.2±6.38	3.26-24.4	12.9±13.6	3.28-68.6	26.1±13.5	10.7-36.0
Ho	2.45±1.44	0.74-5.67	3.15±2.98	0.86-15.0	5.41±2.60	2.41-7.08
Er	7.58±4.21	2.87-16.2	10.2±9.01	3.08-45.3	16.7±7.31	8.32-21.7
Tm	1.101±0.586	0.471-2.330	1.481±1.207	0.461-6.040	2.480±0.997	1.329-3.080
Yb	6.73±3.52	2.83-14.5	9.06±6.88	2.83-34.2	14.5±5.23	8.49-17.6
Lu	1.056±0.554	0.432-2.350	1.390±0.962	0.438-4.740	2.248±0.785	1.358-2.842
$Ce/Ce^*_{(SN)}$	0.305±0.174	0.156-0.780	0.113±0.027	0.084-0.188	0.701±0.089	0.612-0.790
$Eu/Eu^*_{(SN)}$	1.102±0.045	1.036-1.182	1.070±0.037	0.970-1.116	1.232±0.045	1.198-1.282

This page left intentionally blank

Appendix. Additonal Geochemical Data

This section presents additional geochemical data on phosphorites and metalliferous black shales in the Carboniferous-Permian Lisburne Group. Table A1 contains complete geochemical analyses for all samples used in our study. Tables A2 and A3 contain results of statistical factor analyses of black shales and phosphorites, respectively.

Samples for geochemical analysis were trimmed of weathered surfaces and veins and then pulverized in an alumina-ceramic mortar. All analyses were done at Activation Laboratories in Ancaster, Ontario. Major, selected trace, and rare earth elements (REE) were determined by inductively coupled plasma-mass spectrometry (ICP-MS) on rock powders fused with lithium metaborate/tetraborate in order to insure complete acid dissolution of minerals such as zircon, monazite, xenotime, and barite prior to analysis. Instrumental neutron activation analysis (INAA) was used for As, Sb, Sc, and Cr. Data for Li, B, Ga, Co, Cd, Au, Pb, Mo, Re, Te, and Se were acquired by a multi-acid digestion of powders followed by ultratrace ICP-MS analysis, which has higher precisions and lower detection limits than the fusion ICP-MS method. Analyses were obtained on duplicate samples and 8-12 standards. One sample, phosphatic limestone 03AD27B, was not analyzed using the ultratrace ICP-MS method; data reported for Ga, Co, Au, Pb, and Mo were determined by fusion ICP-MS; data for Cd and Se were determined by INAA; Li, B, Re, and Te were not analyzed. Results for the following elements (by fusion ICP-MS) generally were below limits of detection as listed in parentheses: Cs (<0.1 ppm), In (<0.1 ppm), Ta (<0.1 ppm), W (<0.5 ppm), and Sn (<1 ppm), and thus are not reported. Details of the various analytical methods are available at www.actlabs.com.

Table A2 lists results of a statistical factor analysis of the bulk compositions of 17 samples of black shale from the Lisburne Group. The limited number of samples in this database restricts the number of elements; hence, those considered the most informative and representative were selected. Elements not included in the factor analysis, among 65 determined, have uniformly very low concentrations, were not detected, or were not analyzed by the ICP-MS or INAA methods used. Examples are the alkali and alkali earth elements Li and Be; transition metals such as Nb, Tc, Ru, Rh, Pd, Hf, Ta, W, Os, Ir, Pt, Au, and Hg; most middle and heavy REE; halogens including Cl, Br, I, and At; all noble gases; and all actinide elements except Th and U. Using four factors, significant loadings of $\geq$0.5 show that predominant factor 1 (31.0 percent) comprises, in decreasing order of loading, V, Ni, Cd, Mo, Cu, Zn, C_{org}, Cr, and Se, which is a factor composed mainly of seawater-and biogenically- derived constituents (for example, Piper, 1994). Factor 2 (25.6 percent) consists of Ge, Re, Ag, Tl, and Se, and may be partly hydrothermal in origin. Factor 3 (17.4 percent) includes Al, Ti, and C_{org}, and clearly is detrital. Factor 4, the least dominant (12.2 percent), comprises P, La, and U, and is a phosphate-related factor. Occurrence of V, Cr, Ni, Cu, Zn, Cd, Mo, and Se together with C_{org} in Factor 1 supports inferred associations for these elements and C_{org} (fig. 9).

A statistical factor analysis of the bulk compositions of 24 phosphorite samples is listed in table A3. Using four factors, significant loadings of $\geq$0.5 show that predominant factor 1 (23.5 percent) comprises, in decreasing order of loading, P, Sr, Ca, and F, and clearly is phosphate-based. Factor 2 (16.0 percent) consists of La, Y, Ce, Gd, and Cr, reflecting a factor composed mainly of LREE and Y. Factor 3 (15.5 percent) includes Mg, Ti, Ba, Al, K, Fe, and V, and largely is detrital in origin, perhaps excluding some Mg and Ba. Factor 4, the least dominant (14.9 percent), comprises Ni, Zn, Cu, U, and C_{org}, suggesting mostly seawater- and biogenically-derived constituents (for example, Piper, 1994). The presence of F and Sr in phosphate-based Factor 1 supports associations of F and Sr with P (fig. 13), but not for Y, LREE, and U that occur in different factors than P. The latter relationships are consistent with the general scatter of these elements relative to P_2O_5 in the phosphorites (fig. 13*C*), implying that they reside only partly in phosphate.

Table A1. Complete geochemical data from black shales and phosphorites from the Lisburne Group, northern Alaska.

[REE anomalies are calculated by shale normalization (SN) using data for PAAS (McLennan, 1989): $Ce/Ce^*_{(SN)} = 2Ce_{SN}/(La_{SN}+Pr_{SN})$; $Eu/Eu^*_{(SN)} = 2Eu_{SN}/(Sm_{SN}+Gd_{SN})$. n.a., not analyzed; phos., phosphatic; ls, limestone]

Sample no.	SKBo-25	92AD31A	92AD31H	92AD32B	03AD27A	03AD38C	05AD6E	CCP-0.4	CCP-1.35
Rock type	Black shale	Black shale	Black shale	Black shale	Black shale	Black shale	Black shale	Black shale	Black shale
Latitude	68°17.773′	68°37.967′	68°37.967′	68°30.660′	68°23.662′	68°27.627′	68°22.900′	68°17.500′	68°17.500′
Longitude	151°54.609′	156°43.750′	156°43.750′	157°30.920′	162°27.326′	161°58.391′	152°51.490′	152°01.061′	152°01.061′
Major elements (weight percent)									
SiO_2	19.54	41.63	39.35	65.97	67.12	61.61	49.25	54.84	65.55
TiO_2	0.166	0.439	0.387	0.258	0.513	0.206	0.279	0.240	0.202
Al_2O_3	3.12	8.39	7.44	5.20	9.27	4.68	4.99	4.23	3.76
$Fe_2O_3^T$	1.36	2.62	2.37	1.65	2.07	1.46	2.09	1.62	1.43
MnO	0.008	0.099	0.033	0.069	0.010	0.101	0.006	0.009	0.005
MgO	1.00	2.39	1.21	3.24	1.37	2.43	0.53	1.31	0.57
CaO	37.50	8.17	12.63	7.61	4.83	6.66	10.77	15.27	8.69
Na_2O	0.01	0.39	0.40	0.09	0.42	0.43	0.21	0.26	0.30
K_2O	0.80	2.09	1.77	1.14	2.46	2.06	1.74	1.14	1.05
P_2O_5	0.54	3.31	7.69	1.33	3.04	0.92	7.91	2.34	3.76
LOI	34.66	29.02	25.33	12.24	8.12	18.22	22.44	19.06	14.49
Total	98.70	98.55	98.61	98.80	99.22	98.78	100.22	100.32	99.81
F	0.17	0.66	1.27	0.56	0.78	0.19	1.27	0.40	0.58
C_{org}	5.32	15.9	14.7	2.69	3.00	7.68	15.0	6.38	8.05
CO_2	27.9	4.45	2.06	8.10	0.73	6.80	0.53	10.1	3.04
S	1.14	1.53	1.16	0.28	1.04	0.60	1.57	0.73	0.82
SO_4	0.23	0.21	0.09	0.03	0.05	0.06	0.50	1.20	0.90
Trace elements (ppm)									
Li	6.4	28.3	25.4	7.6	34.4	35.1	14.2	9.9	11.7
Be	<2	2	2	<1	2	1	6	2	2
B	31	65	66	73	67	53	31	23	23
Sc	4.6	11.0	8.0	7.0	12.4	6.6	7.7	6.5	6.1
V	1,870	1,720	1,180	169	249	160	2,831	346	576
Zr	52	116	79	86	120	69	89	68	67
Hf	1.1	3.1	3.0	2.1	3.5	1.7	1.6	1.8	1.7
Nb	2.3	5.8	4.9	3.8	8.7	3.9	3.4	3.1	2.6
Cr	241	1,690	1,340	573	205	39	1,660	1,060	1,070
Ni	423	461	379	135	87	285	551	263	268
Co	2.9	6.5	3.3	5.2	5.6	8.2	1.8	3.3	2.1
Cu	127	200	230	100	84	140	312	139	131
Pb	8.99	13.9	15.2	5.65	8.61	6.86	15.9	9.07	8.92
Zn	4,670	882	1,300	436	176	639	1,740	895	1,050
Cd	142	126	52.6	10.3	1.01	3.3	136	44.1	43.9
Mo	110	74.6	92.6	26.0	18.8	23.5	135	18.5	46.8
Re	0.239	0.187	0.166	0.112	0.084	0.114	0.495	0.321	0.367
Au (ppb)	0.3	58.7	21.4	<0.5	<0.5	<0.5	9.1	<0.5	<0.5
Ag	8.7	32.1	25.8	0.3	2.1	6.0	43.5	18.2	17.9
Tl	12.3	0.54	0.05	0.0	0.61	0.06	1.80	0.64	0.65
Ga	2.48	4.06	4.92	4.54	6.76	3.64	3.80	3.20	3.26
Ge	1.00	0.50	0.50	0.50	0.50	0.80	10.0	2.20	4.10
Rb	21	70	56	40	88	36	44	35	31
Sr	301	129	293	68	328	136	226	186	146
Th	2.09	6.82	7.18	4.61	5.42	3.88	4.22	3.87	3.40
U	53.5	31.4	49.9	13.0	22.3	14.7	59.4	16.7	25.7
As	61.9	45.0	44.0	27.0	13.3	9.84	23.9	21.3	22.0
Sb	11.0	19.0	18.0	7.2	2.4	5.9	15.4	5.9	6.6
Te	0.18	0.61	0.67	0.25	0.34	0.18	0.53	0.28	0.24

Table A1. Complete geochemical data from black shales and phosphorites from the Lisburne Group, northern Alaska.—Continued

Sample no.	SKBo-25	92AD31A	92AD31H	92AD32B	03AD27A	03AD38C	05AD6E	CCP-0.4	CCP-1.35
Rock type	Black shale	Black shale	Black shale	Black shale	Black shale	Black shale	Black shale	Black shale	Black shale
Latitude	68°17.773′	68°37.967′	68°37.967′	68°30.660′	68°23.662′	68°27.627′	68°22.900′	68°17.500′	68°17.500′
Longitude	151°54.609′	156°43.750′	156°43.750′	157°30.920′	162°27.326′	161°58.391′	152°51.490′	152°01.061′	152°01.061′
Se	48.9	65.0	55.8	51.3	29.2	33.9	111	25.7	38.0
Ba	91	850	980	326	2,050	150	291	122	106
Y	90.8	160	340	87	26.1	52.2	232	157	250
La	65.8	76.2	150	46.2	26.4	27.6	117	73.0	121
Ce	22.8	45.0	57.4	29.0	37.0	23.7	39.4	30.6	33.2
Pr	9.49	11.7	25.3	8.21	4.42	5.09	18.9	12.6	19.3
Nd	39.8	54.1	117	35.9	16.1	21.5	73.1	46.2	72.9
Sm	7.48	9.73	20.9	6.64	2.87	4.66	13.9	9.38	13.8
Eu	1.677	2.183	4.978	1.531	0.619	1.067	3.570	2.400	3.540
Gd	8.65	11.3	26.1	7.47	2.50	4.69	16.7	10.5	15.3
Tb	1.39	1.82	3.89	1.24	0.47	0.83	2.88	1.90	2.82
Dy	8.45	11.6	24.4	7.29	3.26	4.91	18.5	12.1	18.1
Ho	1.85	2.53	5.67	1.62	0.74	1.07	4.00	2.56	3.87
Er	5.97	8.47	16.2	5.08	2.87	3.52	12.3	7.63	11.6
Tm	0.891	1.263	2.163	0.719	0.528	0.544	1.820	1.130	1.600
Yb	5.45	7.48	12.0	4.11	3.62	3.35	11.6	6.98	9.49
Lu	0.844	1.154	1.785	0.638	0.599	0.542	1.890	1.090	1.440
Ce/Ce^*_{SN}	0.205	0.341	0.212	0.341	0.780	0.459	0.190	0.230	0.156
Eu/Eu^*_{SN}	1.037	1.036	1.101	1.066	1.047	1.081	1.138	1.144	1.143

Table A1. Complete geochemical data from black shales and phosphorites from the Lisburne Group, northern Alaska.—Continued

Sample no.	CCP-3.4	CCP-5.8	CCP-5.8A	CCP-7.5	JS-00-02	JS-04-23A	JS-05-82C	JS-05-93	03AD27B
Rock type	Black shale	Black shale	Black shale	Black shale	Black shale	Black shale	Black shale	Black shale	Phos. ls.
Latitude	68°17.500′	68°17.500′	68°17.500′	68°17.500′	68°17.370′	68°23.662′	68°28.906′	68°31.263′	68°23.662′
Longitude	152°01.061′	152°01.061′	152°01.061′	152°01.061′	163°22.040′	162°27.326′	155°42.703′	157°30.214′	162°27.326′
Major elements (weight percent)									
SiO_2	34.63	22.21	26.07	12.44	49.42	11.91	49.59	34.36	8.94
TiO_2	0.222	0.207	0.163	0.098	0.457	0.017	0.316	0.189	0.028
Al_2O_3	4.51	4.01	3.13	2.01	8.12	0.46	5.98	3.65	0.58
$Fe_2O_3^T$	1.57	1.39	1.21	0.91	2.12	0.70	2.12	1.32	0.98
MnO	0.006	0.008	0.008	0.005	0.038	0.190	0.010	0.109	0.212
MgO	0.65	0.95	0.91	0.91	1.28	0.93	1.21	9.90	1.38
CaO	24.34	35.54	34.89	44.13	14.37	47.21	4.22	17.36	48.48
Na_2O	0.35	0.15	0.13	0.09	0.18	0.18	0.65	0.84	<0.02
K_2O	1.26	0.83	0.73	0.24	2.72	0.13	1.57	0.72	0.02
P_2O_5	11.54	1.96	1.79	1.76	9.51	10.12	2.42	1.42	9.14
LOI	21.29	33.05	31.08	36.06	11.43	26.85	27.22	28.83	28.96
Total	100.37	100.31	100.11	98.65	99.65	98.70	95.31	98.70	98.74
F	2.01	0.36	0.35	0.31	1.53	1.88	0.43	0.21	1.86
C_{org}	9.43	5.14	4.19	2.92	4.41	1.34	17.4	4.47	0.91
CO_2	7.18	26.5	26.3	33.4	1.65	25.6	1.14	25.5	27.50
S	0.91	0.50	0.50	0.52	0.38	0.55	2.60	0.32	0.62
SO_4	2.10	1.00	1.40	1.60	0.09	0.31	0.90	0.60	0.34
Trace elements (ppm)									
Li	34.5	10.8	8.4	3.4	43.7	4.4	17.6	2.4	n.a.
Be	3	3	3	2	1	<1	6	1	<2
B	82	37	30	17	104	10	33	13	n.a.
Sc	7.2	6.6	5.9	2.5	19.3	3.6	7.1	4.7	4.3

Table A1. Complete geochemical data from black shales and phosphorites from the Lisburne Group, northern Alaska.—Continued

Sample no.	CCP-3.4	CCP-5.8	CCP-5.8A	CCP-7.5	JS-00-02	JS-04-23A	JS-05-82C	JS-05-93	03AD27B
Rock type	Black shale	Black shale	Black shale	Black shale	Black shale	Black shale	Black shale	Black shale	Phos. ls.
Latitude	68°17.500′	68°17.500′	68°17.500′	68°17.500′	68°17.370′	68°23.662′	68°28.906′	68°31.263′	68°23.662′
Longitude	152°01.061′	152°01.061′	152°01.061′	152°01.061′	163°22.040′	162°27.326′	155°42.703′	157°30.214′	162°27.326′
V	906	1,134	905	947	190	55	1,499	233	52
Zr	76	74	61	34	113	26	92	51	15
Hf	2.0	1.6	1.3	0.7	3.5	0.7	2.4	1.5	0.6
Nb	2.9	2.8	2.2	1.5	4.5	1.2	4.1	2.8	0.9
Cr	1,290	951	765	170	210	77	1,150	410	79
Ni	260	410	298	176	150	105	394	159	97
Co	4.5	3.3	2.5	1.4	12.8	7.3	2.4	8.7	5
Cu	234	176	136	72	104	28	179	54	29
Pb	19.6	7.33	5.87	5.06	11.1	7.55	13.0	3.79	13
Zn	981	1,520	1,110	2,130	15	188	835	338	117
Cd	86.0	40.5	33.2	81.9	1.89	2.63	80.3	6.55	2.3
Mo	80.3	54.0	49.4	50.4	15.8	56.0	84.1	24.7	53
Re	0.855	0.260	0.274	0.091	0.200	0.527	0.695	0.093	n.a.
Au (ppb)	<0.5	<0.5	<0.5	<0.5	<0.5	<0.5	<0.5	<0.5	3
Ag	20.2	11.8	10.5	1.6	0.3	1.5	19.5	8.3	2.0
Tl	0.73	3.88	3.47	7.33	0.03	0.69	1.99	0.44	1.43
Ga	8.67	3.30	2.39	1.63	7.66	0.58	3.12	1.52	<1
Ge	5.2	5.0	3.6	2.3	0.3	0.3	1.0	0.9	<0.5
Rb	36	29	26	12	65	2.5	56	25	2
Sr	432	282	311	482	875	1,010	77	67	1,100
Th	3.58	2.81	2.21	1.42	4.91	0.93	5.13	3.20	1.16
U	45.2	36.7	28.4	41.2	35.9	118	27.2	9.47	66.0
As	20.5	22.1	19.2	21.3	22.7	77.9	26.1	14.5	30.0
Sb	7.7	8.0	6.0	8.9	4.3	6.1	11.8	4.7	6.5
Te	0.55	0.28	0.21	0.16	0.42	0.15	0.40	0.19	n.a.
Se	52.9	24.3	42.3	22.7	25.2	23.8	85.8	32.8	8
Ba	150	122	97.0	83.0	8,770	237	715	147	210
Y	314	101	89.6	59.1	112	130	97.2	58.9	208
La	147	47.1	41.7	33.7	56.5	80.5	51.4	32.3	140
Ce	40.6	20.2	16.8	12.3	68.4	23.0	28.7	20.1	41.2
Pr	22.4	8.59	7.31	4.26	10.7	13.2	9.31	5.65	23.9
Nd	83.9	35.8	29.8	16.2	46.8	57.3	33.4	20.6	103
Sm	15.8	7.23	5.87	2.97	10.4	11.5	6.70	4.12	20.9
Eu	4.110	1.920	1.540	0.779	2.480	2.670	1.600	0.992	4.65
Gd	19.1	8.46	6.91	3.61	12.7	13.1	7.21	4.50	22.9
Tb	3.43	1.48	1.25	0.65	2.20	2.08	1.22	0.80	3.53
Dy	22.5	9.32	7.96	4.43	14.1	11.8	7.28	5.03	19.9
Ho	4.96	1.95	1.65	1.00	3.10	2.46	1.58	1.07	4.15
Er	15.5	5.85	5.14	3.16	9.62	7.86	4.83	3.24	12.9
Tm	2.330	0.842	0.751	0.479	1.390	1.110	0.682	0.471	1.71
Yb	14.5	5.25	4.73	3.09	9.36	6.37	4.19	2.83	9.35
Lu	2.350	0.864	0.778	0.529	1.460	0.943	0.612	0.432	1.38
Ce/Ce^*_{SN}	0.160	0.230	0.220	0.226	0.639	0.161	0.300	0.340	0.154
Eu/Eu^*_{SN}	1.129	1.182	1.148	1.135	1.047	1.086	1.115	1.095	0.653

Table A1. Complete geochemical data from black shales and phosphorites from the Lisburne Group, northern Alaska.—Continued

Sample no.	65ATR-75	CMD-4518	CMD-4617	CMD-5803	03AD2B	03AD10B	04AD8D	04AD9G	04AD9H
Rock type	Phosphorite	Phosphorite	Phosphorite	Phosphorite	Phosphorite	Phosphorite	Phosphorite	Phosphorite	Phosphorite
Latitude	68°38.070′	68°22.900′	68°18.180′	68°38.070′	68°17.735′	68°17.860′	68°18.180′	68°17.500′	68°17.500′
Longitude	156°44.526′	152°51.490′	151°50.400′	156°44.526′	151°54.869′	151°42.660′	151°50.400′	152°01.061′	152°01.061′
Major elements (weight percent)									
SiO_2	5.42	44.24	5.42	14.68	28.32	5.25	36.99	41.30	2.44
TiO_2	0.027	0.012	0.009	0.022	0.006	0.004	0.008	0.0005	0.0005
Al_2O_3	0.51	0.28	0.37	0.51	0.33	0.36	0.31	0.11	0.18
$Fe_2O_3^T$	0.31	0.07	0.12	1.25	0.17	0.09	0.24	0.52	0.09
MnO	0.042	0.002	0.003	0.148	0.002	0.002	0.002	0.004	0.005
MgO	3.39	0.07	0.34	4.70	0.07	0.12	0.06	0.05	0.70
CaO	45.34	29.41	49.91	38.77	32.99	45.99	28.47	30.89	51.39
Na_2O	0.26	0.21	0.13	0.17	0.17	0.19	0.14	0.18	0.14
K_2O	0.14	0.08	0.12	0.15	0.06	0.06	0.09	0.07	0.12
P_2O_5	26.02	19.35	22.04	20.73	23.84	28.62	21.04	21.54	21.83
LOI	14.6	5.03	14.6	13.1	8.56	12.3	8.00	3.98	21.49
Total	96.10	98.75	93.06	94.26	94.52	92.96	95.35	98.64	98.39
F	5.09	4.17	1.95	3.01	5.84	6.67	4.89	2.93	3.01
C_{org}	3.84	1.48	3.16	1.99	3.78	1.21	3.57	2.97	6.73
CO_2	9.45	5.15	14.9	12.7	2.58	12.0	1.10	1.21	18.1
S	0.49	0.45	0.68	0.90	0.56	0.28	0.54	0.32	0.46
SO_4	0.12	0.84	1.62	1.62	0.50	0.90	0.80	0.60	1.30
Trace elements (ppm)									
Li	2.3	10.5	2.3	1.7	2.7	2.2	4.7	2.1	1.7
Be	<1	<1	<1	<1	2	2	2	1	1
B	13	23	9	10	11	11	13	11	5
Sc	3.2	3.2	3.2	3.9	1.4	2.2	1.0	0.6	1.2
V	419	329	404	442	466	185	318	215	325
Zr	29	9	17	39	22	19	20	9	16
Hf	0.8	0.3	0.4	0.6	0.4	0.2	0.4	0.1	0.3
Nb	0.1	1.0	1.1	1.1	0.5	1.4	0.4	0.1	0.1
Cr	133	160	89	100	84	58	88	188	79
Ni	62	24	51	58	45	20	41	40	60
Co	1.1	0.6	0.8	1.3	0.7	0.8	0.6	0.7	0.6
Cu	48	5	28	67	18	18	16	30	40
Pb	4.61	4.03	6.32	5.71	5.72	2.97	3.63	4.08	3.38
Zn	172	137	298	540	312	224	264	170	390
Cd	14.3	17.2	22.9	33.9	23.9	15.0	13.2	6.63	11.9
Mo	6.31	4.37	10.3	14.4	8.85	5.15	7.56	13.3	3.17
Re	0.036	0.259	0.236	0.033	0.172	0.048	0.124	0.046	0.083
Au (ppb)	<0.5	<0.5	<0.5	<0.5	<0.5	<0.5	<0.5	<0.5	<0.5
Ag	2.5	1.6	1.0	1.6	0.3	0.9	0.6	0.9	0.9
Tl	0.23	0.03	0.03	0.11	0.20	5.94	0.27	0.21	0.27
Ga	0.23	0.39	0.32	0.43	0.32	0.01	0.04	0.06	0.01
Ge	0.3	0.9	0.3	0.3	0.3	0.3	0.3	0.3	0.3
Rb	4	3	3	4	2	2	2	0.5	1
Sr	467	499	770	666	675	903	627	703	642
Th	0.90	0.25	0.31	0.41	0.28	0.18	0.24	0.18	0.16
U	65.3	79.6	162	68.0	120	66.1	64.9	60.2	83.9
As	6.6	1.0	4.2	24.8	0.3	1.9	2.3	1.0	0.3
Sb	2.0	1.7	1.5	9.9	0.9	0.7	1.4	0.7	0.8
Te	0.06	0.03	0.07	0.07	0.10	0.06	0.03	<0.02	0.06
Se	19.3	8.0	13.2	17.3	8.6	5.7	9.6	5.8	7.6
Ba	316	101	259	4,060	79	272	61	62	39

Table A1. Complete geochemical data from black shales and phosphorites from the Lisburne Group, northern Alaska.—Continued

Sample no.	65ATR-75	CMD-4518	CMD-4617	CMD-5803	03AD2B	03AD10B	04AD8D	04AD9G	04AD9H
Rock type	Phosphorite	Phosphorite	Phosphorite	Phosphorite	Phosphorite	Phosphorite	Phosphorite	Phosphorite	Phosphorite
Latitude	68°38.070′	68°22.900′	68°18.180′	68°38.070′	68°17.735′	68°17.860′	68°18.180′	68°17.500′	68°17.500′
Longitude	156°44.526′	152°51.490′	151°50.400′	156°44.526′	151°54.869′	151°42.660′	151°50.400′	152°01.061′	152°01.061′
Y	270	237	284	251	160	93	96	72.7	112
La	127	109	135	108	72.3	42.8	45.7	35.9	49.4
Ce	22.9	15.6	28.7	25.5	11.5	5.20	7.26	5.20	7.33
Pr	14.0	12.2	14.2	11.7	7.81	3.91	4.97	3.56	4.57
Nd	58.2	50.3	56.4	46.6	28.6	13.9	17.3	11.6	15.4
Sm	9.02	7.97	8.89	7.54	5.14	2.54	3.22	2.17	3.04
Eu	2.288	1.972	2.257	2.007	1.310	0.688	0.803	0.560	0.786
Gd	14.5	12.7	14.4	12.3	6.86	3.46	4.08	3.62	5.22
Tb	2.15	1.69	2.07	1.83	1.18	0.62	0.71	0.51	0.75
Dy	14.8	11.6	14.7	13.1	8.07	4.52	4.73	3.28	4.92
Ho	4.21	2.86	3.73	3.38	2.03	1.15	1.13	0.86	1.35
Er	13.1	9.19	12.5	11.3	6.91	3.85	3.89	3.08	4.48
Tm	1.811	1.384	1.960	1.854	1.040	0.610	0.589	0.461	0.662
Yb	12.5	7.85	11.4	11.1	6.92	4.01	3.77	2.83	4.17
Lu	2.007	1.248	1.851	1.829	1.130	0.652	0.604	0.438	0.666
Ce/Ce^*_{SN}	0.118	0.093	0.140	0.154	0.104	0.084	0.104	0.097	0.102
Eu/Eu^*_{SN}	1.056	1.085	1.069	1.100	1.080	1.116	1.075	1.082	1.060

Table A1. Complete geochemical data from black shales and phosphorites from the Lisburne Group, northern Alaska.—Continued

Sample no.	04AD9J	04AD9K	04AD9L	05AD2C	05AD65K1	05AD65K2	05PP063	SKB-28.5C	TNC-191.6F
Rock type	Phosphorite	Phosphorite	Phosphorite	Phosphorite	Phosphorite	Phosphorite	Phosphorite	Phosphorite	Phosphorite
Latitude	68°17.500′	68°17.500′	68°17.500′	68°22.595′	68°22.055′	68°22.055′	68°19.015′	68°17.735′	68°21.870′
Longitude	152°01.061′	152°01.061′	152°01.061′	151°57.078′	154°10.401′	154°10.401′	152°20.216′	151°54.869′	151°52.440′
Major elements (weight percent)									
SiO_2	1.99	39.60	4.80	42.22	13.90	3.71	6.83	46.89	32.16
TiO_2	0.009	0.0005	0.004	0.010	0.015	0.015	0.008	0.013	0.008
Al_2O_3	0.19	0.13	0.17	0.41	0.88	0.48	0.39	0.34	0.28
$Fe_2O_3^T$	0.09	0.42	0.10	0.18	0.17	0.21	0.19	0.30	0.27
MnO	0.003	0.004	0.002	0.001	0.049	0.003	0.007	0.002	0.002
MgO	0.24	0.04	0.24	0.05	1.25	0.14	0.32	0.06	0.13
CaO	53.72	32.75	51.57	27.60	41.34	46.42	46.27	24.85	32.25
Na_2O	0.01	0.13	0.13	0.15	0.16	0.23	0.21	0.15	0.24
K_2O	0.01	0.06	0.04	0.09	0.22	0.13	0.09	0.09	0.05
P_2O_5	21.68	22.13	21.51	21.35	19.27	36.98	20.57	17.63	20.62
LOI	20.8	5.35	20.07	4.36	17.7	4.71	20.0	5.48	8.66
Total	98.71	100.61	98.64	96.42	94.94	93.03	94.90	95.81	94.67
F	3.43	3.07	3.06	4.34	4.03	7.63	5.24	3.68	4.45
C_{org}	2.43	2.24	3.34	1.84	1.23	1.52	3.52	2.53	2.25
CO_2	17.7	2.04	17.9	0.94	15.0	1.74	14.2	0.90	4.64
S	0.41	0.28	0.34	0.32	0.25	0.43	0.60	0.38	0.58
SO_4	0.32	0.60	1.00	0.70	0.80	1.30	1.60	0.50	1.60
Trace elements (ppm)									
Li	2.0	2.0	1.8	2.2	1.7	2.9	2.0	1.8	2.9
Be	<1	1	<1	2	1	2	3	2	<1
B	7	14	5	6	5	11	6	9	8
Sc	0.8	1.1	1.0	1.7	2.8	2.8	3.0	1.6	2.4
V	258	309	188	435	320	415	763	582	79

Table A1. Complete geochemical data from black shales and phosphorites from the Lisburne Group, northern Alaska.—Continued

Sample no.	04AD9J	04AD9K	04AD9L	05AD2C	05AD65K1	05AD65K2	05PP063	SKB-28.5C	TNC-191.6F
Rock type	Phosphorite	Phosphorite	Phosphorite	Phosphorite	Phosphorite	Phosphorite	Phosphorite	Phosphorite	Phosphorite
Latitude	68°17.500′	68°17.500′	68°17.500′	68°22.595′	68°22.055′	68°22.055′	68°19.015′	68°17.735′	68°21.870′
Longitude	152°01.061′	152°01.061′	152°01.061′	151°57.078′	154°10.401′	154°10.401′	152°20.216′	151°54.869′	151°52.440′
Zr	8	20	21	12	10	21	15	28	12
Hf	0.3	0.3	0.4	0.3	0.3	0.7	0.3	0.4	1.0
Nb	0.5	0.1	0.1	0.3	0.7	0.6	0.4	0.4	0.3
Cr	35	141	52	132	106	297	105	142	151
Ni	28	50	60	33	22	60	47	43	69
Co	0.8	1.7	0.7	0.6	0.8	1.0	0.8	0.6	0.6
Cu	10	30	40	22	10	62	13	19	22
Pb	4.06	3.67	5.45	4.78	2.85	10.1	3.66	3.38	5.18
Zn	222	150	460	179	173	390	501	203	230
Cd	16.3	5.74	25.8	23.1	41.7	15.4	35.1	14.9	8.56
Mo	5.27	9.60	7.63	2.25	2.89	21.0	9.05	14.1	7.06
Re	0.096	0.080	0.104	0.075	0.137	0.274	0.085	0.103	0.174
Au (ppb)	<0.5	<0.5	<0.5	<0.5	<0.5	<0.5	<0.5	<0.5	<0.5
Ag	0.6	0.7	0.7	0.3	1.1	1.3	0.3	1.1	0.3
Tl	0.13	0.19	1.21	1.86	0.52	0.30	0.55	1.03	2.84
Ga	0.01	0.01	0.01	0.48	0.27	0.39	0.21	0.25	0.54
Ge	0.3	0.3	0.3	0.3	0.6	1.2	0.3	0.3	1.0
Rb	0.5	2	2	3	7	5	3	3	2
Sr	656	648	818	457	528	969	750	567	744
Th	0.21	0.11	0.14	0.34	0.37	0.85	0.39	0.28	3.36
U	92.0	88.6	140	86.3	57.5	129	78.2	45.2	81.5
As	33.4	4.0	3.0	1.6	2.1	3.2	0.3	3.4	0.3
Sb	0.9	0.5	1.6	0.7	1.4	3.1	1.5	1.3	1.3
Te	0.05	0.02	0.05	0.07	0.04	0.10	0.08	0.06	0.12
Se	10.1	7.1	12	12.4	7.3	24.5	10.5	9.4	23.5
Ba	37	72	64	592	295	679	318	71	230
Y	118	125	166	219	165	532	175	111	1030
La	63.3	63.7	75.6	116	63.2	275	85.4	50.1	517
Ce	12.5	7.81	10.6	16.6	14.8	46.1	17.1	6.90	132
Pr	6.55	5.97	7.19	12.5	7.66	37.9	8.70	5.69	82.8
Nd	27.5	20.3	24.8	42.1	26.7	139	29.9	19.6	298
Sm	4.58	3.88	4.94	7.41	5.18	25.4	5.35	3.71	58.5
Eu	1.101	0.966	1.210	1.910	1.310	6.260	1.430	0.971	14.30
Gd	6.41	6.03	8.75	9.65	6.27	31.9	7.37	5.01	75.6
Tb	1.03	0.92	1.31	1.64	1.22	5.31	1.29	0.87	11.3
Dy	6.62	6.16	8.65	11.2	8.46	33.4	8.69	5.76	68.6
Ho	1.62	1.58	2.29	2.68	2.07	7.85	2.14	1.46	15.0
Er	5.44	5.45	7.38	8.84	6.74	25.3	7.28	4.98	45.3
Tm	0.819	0.840	1.050	1.330	1.020	3.680	1.130	0.761	6.040
Yb	4.86	5.32	6.30	8.65	6.71	22.4	7.04	4.89	34.2
Lu	0.781	0.898	0.957	1.380	1.030	3.330	1.050	0.798	4.740
Ce/Ce^*_{SN}	0.130	0.084	0.095	0.094	0.147	0.101	0.133	0.089	0.145
Eu/Eu^*_{SN}	1.025	1.039	0.970	1.110	1.059	1.087	1.107	1.098	1.115

Table A1. Complete geochemical data from black shales and phosphorites from the Lisburne Group, northern Alaska.—Continued

Sample no.	CCP-1.8	CCP-3.7	CCP-4.85	CCP-10.1	JS-05-82A	JS-05-82B	00AD4A	03AD27C	03AD27L
Rock type	Phosphorite	Phosphorite	Phosphorite	Phosphorite	Phosphorite	Phosphorite	Phos. nodule	Phos. nodule	Phos. nodule
Latitude	68°17.500′	68°17.500′	68°17.500′	68°17.500′	68°28.906′	68°28.906′	68°17.370′	68°23.662′	68°23.662′
Longitude	152°01.061′	152°01.061′	152°01.061′	152°01.061′	155°42.703′	155°42.703′	163°22.040′	162°27.326′	162°27.326′
Major elements (weight percent)									
SiO_2	6.82	43.23	5.68	3.11	7.62	10.38	13.31	21.43	21.32
TiO_2	0.009	0.0005	0.004	0.0005	0.013	0.018	0.018	0.018	0.036
Al_2O_3	0.50	0.15	0.47	0.14	0.45	0.49	1.89	0.49	1.34
$Fe_2O_3^T$	0.22	0.48	0.23	0.10	0.18	0.23	0.67	0.35	0.54
MnO	0.005	0.004	0.007	0.002	0.005	0.005	0.017	0.035	0.024
MgO	1.35	0.03	1.12	0.21	1.11	0.64	0.06	1.90	1.74
CaO	48.46	29.42	50.28	52.97	44.31	42.89	44.76	41.58	40.92
Na_2O	0.02	0.09	0.02	0.12	0.32	0.26	0.06	0.08	0.38
K_2O	0.03	0.02	0.005	0.15	0.08	0.17	0.13	0.01	0.04
P_2O_5	24.86	20.71	25.67	22.90	31.28	31.56	30.91	25.80	26.22
LOI	15.42	4.78	15.12	19.26	8.48	7.67	6.84	6.87	6.26
Total	97.69	98.91	98.61	98.96	93.85	94.31	98.67	98.56	98.82
F	3.55	2.98	3.42	3.13	6.78	6.66	6.43	4.51	4.28
C_{org}	5.52	3.57	3.90	3.74	2.75	3.22	2.76	1.50	0.81
CO_2	11.9	0.95	12.9	17.8	4.89	2.51	0.92	4.90	4.75
S	0.46	0.27	0.35	0.26	0.60	0.60	0.30	0.51	0.66
SO_4	1.40	0.60	1.10	0.80	1.90	1.80	0.45	0.40	0.41
Trace elements (ppm)									
Li	2.6	1.3	2.4	1.1	1.9	1.8	1.1	1.3	1.8
Be	1	1	2	<1	2	2	<1	<1	<2
B	5	7	5	5	11	9	11	5	7
Sc	2.8	0.6	2.4	1.4	2.6	2.4	9.9	8.0	6.8
V	537	327	383	106	505	597	23	21	34
Zr	27	22	19	19	15	17	35	16	28
Hf	0.7	0.5	0.3	0.3	0.3	0.5	1.0	0.5	0.9
Nb	0.5	1.3	0.2	0.1	0.4	0.4	2.0	0.7	1.1
Cr	137	139	114	53	95	137	32	38	23
Ni	110	50	80	30	39	73	16	23	21
Co	0.8	0.7	0.8	0.6	0.9	1.5	3.7	0.8	1.6
Cu	300	30	40	30	13	35	140	13	18
Pb	6.07	2.51	6.40	3.39	6.29	7.42	3.46	4.58	2.89
Zn	710	160	290	90	274	243	242	32	69
Cd	61.0	18.6	20.3	7.64	21.8	41.8	0.77	0.47	0.42
Mo	6.32	8.54	8.58	2.38	20.6	11.8	5.92	4.2	3.74
Re	0.227	0.122	0.307	0.080	0.078	0.326	0.043	0.037	0.022
Au (ppb)	<0.5	<0.5	<0.5	<0.5	<0.5	<0.5	<0.5	<0.5	<0.5
Ag	0.3	0.8	0.3	0.6	1.0	0.9	0.3	0.3	0.2
Tl	0.51	0.05	0.55	0.11	0.42	0.70	0.09	0.03	0.03
Ga	0.60	0.01	0.27	0.01	0.31	0.37	1.39	0.32	0.66
Ge	2.3	0.3	0.7	0.3	0.3	0.3	0.3	0.3	0.3
Rb	0.5	2	0.5	1	4	4	4	0.5	4
Sr	711	604	879	786	778	657	1,900	1,800	2,090
Th	0.56	0.25	0.35	0.13	0.46	0.50	0.88	0.34	2.86
U	141	50.8	166	82.7	99.4	130	89.2	125	60.2
As	0.3	3.0	0.3	2.0	3.0	7.3	2.1	6.3	10
Sb	1.0	0.8	0.9	0.5	1.5	3.0	0.9	0.9	1.3
Te	0.06	0.08	0.09	0.05	0.10	0.08	0.08	0.14	0.09
Se	16.1	7.5	27.2	4.6	12.1	13.1	16.9	8.3	10.5
Ba	44	52	60	61	3,850	2,598	4,380	3,140	3,600

Table A1. Complete geochemical data from black shales and phosphorites from the Lisburne Group, northern Alaska.—Continued

Sample no.	CCP-1.8	CCP-3.7	CCP-4.85	CCP-10.1	JS-05-82A	JS-05-82B	00AD4A	03AD27C	03AD27L
Rock type	Phosphorite	Phosphorite	Phosphorite	Phosphorite	Phosphorite	Phosphorite	Phos. nodule	Phos. nodule	Phos. nodule
Latitude	68°17.500′	68°17.500′	68°17.500′	68°17.500′	68°28.906′	68°28.906′	68°17.370′	68°23.662′	68°23.662′
Longitude	152°01.061′	152°01.061′	152°01.061′	152°01.061′	155°42.703′	155°42.703′	163°22.040′	162°27.326′	162°27.326′
Y	435	105	215	124	199	281	308	94.4	247
La	218	55.6	94.3	57.4	90.7	153	84.6	40.9	122
Ce	34.2	7.57	27.9	7.45	15.9	28.7	114	55.4	201
Pr	23.9	5.68	11.2	4.90	9.90	22.1	21.7	8.05	28.3
Nd	79.6	18.4	38.9	16.4	34.8	78.0	98.8	34.5	127
Sm	15.4	3.50	8.09	3.08	6.65	15.1	25.0	8.58	33.8
Eu	3.680	0.888	1.960	0.825	1.710	3.710	7.221	2.319	8.932
Gd	22.9	5.37	11.8	5.68	8.36	17.4	30.0	9.41	34.7
Tb	3.42	0.78	1.89	0.89	1.53	3.05	5.16	1.78	6.40
Dy	21.2	5.02	11.8	6.06	10.5	18.6	31.6	10.7	36.0
Ho	5.30	1.33	3.06	1.68	2.63	4.21	6.73	2.41	7.08
Er	17.0	4.23	9.87	5.71	8.89	13.1	20.1	8.32	21.7
Tm	2.380	0.623	1.440	0.855	1.390	1.810	3.031	1.329	3.080
Yb	14.0	3.85	8.98	5.52	9.19	10.9	17.6	8.49	17.5
Lu	2.100	0.593	1.410	0.890	1.420	1.570	2.842	1.358	2.543
Ce/Ce^*_{SN}	0.102	0.091	0.188	0.091	0.114	0.111	0.612	0.702	0.790
Eu/Eu^*_{SN}	1.027	1.089	1.018	1.017	1.088	1.100	1.282	1.198	1.216

Table A2. Varimax normalized factor loadings for bulk compositions of 17 black shales from the Lisburne Group, northern Alaska.
[Significant loadings of ≥0.5 are shown in bold type]

Element	Factor 1	Factor 2	Factor 3	Factor 4
Al	0.0621	-0.2565	**0.8743**	0.0096
Ti	0.0555	-0.2158	**0.8676**	0.0194
P	-0.0115	-0.2344	0.0842	**0.9205**
C_{org}	**0.6826**	-0.0880	**0.5473**	0.2265
V	**0.9408**	-0.0839	0.0734	0.0469
Cr	**0.6475**	-0.0381	0.4869	0.3320
Ni	**0.9011**	-0.1421	0.1928	0.0017
Cu	**0.7533**	0.0695	0.4072	0.3245
Zn	**0.6961**	-0.2778	-0.4369	-0.2710
Cd	**0.8488**	0.3136	-0.1521	0.0060
Mo	**0.7979**	0.3657	-0.2267	0.2877
Re	-0.1340	**0.9377**	-0.2324	-0.0290
Ag	0.2603	**0.9229**	-0.0294	0.1348
Tl	-0.0734	**0.9100**	-0.3131	-0.0924
Ge	-0.0796	**0.9417**	-0.2382	-0.0062
U	0.0377	0.3981	-0.5973	**0.5315**
Se	**0.5764**	**0.6552**	0.1554	0.1448
La	0.3754	0.2500	0.0078	**0.7631**
Proportion	31.0 %	25.6 %	17.4 %	12.2 %

Table A3. Varimax normalized factor loadings for bulk compositions of 24 phosphorites from the Lisburne Group, northern Alaska.
[Significant loadings of ≥0.5 are shown in bold type]

Element	Factor 1	Factor 2	Factor 3	Factor 4
Si	-0.0165	0.0197	-0.1160	-0.6514
Al	0.3468	0.1996	**0.6890**	0.0620
Fe	-0.0426	-0.0771	**0.6044**	-0.0386
Mg	-0.0433	-0.1026	**0.8228**	0.2888
Ca	**0.7760**	-0.1216	0.0494	0.4230
K	0.2476	0.0142	**0.6215**	-0.2391
Ti	-0.2951	0.2746	**0.7959**	0.0133
P	**0.8596**	0.2490	0.2121	0.0904
F	**0.6522**	0.3676	0.2799	-0.1809
C_{org}	0.4307	-0.3136	-0.1331	**0.5435**
V	0.3252	-0.0984	**0.5245**	0.1863
Cr	0.0656	**0.6160**	0.1572	-0.1603
Ni	-0.4099	0.3009	0.0235	**0.7653**
Cu	-0.1962	0.1065	0.0775	**0.7454**
Zn	0.2745	0.0206	0.2657	**0.7526**
Mo	-0.8714	0.1239	-0.0291	0.1173
Sr	**0.8211**	0.1693	-0.1265	0.2333
U	0.1534	0.2110	-0.1887	**0.6888**
Ba	0.0508	0.0721	**0.7415**	0.0566
Y	0.0946	**0.9075**	0.0241	0.1904
La	0.0033	**0.9294**	-0.0136	0.1974
Ce	-0.5267	**0.7768**	-0.0919	0.1888
Gd	-0.7301	**0.6242**	-0.1348	0.1802
Yb	-0.8676	0.3700	-0.0838	0.1737
Proportion	23.5 %	16.0 %	15.5 %	14.9 %

Produced in Menlo Park, California
Manuscript approved for publication February 3, 2011
Edited by Tracey Suzuki
Layout by David R. Jones